COMMITTEE CERTIFICATION OF APPROVED VERSION

The committee for Naomi Oshiro certifies that this is the approved version of the following dissertation:

SUBSTRATE SPECIFICITY AND FUNCTIONAL CHARACTERIZATION OF SODIUM/DICARBOXYLATE COTRANSPORTERS

Committee:

Dr. Ana M. Pajor, Supervisor

Dr. James C. Lee

Dr. Lucie Parent

Dr. Guillermo Altenberg

Dr. Owen P. Hamill

Dean, Graduate School

SUBSTRATE SPECIFICITY AND FUNCTIONAL CHARACTERIZATION OF SODIUM/DICARBOXYLATE COTRANSPORTERS

By

Naomi Oshiro, M.S.

Dissertation
Presented to the Faculty of the University of Texas Graduate School of
Biomedical Sciences at Galveston
in Partial Fulfillment of the Requirements
for the Degree of

Doctor of Philosophy

Approved by the Supervisory Committee

Ana M. Pajor, Ph.D.
James C. Lee, Ph.D.
Lucie Parent, Ph.D.
Guillermo Altenberg, M.D., Ph.D.
Owen P. Hamill, Ph.D.

May 2006
Galveston, Texas

Key words: Citric acid cycle intermediates, Two-electrode voltage clamp, *Xenopus laevis* oocytes, Glutarate, Adipate, Succinate, Transport specificity ratio

To my father, and in memory of my mother

ACKNOWLEDGMENTS

Words are never enough to express all my gratitude to those who have generously offered me their support, encouragement, and guidance in the last five years of my graduate school at the University of Texas Medical Branch. My life as a graduate student could not have been so meaningful or enjoyable without them.

I wish to thank all of my dissertation committee members:

Dr. Ana M. Pajor, my supervising professor, for training me to be a critical thinker as well as to be professional. Her enormous patience is unsurpassed, and her enthusiasm, support, humor, and kindness have led me to completion of the graduate studies. I am forever grateful for it.

Dr. James C. Lee, my out-of-program committee member, for providing valuable insights into intramolecular interaction between transmembrane helices of Na^+/dicarboxylate cotransporters using thermodynamics. The point to which he has directed his attention broadens and changes an approach to a problem.

Dr. Lucie Parent, my off-campus committee member from the University of Montreal, for shearing her expertise in electrophysiology, which offered me significant guidance to improve experimental design.

Dr. Guillermo Altenberg, my committee member from the graduate program of Cellular Physiology and Molecular Biophysics, for providing critical discussion and valuable advice on experimental design in electrophysiology and data interpretation.

Dr. Owen P. Hamill, my committee member from the graduate program of Cellular Physiology and Molecular Biophysics, whose humanity and enthusiasm have guided me through to find out solutions of problems. Although he has a number of obligations, he is always willing to take time to discuss not only science but also my career as a young scientist.

I would also like to thank Dr. Steven C. King at the Oregon Health & Science University, whose idea for Transport Specificity Ratio (TSR) was a unique and insightful tool to

detect changes in substrate specificity in transport proteins. His knowledge and passion to thermodynamics was unexceeded, and his discussion and interpretation of experimental results were undoubtedly valuable.

Thanks also to my colleagues and everyone on the 4th floor of Basic Science Building who helped me in various ways Kathleen M. Randolph, Jittima Weerachayaphorn, Aditya D. Joshi, Dr. Jason A. Hall, Donovan E. Randolph, Sheri M. Foltz, Dr. Simon A. Lewis, Jamie R. Lewis, Dr. Aileen K. Ritchie, Dr. Nancy K. Wills, and Dr. Steven A. Weinman for not only their scientific suggestion and help but also cheerful encouragement, joyful noise, great friendship, and enthusiasm about hallway parties, which certainly made my life as a graduate student memorable.

There are many of my friends who deserve acknowledgements in this dissertation. I am very grateful to Kay and Bob Mitchell for their consistent love, generosity, and support, especially as I went through a difficult time of my life; Dr. Yasuna Kobayashi and his family, Shigeko and Atsuko, for their loyal friendship, sincere caring, and great encouragement despite a long distance; Dr. Tadahide Izumi and Kuniko Izumi for scientific advice as well as for being open-hearted friends; Janel and Jerry Sprayberry, and Yvonne and Fritz Poppe for their amazing patience, kindness, and support when I had many difficulties with English. Without that time, I would not have been where I am now; Linda and Joe Davis for inviting me to be a part of their family; Dr. Rosario Maroto and her son, Alan Hamill, for being wonderful supporters and his entertaining me with artistic dance sometimes; Dr. Toshinori Yamamoto for his warm thought for me over six years. Lastly, many thanks are offered to Jung Won Kim, a gifted organist from Pusan, South Korea, and Dr. Ibironke V. Adelaja, a promising young surgeon, for their love and faithful friendship, and for sharing their lives with me in many occasions. I am very lucky to have both of them as my precious friends who have been there for me.

In order to make my five years of graduate studies possible, my family has shown the invaluable contribution. Thanks to my two brothers, Masahiro and Seiji, for their support and cheering. I sincerely appreciate my parents who always believe in me and offer me everything they have to make my wishes come true. Their understanding, quiet enduring love, and strength are my anchor.

SUBSTRATE SPECIFICITY AND FUNCTIONAL CHARACTERIZATION OF SODIUM/DICARBOXYLATE COTRANSPORTERS

Publication No._____

Naomi Oshiro, M.S.
The University of Texas Medical Branch at Galveston, May 2006

Supervisor: Ana M. Pajor

Transport of dicarboxylates across the plasma membrane is mediated by the Na^+/dicarboxylate cotransporters (NaDCs) belonging to the SLC13 gene family. These transporters play important roles in the homeostasis of dicarboxylates. The studies in this dissertation focused on two aspects of the NaDCs: structure-function studies of two low-affinity transporters, mouse (m) and rabbit (rb) NaDC1, and functional characterization of a high-affinity NaDC transporter from *Xenopus laevis*, xNaDC3.

Although sharing strong sequence identity, mNaDC1 and rbNaDC1 differ in their ability to transport certain dicarboxylates. For example, oocytes expressing mNaDC1 exhibit large inward currents in the presence of glutarate, adipate, and succinate, whereas oocytes expressing rbNaDC1 have currents only with succinate. To identify NaDC1 domains involved in different ability to transport glutarate and adipate, I constructed a series of mNaDC1-rbNaDC1 chimeras, and used both electrophysiological and dual-radiolabel competitive uptake techniques to exam their transport properties. My work indicates that different multiple transmembrane helices (TMs) are involved in NaDC1 substrate recognition, with the region of TM 3-4 and the C-terminus required for glutarate while the TM 8-10 region is necessary for adipate transport. Further analysis of these two regions provided evidence that they contained residues important for both apparent substrate affinity and catalytic efficiency of NaDC1.

The functional properties of non-mammalian vertebrates in the SLC13 family are not well characterized. Therefore, an initial functional characterization of xNaDC3 was performed using electrophysiological techniques. Like other members of the SLC13 family, xNaDC3 is electrogenic and exhibits inward substrate-dependent currents in the presence of sodium. However, other electrophysiological properties of xNaDC3 are unique and involve large cation-activated leak currents possibly mediated by anions.

Taken together, these studies have provided insight into the mechanism of substrate recognition and transport by NaDCs. My work not only contributes to a more detailed analysis of NaDC structure-function relationships, but also demonstrates how transport protein structural information can be obtained using a biochemical approach. The need for such an approach can be explained by the fact that only a limited number of transporters have had their structures solved to an atomic resolution despite the critical involvement of transporters in cellular functions.

TABLE OF CONTENTS

LIST OF TABLES

LIST OF FIGURES

ABBREVIATIONS

2,2-DMS	2,2-Dimethylsuccinate
2,3-DMS	2,3-Dimethylsuccinate
f	Prefix, Flounder
h	Prefix, Human
Indy	Na^+-independent succinate transporter from *Drosophila*
m	Prefix, Mouse
NaDC1	Low-affinity Na^+/dicarboxylate cotransporter
NaDC3	High-affinity Na^+/dicarboxylate cotransporter
NaCT	Na^+-citrate transporter
NaS	Na^+/sulfate cotransporter
o	Prefix, Opossum
OAT	Organic anion transporter
r	Prefix, Rat
rb	Prefix, Rabbit
RT-PCR	Reverse transcription-polymerase chain reaction
SLC	Solute carrier gene family
TEVC	Two-electrode voltage clamp
TM	Transmembrane helix
TSR	Transport Specificity Ratio
x	Prefix, *Xenopus laevis*

CHAPTER 1: INTRODUCTION

This dissertation focuses on two major aspects of the Na^+/dicarboxylate cotransporters (NaDCs). The first section described in Chapters 2 and 3 centers on the relationship between structure and function of the low-affinity Na^+/dicarboxylate cotransporter, NaDC1. In the second part described in Chapter 4, the electrophysiological properties of the high-affinity Na^+/dicarboxylate cotransporter, NaDC3, were investigated by the two-electrode voltage clamp. All of the studies in this dissertation were carried out using *Xenopus laevis* oocytes as an expression system. This introduction will begin with a simplified general classification of membrane transport proteins, and it will continue with further detail of NaDCs.

GENERAL CLASSIFICATION OF MEMBRANE TRANSPORT PROTEINS

In the genome of *Saccharomyces cerevisiae* and *Escherichia coli*, approximately 15% of the cellular proteins contain two or more predicted transmembrane helices and are considered as potential membrane transport proteins (89). Due to recent increases in the information on gene sequences, structures and functional mechanisms of the membrane transport proteins, a novel classification system of the transport proteins was proposed by Saier in 1999, called the Transporter Classification system (15). The Transporter Classification system is based on the functional and phylogenetic characterization of about 250 families of sequence-related transporters in bacteria, archaea, and eukaryotes. Currently, nearly 400 families are included in the TC system, which was formally adopted by the International Union Biochemistry and Molecular Biology (15).

In the Transporter Classification system, the membrane transport proteins are initially classified into two major types, channels and carriers, as shown in Figure 1.1

(15). Ion channels are traditionally considered to be selective pores that use pre-existing electrochemical gradient for their ion transport.

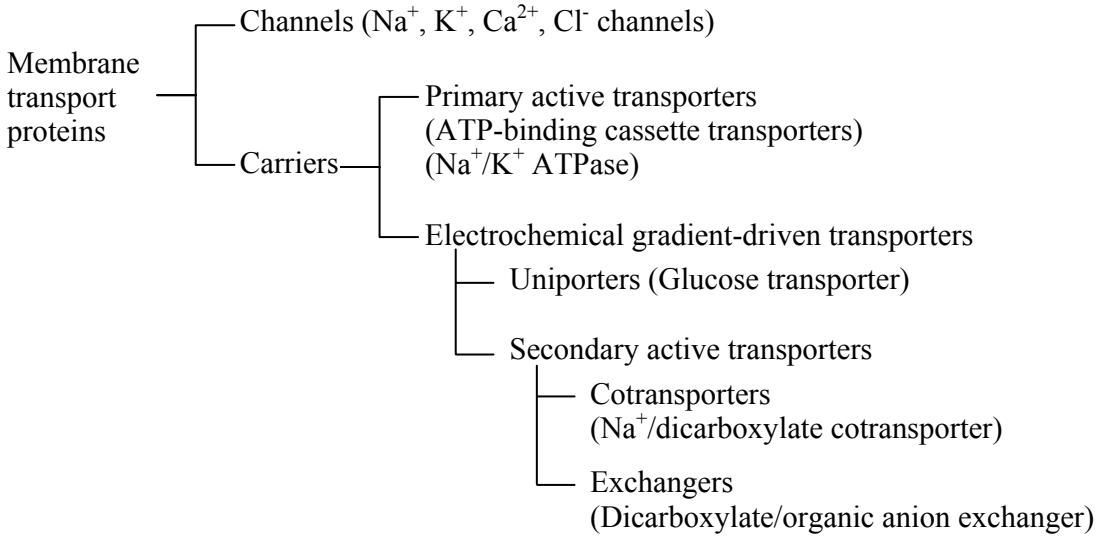

Figure 1.1 General classification of membrane transport proteins. The transport proteins are classified according to the Transporter Classification system (15; 93). The scheme shows the simplified first three classes in the classification system. The transport proteins are divided into two major types, channels and carriers. Carriers are subdivided into primary active transporters, secondary active transporters, and uniporters.

More diverse groups of transport proteins can be found in carrier proteins, subdivided into primary active transporters, secondary active transporters, and uniporters depending on the nature of the transport proteins and their energy sources (Figure 1.1). Majority of primary active transporters use hydrolysis of diphosphate bond of inorganic pyrophosphate or a nucleoside triphosphate such as ATP to drive the transport of solutes against their electrochemical gradient. For example, the multidrug resistance protein 1, a member of the ATP-binding cassette transporter family, transports variety of compounds using energy of ATP hydrolysis. The Na^+/K^+ ATPase also hydrolyzes ATP to pump sodium ions out and potassium ions in to maintain the electrochemical gradient of sodium and potassium ions across membranes. Secondary active transporters and uniporters do not couple directly to ATP hydrolysis during transport cycles but use electrochemical

gradient created by the primary active transporters to drive active solute transport across membranes. Major driving forces of the secondary active transporters are sodium- and proton- electrochemical gradients. Among the secondary active transporters, there are two main subclasses, cotransporters and exchangers. Cotransporters involve two or more solutes and ions transported in the same direction, whereas exchangers transport substrates in opposite directions. Uniporters such as glucose transporters (GLUTs) are facilitated diffusion carriers transporting a single solute by facilitated diffusion. The NaDCs, the major focus of this dissertation, belong to the secondary active cotransporters.

THE SOLUTE CARRIER 13 GENE FAMLY

According to the Human Genomic Organization (HUGO) Gene Nomenclature Committee, the solute carrier (SLC) families currently consist of 49 families and 352 transporter genes. The genes encoding human NaDCs are grouped into the SLC13 family in the human gene nomenclature (see http://www.gene.ucl.ac.uk/nomenclature/). In particular, genes coding for the low-affinity Na^+/dicarboxylate cotransporter, NaDC1, and the high-affinity Na^+/dicarboxylate cotransporter, NaDC3, are designated as SLC13A2 and SLC13A3, respectively (Table 1.1). The SLC13 family also includes genes corresponding to the Na^+/sulfate cotransporters (NaS1 and NaS2) and the Na^+/citrate transporter (NaCT) named SLC13A1, SLC13A4, and SLC13A5, respectively (Table 1.1).

Table 1.1 General characteristics of vertebrate members of the SLC13 family

Protein	Substrates	Tissue distribution	Orthologs	%[1]	Reference
NaDC1	Dicarboxylates	Kidney (apical	Human (h)	76	(69)
SLC13A2	K_m succinate 800 μM	membranes),	Rabbit (rb)	74	(72)
		small intestine	Rat (r)	92	(21; 94)
			Mouse (m)	100	(85)
			Opossum (o)	70	(3)
			Xenopus laevis (x)	62	(6)
NaDC3	Dicarboxylates	Kidney	Human	46	(108)
SLC13A3	K_m succinate 20 μM	(basolateral	Rat	47	(17; 40)
		membranes),	Mouse	46	(75)
		brain, liver,	*Xenopus laevis*	48	(67)
		placenta	Flounder (f)	44	(101)
NaS1	Sulfate	Kidney,	Human	44	(49)
SLC13A1	K_m sulfate 0.4 mM	intestine	Rat	43	(60)
			Mouse	42	(9)
			Eel	39	(65)
NaS2	Sulfate	Placenta,	Human	41	(27; 61)
SLC13A4	K_m sulfate 0.4 mM	endothelial			
		venules, testis,			
		heart, liver			
NaCT	Citrate	Liver, brain,	Human	54	(34)
SLC13A5	K_m citarate 0.6 mM,	testis	Rat	50	(35)
	dicarboxylates		Mouse	50	(33)

[1] The percentage of amino acid sequence identity to mouse NaDC1.

[2] K_m values are for human.

THE LOW-AFFINITY Na^+/DICARBOXYLATE COTRANSPORTER, NaDC1

Isolation of the NaDC1 cDNA

The first cDNA of NaDC1 designated rabbit NaDC1 (rbNaDC1) was isolated from rabbit kidney by the expression cloning method using *Xenopus laevis* oocytes (72). Since then, NaDC1 orthologs have been cloned from various species. The human NaDC1 (hNaDC1) was also cloned from kidney. The gene is found on chromosome 17 p11.1-q11.1 (57; 69), and the intron-exon boundaries are identical to those of mouse NaDC1 (mNaDC1) when the sequence of chromosome 11 of mNaDC1 was mapped on those of human chromosome 17. The amino acid sequence of hNaDC1 is 76% identical to mNaDC1. The mNaDC1 was isolated from kidney, and the gene Slc13a2 is localized on chromosome 11. The gene is about 25 kb and includes 12 exons. The amino acid sequence of mNaDC1 is 74% identical to rbNaDC1. The cDNA encoding rat NaDC1 (rNaDC1) was screened from a rat kidney cDNA library, and the amino acid sequence of rNaDC1 is 92% identical to mNaDC1 (18; 94). The NaDC1 transporter has also been isolated from amphibian intestine, *Xenopus laevis*. The transporter was initially named xNaDC2 due to its unique cation specificity. The xNaDC2 transporter shows uptake activity for succinate in the presence of either Na^+ or Li^+. However, the amino acid sequence of xNaDC2 is similar to other NaDC1 orthologs, 62% to mNaDC1. Therefore, recently xNaDC2 has been renamed xNaDC1 (74).

Functional characterization of NaDC1 and substrate specificity

Functional characterization of NaDC1 has been performed mostly in *Xenopus* oocytes by either radiotracer uptake assays or the use of two-electrode voltage clamp (TEVC). In the radiotracer assays, the Michaelis-Menten constant (K_m) for succinate in all of NaDC1 orthologs is between 0.3 and 1 mM (74). The half-saturation constant for sodium varies between 10 and 50 mM, and a Hill coefficient for sodium- coupled transport is between 2 and 3 (3; 6; 72; 85). This is consistent with a stoichiometry in

which three sodium ions are coupled to the transport of a divalent dicarboxylate, suggesting that the transport process mediated by NaDC1 is electrogenic. Despite the fact that there are differences in substrate specificity between the species, NaDC1 generally transports divalent dicarboxylates such as succinate, fumarate, and the divalent form of citrate, citrate^{2-} (Figure 1.2). A preferred conformation of four carbon dicarboxylates appears to be *trans* configuration, evidenced by the inhibition of succinate uptake by *trans* configuration dicarboxylates in purified brush border membrane vesicles (112). Also, computational analysis of conformers for succinate has predicted that a planar and *trans* configuration is most stable in aqueous solutions (66). Currently, there is no information for actual conformations of dicarboxylates at the substrate binding site of NaDCs.

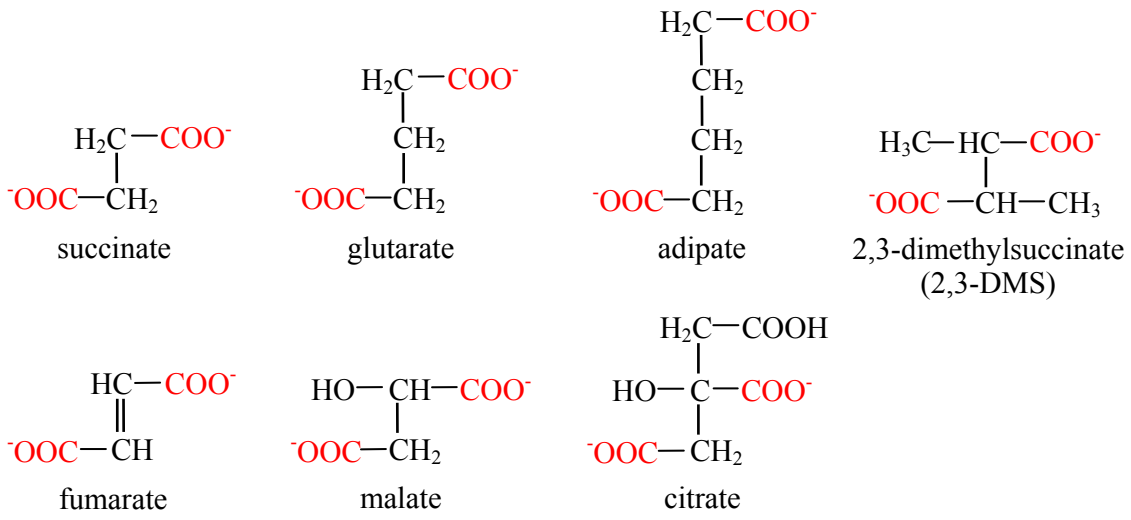

Figure 1.2 Substrates of the Na$^+$/dicarboxylate cotransporters. Divalent form (red) of di- and tricarboxylates such as citric acid cycle intermediates are preferred substrates of NaDCs.

Substrate specificity for each ortholog has been studied by inhibition of radiotracer uptake. For example, succinate and fumarate show similar inhibition of ^{3}H-succinate uptake in all tested NaDC1 transporters (3; 6; 72; 85; 94). On the other hand, in mNaDC1, 2.2-dimethylsuccinate (DMS) shows about 85% inhibition of ^{3}H-siccunate

uptake, whereas rbNaDC1exhibits 20% inhibition by 2,3-DMS (72; 85). Therefore, the difference in substrate specificity between mouse and rabbit NaDC1 transporters can be used to obtain further structural and functional information, especially TM and amino acid residues determining different substrate specificity.

Using the TEVC technique, functional characterization of NaDC1 was carried out in mammalian NaDC1 transporters (18; 76; 85; 94; 117). The NaDC1 mediated dicarboxylate transport is electrogenic. Also, this dicarboxylate transport is accompanied by water influx in the absence of osmotic gradient (62). The stoichiometry for transport of a divalent dicarboxylate, sodium, and water molecule is 1 dicarboxylate: 3 sodium ions: 182 water molecules (62). The half-saturation constant ($K_{0.5}$) for succinate in rabbit and mouse NaDC1 transporters are approximately 100 and 200 μM, respectively, whereas rNaDC1 shows a lower $K_{0.5}^{succinate}$ of about 25 μM (17; 76; 94). The hNaDC1 is different from mNaDC1 and rbNaDC1 by showing at least 5-fold higher $K_{0.5}^{succinate}$ (117). The half-saturation constant for sodium ($K_{0.5}^{sodium}$) and the apparent Hill coefficient are similar to those detected in the radiotracer assays (72; 76). By measuring net substrate-induced inward currents in the steady states, substrate specificity of the NaDC1 orthologs is consistent with the results in radiotracer assay. For example, fumarate induces inward currents as large as succinate does in both mouse and rabbit NaDC1 transporters. However, 2,2-DMS-dependent currents in mNaDC1 are about 60% of succinate-induced currents, whereas rbNaDC1 exhibits only 5% of succinate-evoked currents with 2,3-DMS (76; 85). Since succinate- and 2,2- or 2,3-DMS-induced currents were measured in the same oocytes expressing either mNaDC1 or rbNaDC1 to calculate the ratio, the difference in expression of both wild-type transporters can be negligible as the ratios are compared. Furthermore, α-ketoglutarate-evoked currents were examined in both transporters. However, the difference in α-ketoglutarate-induced currents between mNaDC1 and rbNaDC1 is less than that in DMS-dependent currents since the concentration of the substrate is ten-fold higher in the study of rbNaDC1 (76; 85). Therefore, in this dissertation, I investigated differences in substrate specificity between

mouse and rabbit NaDC1 transporters using dicarboxylates that have been tested in different experimental conditions using either radiotracer assays or TEVC.

Cation selectivity

The transport of dicarboxylates by NaDC1 is highly specific for sodium ions. Lithium can replace sodium partially. When sodium was replaced by lithium, succinate-dependent inward currents were approximately 20% of those measured in sodium, and the K_m for succinate in lithium is 15-fold higher than in sodium at -50 mV (76). The half-saturation constant and the apparent Hill coefficient for lithium, $K_{0.5}^{lithium}$ and n_{Li}, respectively, in xNaDC1 are similar to those for sodium by about 50 mM and 1.3, respectively. Lithium activated dicarboxylate transport occurs in rabbit, mouse, opossum, and *Xenopus* NaDC1 transporters, whereas human and rat NaDC1 transporters do not support succinate transport in the presence of lithium (3; 70; 85). Another role of lithium in NaDC1 mediated transport is to act as an inhibitor of succinate transport by competition with sodium for the same cation binding site. At 2.5 mM lithium in the presence of 97.5 mM sodium, succinate uptake is inhibited about 60% in rbNaDC1 (81). Therefore, high concentration of lithium can substitute sodium partially in terms of succinate transport in rbNaDC1, and low concentration of lithium inhibits succinate transport by competing with sodium for the same cation binding site. This inhibitory effect of lithium is also seen in rNaDC1 and oNaDC1 but not hNaDC1, mNaDC1, or xNaDC1 (3; 70; 85).

Voltage-dependent steady state kinetics

At a saturating sodium concentration, 100 mM, the $K_{0.5}^{succinate}$ is relatively independent of the membrane potential in the range from -150 and -50 mV, and increases nonlinearly at more positive membrane potentials than -50mV (76; 117). This finding indicates that succinate binding to NaDC1 is voltage-dependent. The $I_{max}^{succinate}$ increases linearly with hyperpolarization of the membrane. Nevertheless, rNaDC1 was reported to

have a different voltage-dependence of $K_{0.5}^{citrate}$ (17). The $K_{0.5}^{citrate}$ in rNaDC1 shows a slope which linearly decreases at voltages between -160 and -80 mV, and at potential more positive than -80 mV, The $K_{0.5}^{citrate}$ is independent of the membrane potential. The voltage-dependence of substrate binding in rNaDC1 differs from that of other NaDC1 orthologs.

Tissue distribution of NaDC1

The tissue distribution of NaDC1 is summarized in Table 1.1. By Northern blot analysis using the full-length rbNaDC1 cDNA as a probe, positive signals of rbNaDC1 mRNA are detected in the small intestine, kidney, and liver at the size of 2.8 kb after an overnight exposure (72). However, after a 7-day exposure, the mRNA at the same size is also found in lung and adrenal at the lower level. The similar expression pattern of NaDC1 transcripts is seen in other species such as mouse, human, and *Xenopus laevis* (6; 69; 85). Unlike mammalian NaDC1, *Xenopus* NaDC1 mRNA is only detected in intestine (6). The transcripts of rNaDC1 is observed in the small intestine, large intestines and kidney in the order of abundance, with the size of 2.4 kb (94). Moreover, the expression of rNaDC1 mRNA is detected in enterocytes lining in intestine, bronchiole and alveolar epithelium in lung, liver, and epididymis by *in situ* hybridization (18). The expression of oNaDC1 mRNA is observed in the opossum kidney cell line using Northern blot analysis (3).

Immunohistochemistry of rNaDC1 provides more detailed localization of rNaDC1 in kidney. Employing a polyclonal anti-rNaDC1 antibody to stain rat kidney sections, positive staining is found in the outer stripe of the outer medulla and in cortex, suggesting that the expression of rNaDC1 is exclusively in the renal proximal tubule S2 and S3 segments (94). At the high magnification, the protein is only detected on the apical membranes of the renal epithelium and not on the basolateral membranes.

Na^+-coupled transport mechanism of NaDC1

The NaDC1 mediated substrate transport relies on the ordered binding mechanism of three sodium ions and one dicarboxylate molecule. This assumption was made due to two types of currents measured in hNaDC1: succinate-dependent currents and cation-dependent succinate-independent currents (117). This result points to a potential 10-stage transport model (Figure 1.3). Three sodium ions bind to the protein prior to the binding of a single divalent dicarboxylate, which triggers the first conformational change and increases the affinity for substrate. After the cation-induced conformational change, substrate binding occurs, and a fully loaded carrier translocates the substrate and cations to the inside of the cell. The order of releasing the substrate and cations is not known. Then, an empty carrier reorients to face the outside the cell to start a new transport cycle. Therefore, one transport cycle leaves one positive net charge inside the cell, indicating that transport reaction mediated by NaDC1 is electrogenic.

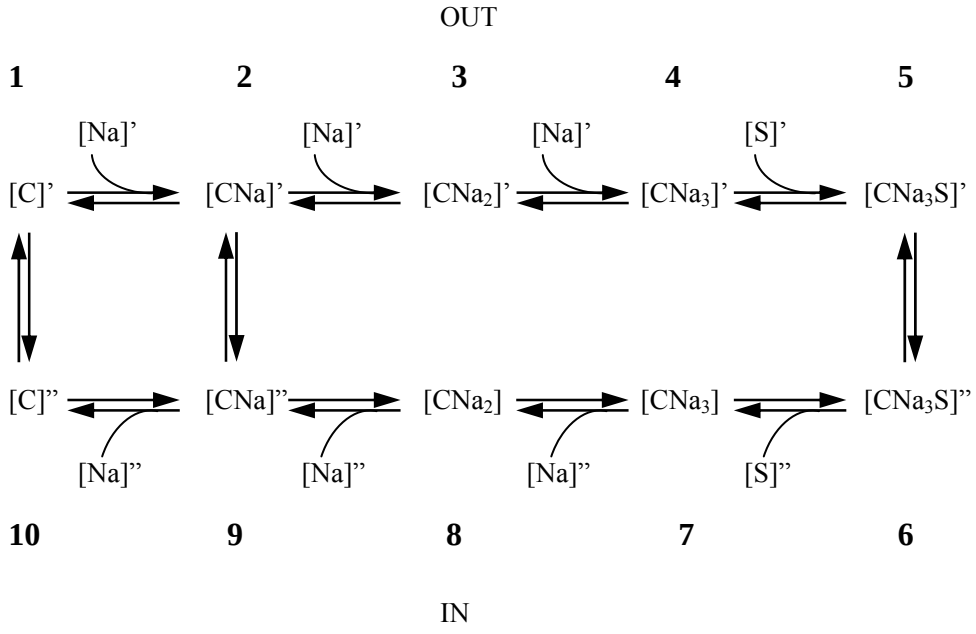

Figure 1.3 Transport model for Na^+/dicarboxylate cotransporter (modified from (117)). C represents a carrier, and S represents a substrate. ' refers to extracellular, and " refers to intracellular. The number represents each transport state.

Two types of currents are measured in NaDC1 at different stages of the transport cycle. The substrate-dependent currents are evoked by translocation of fully loaded carrier proteins with three sodium ions and one divalent dicarboxylate (Figure 1.3, states 5 and 6). The cation-dependent substrate-independent currents called cation leak currents are activated by translocation of cation-loaded carrier proteins, uncoupling with a substrate (Figure 1.3, states 2 and 9). For comparison, the leak currents in NaDCs are smaller than the substrate-induced currents (117). This leak current is an electrophysiological property of NaDC1 and not all membrane transporters exhibit the leak currents. Within NaDCs, rat (r) and human (h) NaDC1 transporters have been reported for substrate-uncoupled leak currents (18; 117). Similar leak currents have also been identified in other families of membrane transport proteins such as Na^+/glucose cotransporter, Na^+/phosphate cotransporter, and thyroid Na^+/I^- symporters (21; 25; 88).

Secondary structure model of NaDC1

The initial secondary structure model of NaDC1 was proposed when the rbNaDC1 transporter was isolated, showing 8 putative transmembrane helices (TMs) with intracellular N- and C- termini (72). This structure model is based on Kyte and Doolittle hydropathy analysis (47) of rbNaDC1 amino acid sequence, which was subsequently revised by different topology algorithm developed by Mohana Rao and Argos (64). As shown in Figure 1.4, the amended secondary structure model of rbNaDC1contains 11 putative TMs, and mutagenesis on two consensus *N*-glycosylation sites, Asn-160 and Asn-578, revealed that Asn-578 located near the C-terminal tail is glycosylated in rbNaDC1. This consensus site is conserved in all members of the SLC13 family (51; 80). This finding points to an extracellular location of the C-terminus of rbNaDC1 (Figure 1.4). Furthermore, positive immunofluorescence in cells expressing rbNaDC1 and Flag-tagged NaDC1 at the amino terminus was observed only after permeabilization of the plasma membrane (120). This result shows that the N-terminus and a part of hydrophilic loop 4 situated between Ser-164 and Ser-233 are inside the cell (Figure 1.4). All together, the current working secondary structure model of NaDC1

contains 11 putative TMs with the intracellular N-terminus and loop 4 and the extracellular C-terminus. The studies in Aims 1 and 2 in this dissertation used this latest published secondary structure model of the NaDC1 transporter.

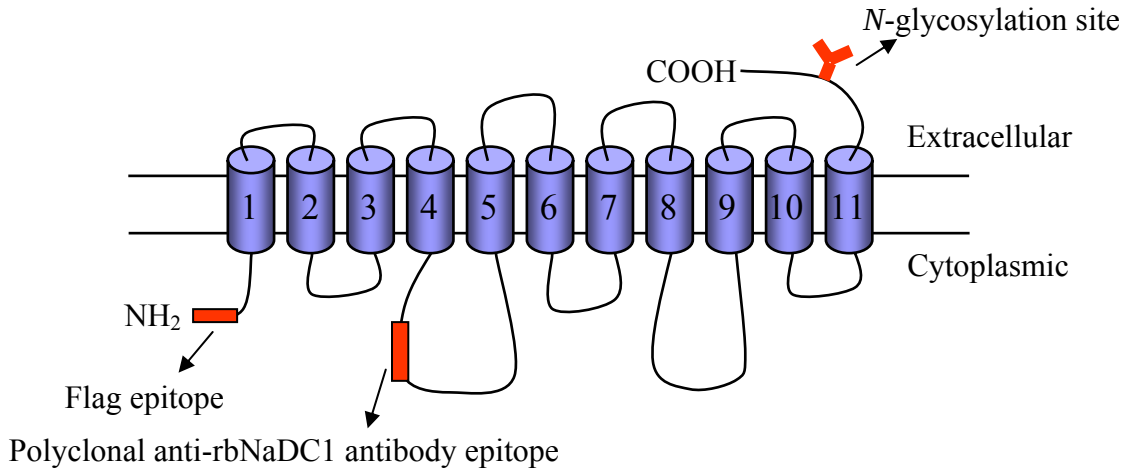

Figure 1.4 Secondary structure model of NaDC1. The current secondary structure model of NaDC1 contains 11 putative TMs (cylinders) with the intracellular N-terminus and hydrophilic loop 4 and the extracellular C-terminus.

Structure-function studies of NaDC1

The relationship between structure and function in rbNaDC1 has been intensively studied by Pajor's group in the last decade. The studies employed construction of chimeric NaDC1 transporters and the site-directed mutagenesis.

Chimeras between rbNaDC1 and the Na^+/sulfate cotransporter

The Na^+/sulfate cotransporter, NaS1, shows 43% identity to rbNaDC1 in amino acid sequence. The rbNaDC1-rNaS1 chimeras suggest that the substrate recognition site of NaDC1 and NaS1 appears to be located after Ser-141 in the C-terminus of the protein. However, the rbNaDC1-rNaS1 chimera has increased substrate affinity and altered cation

selectivity and sensitivity to inhibitor. Therefore, the amino acid residues in the first four TMs may be involved in determination of substrate affinity and cation selectivity (83).

Chimeras between rbNaDC1 and hNaDC1

Another study using chimeric NaDC1 transporters was performed between rabbit and human NaDC1, which share 78% sequence identity but also exhibit functional differences in terms of citrate kinetics (38). The rbNaDC1 transporter has higher affinity for citrate than hNaDC1. The study suggests that TM 7, 10, and 11 including their associated loops appear to contain at least one of the cation binding sites located close to the substrate binding site. In a crystal structure of the Na^+/Cl^--dependent leucine transporter ($LeuT_{Aa}$), one of sodium ions interacts with the carboxy oxygen of the substrate, leucine, by an ionic interaction (116). Therefore, it is possible that in NaDC1, at least one of three sodium ions might interact with the carboxy oxygen of a bound succinate in the binding pocket.

The site-directed mutagenesis on charged amino acids

Acidic amino acid residues in rbNaDCl at Asp-373 and Glu-475 in TM 8 and 9, respectively, may be involved in the transport activity since mutations at these positions change the affinity for both succinate and sodium (28). Additionally, charge neutralization of two conserved cationic amino acids, Lys-84 and Arg-349, causes decreases in activity and changes in K_m for succinate, suggesting that these residues have roles in substrate binding (77). Some residues are not necessary for transport function of NaDC1 but rather may be involved in expression and stability in the membrane. Mutagenesis of all 11 histidine residues in rbNaDC1 revealed that mutation at position 106 shows decreased uptake of succinate. However, this change is due to a decrease in V_{max} without a significant change in K_m for succinate. Also, transport activity corresponds to the abundance of cell surface expression of the H106A, H106R, H106D, and H106N mutants. Therefore, His-106 might be involved in protein expression rather

than function (84). The mechanism of protein expression regulation by His-106 remains unknown except the size of the residue at this position might be a key to control the expression of the NaDC1 proteins. Possible mechanism of decreased cell surface expression of the H106A and H106R mutants can be described by either a decrease in a trafficking rate of the proteins to the plasma membrane or an increased rate in membrane protein degradation, or both. Mutations of multiple cysteine residues may alter the protein shape and configuration, resulting in changes in membrane trafficking or stability of the mutants in the membranes (78).

Cysteine-scanning mutagenesis in TM 7-8 and TM 9-10

Cysteine-scanning mutagenesis in putative TM 9 of rbNaDC1 had identified that the transport activity of cysteine substituted mutants at Ser-478, Ala-480, Ala-481, and Thr-482 is inhibited by a membrane-impermeant cysteine specific reagent [2-(trimethylammonium)ethyl]-methanethiosulfonate (MTSET) and protected by substrate. Subsequent cysteine-scanning mutagenesis in TM 10 has found that cysteine mutation at Thr-483, Thr-484, Leu-485, Leu-487, Ile-489, and Met-493 makes the mutants sensitive to inhibition by MTSET, and depending on the conformational stages of NaDC1, the accessibility of MTSET changes. Therefore, TM 9-10 appear to be involved in a transducing conformational change in the cation-binding sites to the substrate-binding, and it is also suggested that TM 9-10 may form part of the permeation pathway through the protein for substrate and cation (71; 79). The same experimental approach was employed in the region of TM 7-8, indicating that the accessibility of Arg-349 and Asp-373 from extracellular medium alters along with the conformational stages in the transport cycle of NaDC1 (118).

Regulation of NaDC1

At physiological pH, 93% of citrate in blood is a trivalent form, $citrate^{3-}$, which is poorly transported by NaDCs (34; 72). The remaining 7% is divalent citrate, $citrate^{2-}$, which is a preferred substrate of NaDCs. Therefore, transport of citrate mediated by NaDCs is stimulated at acidic pH due to increased population of the divalent form of citrate in urine filtrate (81; 113). Also, in abnormal physiological conditions such as chronic metabolic acidosis, K^+ deficiency, and starvation, elevated citrate uptake was reported due to increased abundance of NaDC1 mRNA and protein (4; 37; 98; 111). Regulation of the amount of $citrate^{2-}$ in urine and expression of NaDC1 transcripts and protein is implicated in calcium kidney stone development since citrate acts as an endogenous chelator (30; 86).

In addition to the long-term regulatory conditions described above, short-term acute regulation of NaDC1 has been studied using protein kinases. The activity of NaDC1 is inhibited by protein kinase C (PKC) activators to great extent, which partially corresponds to decreased cell surface expression of the transporter (82). Therefore, PKC appears to regulate NaDC1 through endocytosis pathway. More recent studies for regulatory mechanisms of NaDC1 in kidney have identified that the Na^+/H^+ exchanger regulating factor (NHERF-2), a key molecule to regulate the trafficking of the Na^+/H^+ exchanger (NHE) and Na^+/HCO_3^- cotransporter into the plasma membrane (97; 109; 119), stimulates NaDC1 mediated currents. The serum and glucocorticoid inducible kinases (SGK1 and SGK3) and protein kinase B (PKB) which is known to govern the trafficking of glucose transporters (16; 48; 100) also increase substrate-induced currents in NaDC1 (11; 106). This functional activation is due to an increase in the maximum velocity of substrate-induced currents and not a change in substrate affinity, indicating that NHERF-2 and the kinases are involved in the functional regulation of NaDC1 by elevating abundance of the protein in the plasma membrane.

THE HIGH-AFFINITY Na^+/DICARBOXYLATE COTRANSPORTER, NaDC3

Isolation and functional characterization of NaDC3

To date, there are five NaDC3 orthologs from different species (Table 1.1). In general, the amino acid sequence of the NaDC3 transporters is about 45% identical to NaDC1, with a secondary structure model that is similar to NaDC1 (17; 40; 75; 101; 108). The gene of human NaDC3 (hNaDC3), designated as SLC13A3 in the human gene nomenclature, is localized on chromosome 20 q12-13.1 and includes 13 exons and 12 introns (108).

The affinity for substrate is different between these transporters. The K_m for succinate in NaDC3 is between 2 and 180 μM in radiotracer assay, which is notably smaller than that of NaDC1, 300-1000 μM (40; 75; 101; 108). The half-saturation constant for sodium is between 20 and 60 mM. The relationship between succinate uptake or succinate-induced currents and the sodium concentration is sigmoidal, suggesting that more than one sodium ions are involved in transport of one dicarboxylate. The calculated Hill coefficient is between 2 and 3, which indicates at least 2 sodium ions couple to one dicarboxylate transport (40; 75; 101; 108). The NaDC3 transporters are electrogenic transporters like NaDC1 and characterized by the two-electrode voltage clamp (TEVC) (14; 17; 108). The cation selectivity of the NaDC3 orthologs is consistent with that of NaDC1 with exception of hNaDC3 (14; 17; 75; 108). For example, the mouse NaDC1 and NaDC3 transporters show partial succinate uptake when sodium is replaced with lithium, and there is no inhibition with 5mM lithium in the presence of 95 mM sodium. However, succinate-induced currents in hNaDC3 are inhibited by 5 mM lithium in the presence of 70 mM sodium and 25 mM choline chloride about 40%, and the inhibition is lithium concentration dependent (108). By contrast, in hNaDC1, lithium has no apparent effect on succinate transport (69).

The substrate specificity of NaDC3 generally overlaps with that of NaDC1. However, a major difference can be found in the ability to handle long or bulky dicarboxylates such as glutarate and 2,3-dimethylsuccinate (2,3-DMS) (Figure 1.2). These substrates can be transported efficiently by NaDC3 (40; 75; 101; 108), whereas NaDC1 transports them with low affinity and activity (72; 81). This implies that longer and bulkier dicarboxylates are preferable substrates for NaDC3 but not for NaDC1. The mNaDC1, however, is an exception to the general substrate specificity differences between NaDC1 and NaDC3. The mNaDC1 transporter exhibits some properties in common with the NaDC3 transporter, which includes transport activity of glutarate and 2,2-DMS (85).

Tissue distribution of NaDC3

Northern blot analysis using mouse and rat NaDC3 cDNA as a probe shows positive signals in kidney, liver, and brain (17; 40; 75). As a result of RT-PCR to detect NaDC3 mRNA transcripts, positive reactions were also seen choroids plexus and placenta (40; 75). The expression of rNaDC3 mRNA was observed in kidney, liver, and brain by *in situ* hybridization, identifying that renal epithelium in the S3 segment, hepatocytes surrounding the central vein, and cells of meningeal layers express rNaDC3 transcripts (17). Immunohistochemistry with renal sections of winter flounder (f) using anti-fNaDC3 antibody determined localization of fNaDC3 at the basolateral membrane of renal epithelial cells, and positive stain was not found at other segments of nephron (31).

PHYSIOLOGICAL SIGNIFICANCE OF NaDCs

The potential physiological roles of NaDCs are summarized in Table 1.2 and illustrated in Figure 1.5 using a renal epithelial cell diagram. Since majority of substrates of NaDCs are the citric acid cycle intermediates such as succinate and citrate, the function of NaDCs is primarily involved in cellular metabolism by absorbing di- and tricarboxylates at small intestine and kidney. Moreover, proper citrate uptake in renal

proximal epithelium regulates the concentration of urinary citrate, may resulting in prevention of kidney stone formation since citrate acts as an endogenous chelator for calcium. Statistically, 50% of kidney stone patients experienced metabolic acidosis, leading to hypocitraturia (86; 87). In addition, metabolic acidosis increases the expression of the NaDC1 mRNA and protein (4; 37) and the population of divalent form of citrate, citrate^{2-}, which can actively be transported by NaDC1. Therefore, upregulation of NaDC1 expression at the transcription and translation levels and an increased concentration of citrate^{2-} in urine in metabolic acidosis may elevate the uptake of urinary citrate, leading to hypocitraturia in kidney stone patients. In renal proximal epithelial cells, the function of NaDCs coordinates with that of dicarboxylate/organic anion exchangers such as organic anion transporter (OAT)1 and OAT3 expressed on the basolateral membrane. Transported dicarboxylates become a substrate for the dicarboxylate/organic anion exchanger, involved in uptake of organ anions such as drugs and toxins from the blood circulation to the cells (20). Eventually, the organic anions are eliminated from the cells by OAT4 or facilitated diffusion carriers on the apical membrane (91; 104).

Table 1.2 Potential physiological roles of the Na^+/dicarboxylate cotransporters

Physiological roles	Function of NaDCs	Organ	Protein
Metabolism	Absorption of di- and tricarboxylates	Small intestine Kidney	NaDC1 NaDC3
Prevention of kidney stone development	Uptake of citrate, regulating urinary citrate concentration	Kidney	NaDC1
Organic anion secretion (drugs, toxins)	Uptake of dicarboxylates, providing substrates to the dicarboxylate/organic anion exchanger	Kidney	NaDC1 NaDC3
Regulation of glutamate synthesis	Uptake of α-ketoglutrate in hepatocytes, providing a substrate to glutamate synthetase	Liver	NaDC3
Replenishing neurotransmitter pool	Uptake of α-ketoglutarate at synapse	Brain	NaDC3

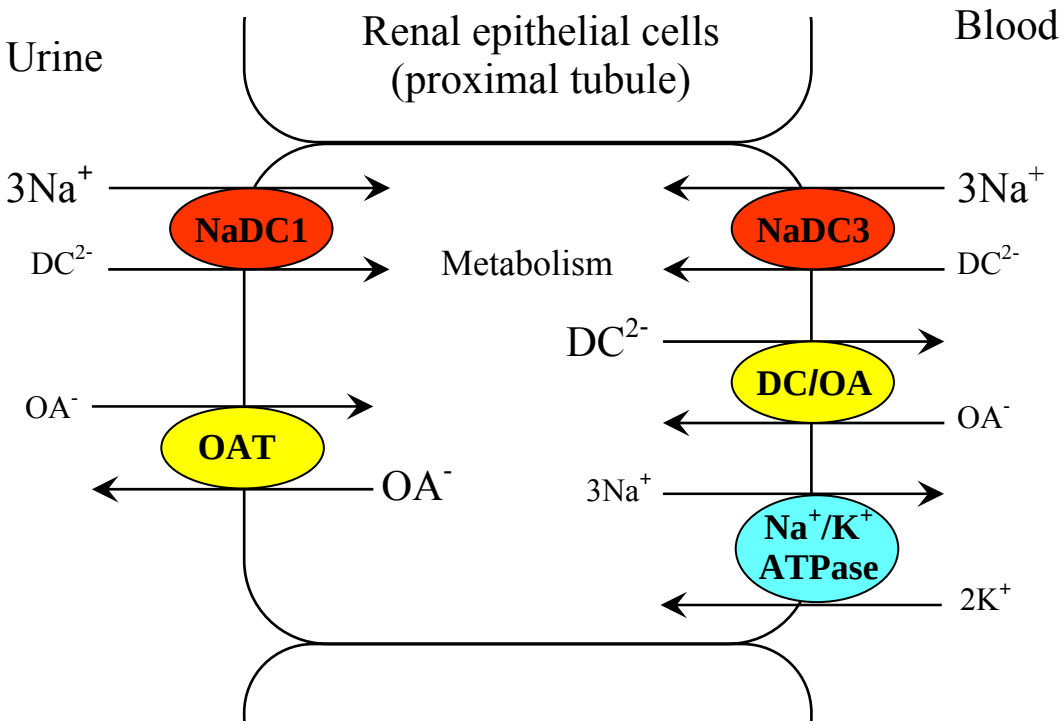

Figure 1.5 Schematic representation of active dicarboxylate transport in renal proximal tubules. The low-affinity Na^+/dicarboxylate cotransporter, NaDC1, is expressed on the apical membrane of renal epithelial cells, and the high-affinity Na^+/dicarboxylate cotransporter, NaDC3, is expressed on the basolateral membrane. Using electrochemical gradient of sodium, NaDC1 and NaDC3 transport one divalent dicarboxylate (DC^{2-}) inside the cell, coupling with three sodium ions. To maintain electrochemical gradient of sodium which is a driving force of NaDCs, the function of Na^+/K^+ -ATPase is essential. Majority of intracellular dicarboxylates are utilized for metabolism. Additionally, the intracellular dicarboxylates are involved in uptake of organic anion (OA^-), drugs and toxins, from the blood circulation, mediated by the dicarboxylate/organic anion exchangers (DC/OA) such as organic anion transporter (OAT) 1 and 3 on the basolateral membrane. The intracellular OA^- is eventually secreted into urine by an exchanger, OAT4, or facilitated-diffusion carriers (not illustrated in the figure)

The NaDC3 transporter plays a role in liver and brain. Uptake of α-ketoglutarate in hepatocytes provides a substrate for glutamine synthetase, regulating glutamine synthesis (102; 122). Uptake of α-ketoglutarate, a neurotransmitter precursor, into the synaptic terminals by NaDC3 appears to contribute to replenishing neurotransmitter and citric acid cycle pools in GABAergic and glutamatergic nerves (95; 96).

Discovery of the Na^+/dicarboxylate cotransporter homolog from *Drosophila* brought a novel insight of the cotransporter to human health (92). The NaDC1 homolog *Indy* (I'm not dead yet) from *Drosophila*, encoding a Na^+-independent succinate transporter, is expressed in midgut which is analogous to the small intestine, and in the fat body and oenocyte which are important for metabolism. Disruptions in one copy of the gene (heterozygotes), which decreases the transport activity, results in doubling of life span of the mutant flies. This result suggests that the low activity of *Indy* affects the metabolism of the flies, leading to longevity. NaDC1 homologs have also been isolated from *Caenorhabditis elegans*, ceNAC1, ceNAC2, and ceNAC3 (23; 24). The ceNAC1 is a low affinity Na^+-dependent dicarboxylate transporter, and the ceNAC2 and ceNAC3 are classified as high affinity Na^+-dependent dicarboxylate transporters. These transporters are expressed in the intestinal tract where not only the digestion and absorption of nutrients but also the storage of energy takes place. The knockdown of the function of ceNAC2 expands the lifespan by about 15%. This result suggests that decrease in the activity of ceNAC2 changes the metabolic state, resulting in lifespan elongation. These functional impairments may be analogous to caloric restriction in human, which suggests that NaDCs might be involved in aging and longevity.

CRYSTALLOGRAPHY IN MEMBRANE TRANSPORT PROTEINS

Despite a great increase in the number of atomic structures of soluble proteins, crystallizing transporters as well as other membrane proteins has been found to be extremely challenging for several reasons. First, membrane proteins are amphipathic,

which incorporate hydrophobic areas in contact with membrane phospholipids and hydrophilic areas in contact with intracellular and extracellular spaces, and aqueous pores in the proteins (68). Therefore, purifying a membrane protein out of the biological lipid bilayer often makes the protein non-functional. Second, in order to obtain sufficient material for crystallization, membrane proteins need to be overexpressed because their abundance is typically low. However, overexpression has proven to be very difficult by the fact that a few of mammalian membrane proteins have been expressed functionally in bacteria, the expression system used to acquire large quantities of proteins (105). Consequently, bacterial membrane proteins are still the primary source for structural studies. For example, recent success in high-resolution crystal structures of membrane carrier proteins such as the lactose permease (LacY) and glycerol-3-phosphate transporter (GlpT) and Na^+/Cl^--dependent leucine transporter ($LeuT_{Aa}$) are from either *Escherichia coli* or *Aquifex aeolicus* (1; 32; 116). Lastly, the conformational flexibility of membrane transport proteins also makes crystallization difficult. To overcome this problem, the application of inhibitors has been proposed as a potential strategy to rigidify their structures for crystallization although this is not applicable to all of membrane proteins (105). The principle of this approach has been employed in the studies of the LacY protein by creating the LacY mutant locked in the inward-facing conformation (1; 99).

Overall, in spite of a large number of amino acid sequences for membrane proteins, their structural information is very limited in terms of crystallography. Accordingly, the structural information of membrane proteins has largely relied on biochemical studies using the use of chimeras, site-directed mutagenesis, cysteine scanning, and cross-linking experiments to identify residues or domains responsible for their function. For example, chimeras constructed using electrogenic and electroneutral Na^+-coupled inorganic phosphate cotransporters, NaPi-IIa and NaPi-IIc, respectively, identified that the first six TMs were important for the electrogenicity of the transporter (5). In the Na^+-HCO_3^- cotransporter kNBC1 belonging to the SLC4 family, substitution of charged amino acids with neutral and oppositely charged residues resulted in the loss of ion transport activity (2). Also, this study provided the information for amino acid

residues constituting the potential ion selectivity filters in both inward- and outward-facing conformations. To test accessibility of amino acids and topology of membrane proteins, cysteine-scanning mutagenesis with chemical modification using methanethiosulfonate (MTS) reagents is a useful tool. Using a membrane permeable MTS reagent, MTSEA, the putative second intracellular loop of the serotonin transporter (SERT) was examined, suggesting that the loop is longer than predicted and may form α-helix (121). The cysteine substitutions can also be employed for cross-linking to measure the distance between the mutated cysteine residues using various lengths of cross-linkers. In the *Vibrio parahaemolyticus* Na^+/glucose cotransporter (vSGLT), two single cysteine mutations in the spilt N- and C-terminal halves of vSGLT were introduced. The double cysteine substituted split vSGLT induced the cross-linking between these cysteine residues in the presence of a sulfhydryl-reactive cross-linker. The cross-linked split vSGLT reserves glucose transport activity as well as the wild-type transporter. This result suggests that these cysteine residue are located in close proximity during glucose transport reaction (115). These biochemical studies also provide the information about functional properties of transporters such as their kinetics which can not be obtained from crystal structures. Therefore, both crystallography and biochemical experiments are necessary for better understanding of the nature of integral membrane proteins.

OVERVIEW

This dissertation is centered on both NaDC1 and NaDC3 from two different experimental interests: the identification of transmembrane helices (TM) and amino acid residues responsible for different substrate specificity between the mouse and rabbit NaDC1 transporters, and functional characterization of *Xenopus laevis* NaDC3 (xNaDC3) using the two-electrode voltage clamp (TEVC). In the initial functional characterization of the NaDC1 orthologs using radiotracer assay and TEVC, distinct differences in substrate specificity were observed between mouse and rabbit NaDC1 transporters, especially handling of longer and bulkier dicarboxylates than succinate such as 2,3-dimethylsuccinate (2,3-DMS) and glutarate (Figure 1.2). Nevertheless, there is no

information for transmembrane helices or amino acid residues that determine the differences in substrate selectivity between these two transporters. Therefore, the studies in Chapters 2 and 3 in this dissertation investigated TM and amino acids responsible for determining differences in substrate specificity between mNaDC1 and rbNaDC1. The other focus of the dissertation is to study electrophysiological properties of xNaDC3 using TEVC. The initial functional characterization of xNaDC3 by radiotracer uptake revealed that xNaDC3 has a unique lithium dependence, which was seen in lithium activation of succinate transport. Therefore, I examined electrophysiological properties of xNaDC3 using TEVC in the presence of sodium and lithium.

AIMS OF STUDIES IN THIS DISSERTATION

This dissertation focuses on two isoforms of the Na^+/dicarboxylate cotransporters (NaDCs): the low affinity Na^+/dicarboxylate cotransporter (NaDC1) and the high affinity Na^+/dicarboxylate cotransporter (NaDC3). The studies in Aims 1 and 2 are to identify transmembrane helices (TM) and amino acid residues involved in determination of different substrate specificity between the mouse and rabbit NaDC1 transporters. The studies in Aim 3 use the two-electrode voltage clamp (TEVC) to perform functional characterization of *Xenopus laevis* NaDC3 (xNaDC3).

Aim 1: To determine transmembrane helices and residues which determine differences in transport of glutarate between NaDC1 orthologs.

The experimental approach for this Aim was to use chimeras between the NaDC1 orthologs which show differences in substrate specificity in order to identify TM involved in different substrate specificity. The mouse (m) and rabbit (rb) NaDC1 transporters exhibit a difference in handling of long and bulky dicarboxylates such as α-ketoglutarate and dimethylsuccinate. Therefore, in the studies in Aim 1, a series of chimeric NaDC1 transporters was constructed between mNaDC1 and rbNaDC1, and TM responsible for glutarate-evoked currents were identified using the two-electrode voltage clamp. The studies were extended to site-directed mutagenesis in the region contributing most to glutarate-dependent currents and determined a residue which affects the $K_{0.5}^{glutarate}$ but not $K_{0.5}^{succinate}$. Furthermore, the studies adapted the idea for the Transport Specificity Ratio (TSR), proposed by King (41), and TSR analysis of the chimeras provided evidence that TM 3 and TM 4 of mNaDC1 interact in the transition state complex during glutarate transport.

Aim 2: To identify domains and amino acid residues involved in different ability to transport adipate by NaDC1 orthologs.

The studies in this Aim employed the same experimental approach as Aim 1. Adipate contains six carbons and is one carbon longer than glutarate. Therefore, to identify TM responsible for adipate-evoked currents, the studies in Aim 2 used some of the chimeras constructed in Aim 1. The chimera studies were extended to mutagenesis in the region which contributes most to adipate-induced currents. Because of high background of ^{14}C-adipate, TSR analysis was not possible in the study. Aim 1 and 2 in this dissertation were to identify domains and residues responsible for transport of longer dicarboxylates such as glutarate and adipate. The results of these studies should contribute to a better understanding of the structural and functional information of NaDC1 as well as NaDC1 homologs in the SLC13 gene family.

Aim 3: To characterize the electrophysiological properties of the high affinity Na^+/dicarboxylate cotransporter, NaDC3, from *Xenopus laevis*.

The information for NaDCs in non-mammalian vertebrates is limited. Only two transporters, *Xenopus* NaDC1 and winter flounder NaDC3, have been studied (6; 101). Therefore, the studies in this Aim were carried out using the TEVC to examine electrophysiological properties of the recently identified high affinity Na^+/dicarboxylate cotransporter found in *Xenopus laevis*, xNaDC3. Results in this study should provide electrophysiological information for non-mammalian vertebrates of NaDCs.

CHAPTER 2: TRANSMEMBRANE HELICES 3 AND 4 ARE INVOLVED IN SUBSTRATE RECOGNITION BY THE Na^+/DICARBOXYLATE COTRANSPORTER, NaDC1

(Studies in this chapter have been published and reproduced with permission from: Oshiro, N., King, S.C., and Pajor, A. M. Transmembrane helices 3 and 4 are involved in substrate recognition by the Na^+/dicarboxylate cotransporter, NaDC1 (2006) *Biochemistry 45*, 2302-2310. Copyright 2006 American Chemical Society.)

INTRODUCTION

The current secondary structure model of NaDC1 contains 11 transmembrane helices (TM) with an intracellular N-terminus and an extracellular C-terminus (80; 120). Residues involved in determining differences in substrate affinity and cation selectivity are found in the C-terminal half of the protein although the first four TMs also affect substrate binding affinity, sensitivity to inhibitors, and cation selectivity (38; 77; 83). NaDC1 generally prefers four-carbon dicarboxylate, such as succinate (76). However, mouse NaDC1 (mNaDC1) exhibits functional properties that differ from those of the rabbit or human NaDC1. Despite the amino acid sequence identity between the mNaDC1 and mNaDC3 transporters, substrate specificity of mNaDC1 resembles that of mNaDC3, including the ability to transport longer or bulkier dicarboxylates than succinate such as 2,2-dimethlysuccinate (2,2-DMS) (Table 1.1). For example, succinate transport was inhibited by 2,2-DMS in mNaDC1 about 85% and in mNaDC3 about 80%, whereas in rbNaDC1, the inhibition was 20% by 2,3-DMS (72; 75; 85). Under the two-electrode voltage clamp (TEVC), 1 mM of 2,2-DMS-induced currents were approximately 60% of succinate-dependent currents in mNaDC1 and about 80% with 0.5 mM 2,3-DMS in mNaDC3 (75; 85). On the other hand, rbNaDC1-expressing oocytes exhibited about 8% of succinate-induced currents with 10 mM 2,3-DMS.

To date, the amino acids or domains responsible for these functional differences between NaDC1 orthologs have not been identified. Therefore, I took advantage of a difference in substrate specificity between mNaDC1 and rbNaDC1 to identify residues and domains which are important for glutarate. I compared mouse and rabbit NaDC1, which have a high sequence identity of 74% but differences in handling of glutarate (Table 1.1 and Figure 2.1). The results of this study show that residues from multiple TMs are involved in glutarate transport, with TM 3 and 4 contributing most to the total glutarate-induced inward currents. Furthermore, I find evidence of functional interaction in the transition state between amino acids in TM 3 and TM 4.

METHODS

Nomenclature of chimeric and mutant transporters

The chimeric transporters constructed with mouse (m) NaDC1 (GenBank AF201903) and rabbit (rb) NaDC1 (GenBank U12186) are designated using the letters M (mouse) and R (rabbit) following the number of transmembrane helices (TM) that are contributed by mNaDC1 at the amino terminus. For example, 2MR contains TM 1-2 of mNaDC1 and the rest from rbNaDC1. The mutant transporters are named using the single letter amino acid code followed by the number of the position that was mutated. The second letter following the sequence number shows the amino acid substituted at that position. The numbering of amino acid sequence is based on the mNaDC1 sequence.

Site-directed mutagenesis

Restriction enzyme sites for preparing chimeras were introduced by silent mutagenesis into intracellular and extracellular loops of mNaDC1 and rbNaDC1. A few of the initial mutants in this study were made using the oligonucleotide-directed Kunkel method (45), but most of the mutants were made using the QuikChange site-directed mutagenesis kit (Stratagene) according to the manufacturer's directions. Briefly, the

parental double-stranded cDNA was heat denatured and annealed with both sense and anti-sense oligonucleotides containing the desired mutations. The parental cDNA was cut with *Dpn*I, and the undigested cDNA incorporating the mutations was transformed into the XL-1 blue strain of *Escherichia coli*. All of the mutants were verified by sequencing at the Protein Chemistry Laboratory of the University of Texas Medical Branch.

Construction of Chimeric Transporter cDNAs

Chimeric transporter cDNAs containing portions of mouse and rabbit NaDC1 cDNAs were constructed by subcloning using endogenous or introduced restriction enzyme sites. The junctions of the chimeras were located in loops outside of putative TMs. The numbering of the junctions is based on the mNaDC1 amino acid sequence, and the equivalent positions in rbNaDC1 were selected to avoid additional mutations in the chimeras. The 2MR chimera was constructed using an introduced *Hind*III site at amino acid position 74 in mNaDC1 and the endogenous *Hind*III site in rbNaDC1. The 4MR chimera was created by using the endogenous *Sac*I sites at position 177. For the 3MR and 6-10MR chimeras, junctions at amino acid 120 (*Ngo*MIV), 284 (*Avr*II), 341 (*Nru*I), 427 (*Nru*I), 489 (*Nde*I), and 518 (*Bsm*I), respectively, were made by introducing restriction enzyme sites. The junctions to construct TM 3 and TM 4 chimeras, R(M3) and R(M4), were the same as those for 2MR, 3MR, and 4MR. All of the chimeras were confirmed by sequencing at the Protein Chemistry Laboratory of the University of Texas Medical Branch.

***Xenopus* Oocyte Injections**

The cDNAs of wild-type, chimeras, and mutant NaDC1 were linearized at the *Xba*I site in the pSPORT1 vector and used as templates for *in vitro* transcription using the T7 mMessage mMachine kit (Ambion). The cRNA was stored at -80°C until use. Female *Xenopus laevis* were either purchased from Xenopus I or donated by Dr. Cheryl

Watson. Stage V and VI oocytes were dissected and treated with collagenase as described previously (72) or by using a modified protocol in which oocytes were incubated for 3 h with 2 mg/mL collagenase without the subsequent phosphate buffer treatment. The defolliculated oocytes were injected with 46-50 nL of cRNA the day after dissection and cultured at 18°C in Barth's medium supplemented with 5% heat-inactivated horse serum, 2.5 mM pyruvate, 100 μg/mL gentamycin sulfate, and either 50 μg/mL tetracycline or a mixture of 5 μg/mL ceftazidime (GlaxoSmithKline) and 100 units/mL penicillin-100 μg/mL streptomycin (Gibco). Experiments were done 3 to 6 days following injection. Culture vials and medium were changed daily.

Electrophysiology

Oocytes expressing each wild-type, chimera, and mutant NaDC1 transporter were used to measure substrate-induced inward currents using the two-electrode voltage clamp (TEVC) method as described previously (76; 117). The 100 ms test pulses were configured by the pClamp6 program (Axon instruments, Inc.) between +50 and -150 mV in decrements of 20 mV. The membrane potential was held at -50 mV between trials, and the average of three measurements was taken for every trial. The resistance of the electrode filled with 3 M KCl was less than 0.5 MΩ .

To obtain a basal current at the holding potential, oocytes were first equilibrated in choline buffer containing 100 mM choline chloride, 2 mM KCl, 1 mM $MgCl_2$, 1 mM $CaCl_2$, and 10 mM HEPES, pH adjusted to 7.5 with 1 M Tris. This was followed by sodium buffer containing 100 mM NaCl instead of choline chloride. The test solutions of 1 mM substrates in sodium buffer were then added, and the voltage pulse protocol was initiated. The substrate was washed away using choline buffer, and subsequent experiments were conducted after recovery of basal currents. Substrate-induced currents were calculated from the difference between steady-state currents in the presence and absence of substrate. The kinetic data were analyzed using SigmaPlot software (Jandel

Scientific). The steady-state substrate-induced currents were fitted to the Michaelis-Menten equation:

$$I = I_{max} \frac{[S]}{K_{0.5} + [S]} \qquad [Eqn.1]$$

where I is the current, I_{max} is the maximum current at saturating substrate concentration, [S] is the substrate concentration, and $K_{0.5}$ is the substrate concentration that produces half I_{max}. Statistical analysis was performed using t-test by the SigmaStat program (Jandel Scientific). Experiments were repeated with oocytes from at least two to four different frogs.

Dual-label Competitive Transport Assay and Transport Specificity Ratio (TSR)

Transport solutions were prepared in sodium buffer containing a mixture of 150 μM ^{14}C-glutarate (American Radiolabeled Chemicals, Inc) and 50 μM ^{3}H-succinate (ViTrax Co.). In the transport assays, oocytes were rinsed with choline buffer to remove sodium and serum as described (72). Transport was initiated by replacing choline buffer with 0.4 mL of the transport solution. The uptake reaction was stopped by adding 4 mL of ice-cold choline buffer followed by three washes with cold choline buffer to remove extracellular radioactivity. Individual oocytes were transferred to scintillation vials and dissolved in 0.25 mL of 10% SDS. Radioactivity of the samples was measured by dual-label scintillation counting. Counts in uninjected oocytes were subtracted from counts obtained in cRNA-injected oocytes.

The transport specificity ratio (TSR) is a constant that reflects a difference in substrate affinities for two competing substrates in their transition states of carrier-substrate complexes (41). Experimentally, the TSR is determined from the initial rates (v) of a competitive transport reaction with both ^{3}H-succinate and ^{14}C-glutarate and the concentrations of the substrates using the following equation:

$$\mathrm{TSR} = \left(\frac{v_{\mathrm{glutarate}}}{v_{\mathrm{succinate}}}\right)\left(\frac{[\mathrm{succinate}]}{[\mathrm{glutarate}]}\right) \qquad [\mathrm{Eqn.2}]$$

The TSR is an expression-independent constant that provides information on the change in binding energy ($\Delta\Delta G_b$) resulting from structural differences between the two competing substrates, in this case succinate and glutarate, as given in the following equation (From (41)):

$$\mathrm{TSR} = \frac{\left(\frac{k_{\mathrm{cat}}}{K_{\mathrm{m}}}\right)_{\mathrm{glutarate}}}{\left(\frac{k_{\mathrm{cat}}}{K_{\mathrm{m}}}\right)_{\mathrm{succinate}}} = \exp(-\Delta\Delta G_b/RT) \qquad [\mathrm{Eqn.3}]$$

where R and T refer to the gas constant (8.31 J/K/mol) and temperature (296 K), respectively. A change in TSR value indicates a change in the transition binding energy of at least one of the two substrates. Changes in free energy associated with the single and double chimeras involving TM 3 and 4 were calculated using the following equation (110):

$$\Delta(\Delta\Delta G_b) = -RT \ln\left(\frac{\mathrm{TSR}_{\mathrm{glutarate}}}{\mathrm{TSR}_{\mathrm{wild\text{-}type}}}\right) \qquad [\mathrm{Eqn.4}]$$

RESULTS

Substrate specificity in wild-type NaDC1 transporters

Since previous experiments were done in different experimental conditions such as substrate concentrations between the NaDC1 orthologs, I performed preliminary substrate specificity screening using TEVC with 1 mM of various di- and tricarboxylates in mNaDC1 and rbNaDC1 (Figure 2.1). The result clearly shows that mNaDC1-expressing oocytes have more than 70% of succinate-induced currents with all of tested

substrates, whereas oocytes expressing rbNaDC1 exhibit very little currents with glutarate, α-ketoglutarate, and 2,3-DMS. There is no current detected with adipate in rbNaDC1.

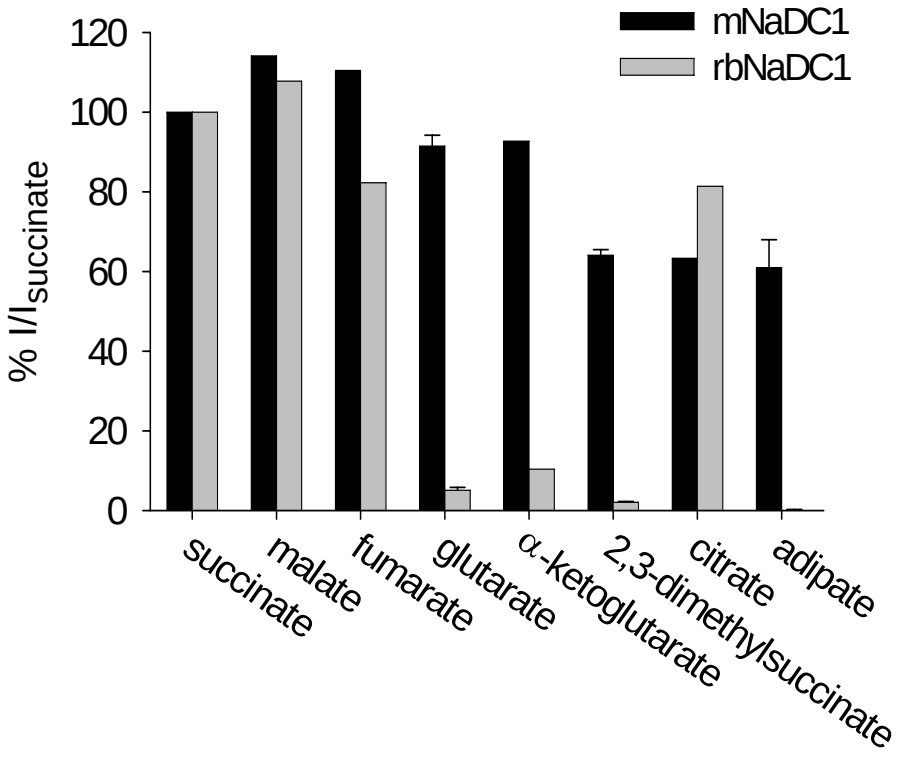

Figure 2.1 Substrate specificity in wild-type NaDC1 transporters. The various di- and tricarboxylates were prepared at 1 mM and tested for substrate-induced currents using the two-electrode voltage clamp. The data represents substrate-dependent currents relative to succinate-evoked currents at -50 mV. Malate, fumarate, α-ketoglutarate, and citrate were tested only once. The data for glutarate, adipate, and 2,3-dimethylsuccinate are shown as mean ±SEM, n=18-25 for glutarate, n= 14 for adipate, and n= 3-4 for 2,3-dimethylsuccinate.

Voltage-Dependent Currents in Mouse and Rabbit NaDC1

Glutarate and succinate are dicarboxylates that differ in length by only one carbon (Figure 1.2). The previous experiments done in our lab using radiotracer uptakes and the

two-electrode voltage clamp (TEVC) measurements indicated that the mouse and rabbit NaDC1 exhibit differences in their ability to transport glutarate (69; 76; 81). Those findings were verified in the preliminary studies for substrate screening in mNaDC1 and rbNaDC1 (Figure 2.1) and extended in this study. As shown in Figure 2.2, mNaDC1 exhibited large voltage-dependent inward currents with both glutarate and succinate at all tested membrane potentials. In contrast, rbNaDC1 exhibited inward currents in the presence of succinate, but only very small currents with glutarate.

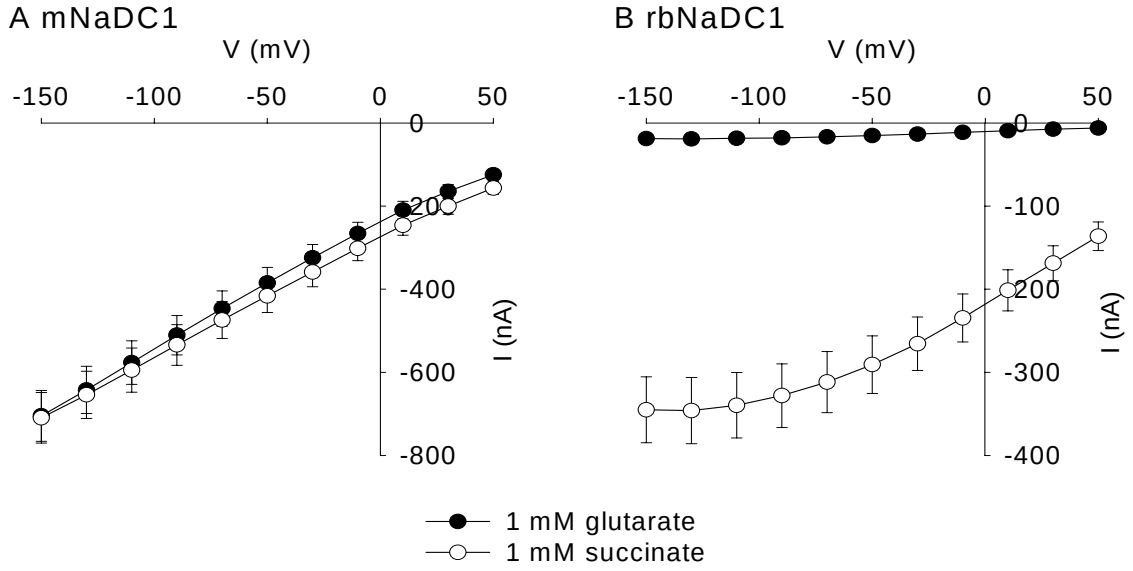

Figure 2.2 Voltage dependence of steady-state substrate-induced currents of wild-type NaDC1 transporters. *Xenopus* oocytes expressing mNaDC1 (A) and rbNaDC1 (B) were superfused with 1 mM succinate or 1 mM glutarate, and the pulse protocol described in Methods was followed. The mNaDC1 expressing oocytes exhibited inward currents with both glutarate and succinate, whereas oocytes expressing rbNaDC1 showed voltage-dependent inward currents with succinate but only small currents with glutarate. The data shown are mean ± SEM, n = 18-25 frogs.

Glutarate Kinetics in Oocytes Expressing mNaDC1 and rbNaDC1

The kinetics for glutarate in mNaDC1 and rbNaDC1 were next examined. The steady-state currents induced by increasing concentrations of glutarate at -50 mV are

shown in Figure 2.3. In the single experiment shown in Figure 2.3A, the $K_{0.5}$ for glutarate in mNaDC1 was 194 μM, and the I_{max} was -386 nA. In three experiments, the mean $K_{0.5}^{glutarate}$ was 252 ± 100 μM (mean ± SEM), and the $I_{max}^{glutarate}$ was -476 ± 112 nA. The kinetics of glutarate were more difficult to measure in rbNaDC1 because the currents were very small at low concentrations. Therefore, the $K_{0.5}$ for glutarate in rbNaDC1 was examined in a single experiment, showing approximately 15 mM of $K_{0.5}$ and -289 nA of I_{max} (Figure 2.3B). For comparison, the K_m for glutarate in rbNaDC1 was 7 mM measured using radiotracer (81). The succinate $K_{0.5}$ values were only about 2-fold different in the two transporters with a mean $K_{0.5}$ in mNaDC1 of 99 ± 15 μM (mean ± SEM, n = 3) (Figure 2.4) and 200 μM in rbNaDC1 (76). By comparison, the succinate K_m measured by radiotracer uptakes is 320 μM in mNaDC1 (69) and 450 μM in rbNaDC1 (72).

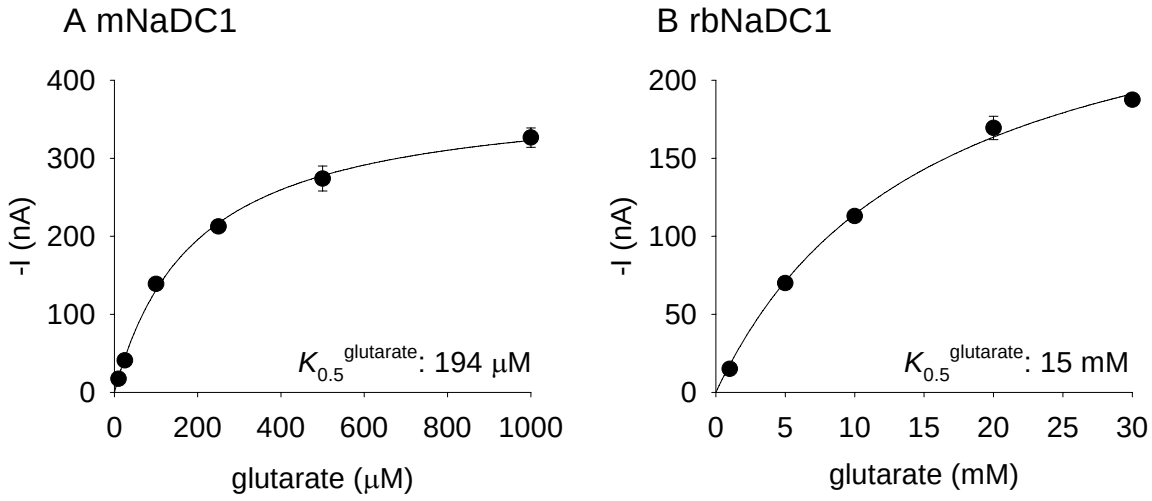

Figure 2.3 Glutarate kinetics in oocytes expressing mNaDC1 (A) and rbNaDC1 (B). Steady-state substrate-dependent currents at -50 mV are shown as a function of different concentrations of glutarate. The figure represents single experiments, and each data point shows mean ± range of duplicate measurements in a single oocyte. The concentrations of glutarate were varied between 10 μM and 1 mM for mNaDC1, and from 1 to 30 mM for rbNaDC1. In mNaDC1, the $K_{0.5}$ for glutarate is 194 μM and I_{max} is -386 nA. In rbNaDC1, the $K_{0.5}$ is 15.3 mM and the I_{max} is -289 nA.

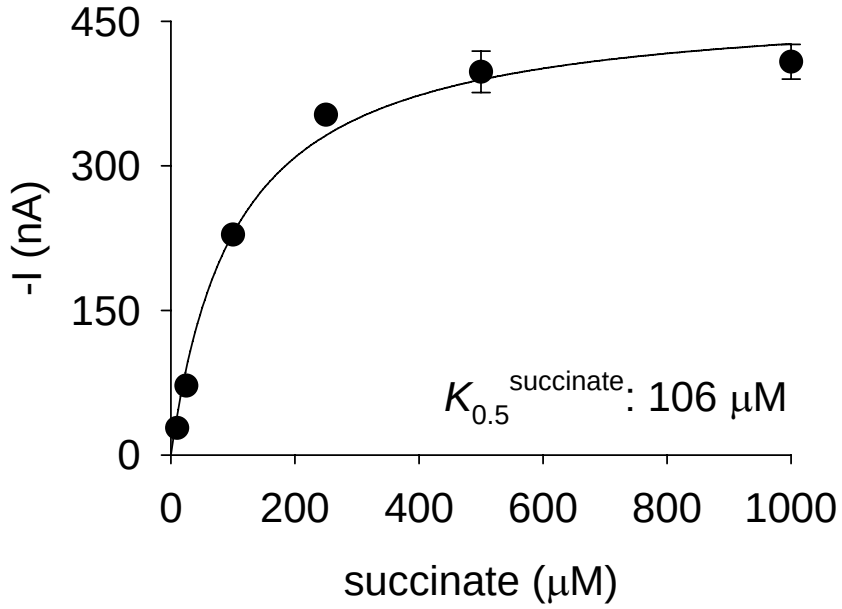

Figure 2.4 Kinetics of succinate-induced currents in mNaDC1. The concentration dependence of steady-state succinate currents at -50 mV in mNaDC1 expressing oocytes. The result from a single experiment is shown in this figure, and each data point represents the mean ± range of duplicate measurements in a single oocyte. The concentrations of succinate were between 10 μM and 1 mM. The $K_{0.5}$ for succinate is 106 μM and I_{max} is -472 nA.

Glutarate-Dependent Currents in Chimeric NaDC1 Transporters

A series of chimeras containing between TM 2 and 10 from mNaDC1 at the N-terminus (shown in Figure 2.5) was constructed and each expressed in *Xenopus* oocytes. The substrate-induced currents were determined as in Figure 2.2, but only the data from -50 mV are shown. The results are similar at all voltages (results not shown). Most of the chimeras had succinate-induced currents similar to those of the wild-type mouse and rabbit NaDC1, suggesting that the expression of these chimeras is similar to the wild-type proteins (Figure 2.6). The 2MR chimera exhibited much smaller currents than the wild-type transporters and may be expressed at a lower level. There are no antibodies available against mNaDC1, and therefore, it was not possible to test cell surface expression of the chimeras directly. The series of chimeras with rbNaDC1 at the N-

terminus was also constructed and tested, but the activity was too low for further experiments, similar to our previous findings with chimeras between rabbit and human NaDC1 (38).

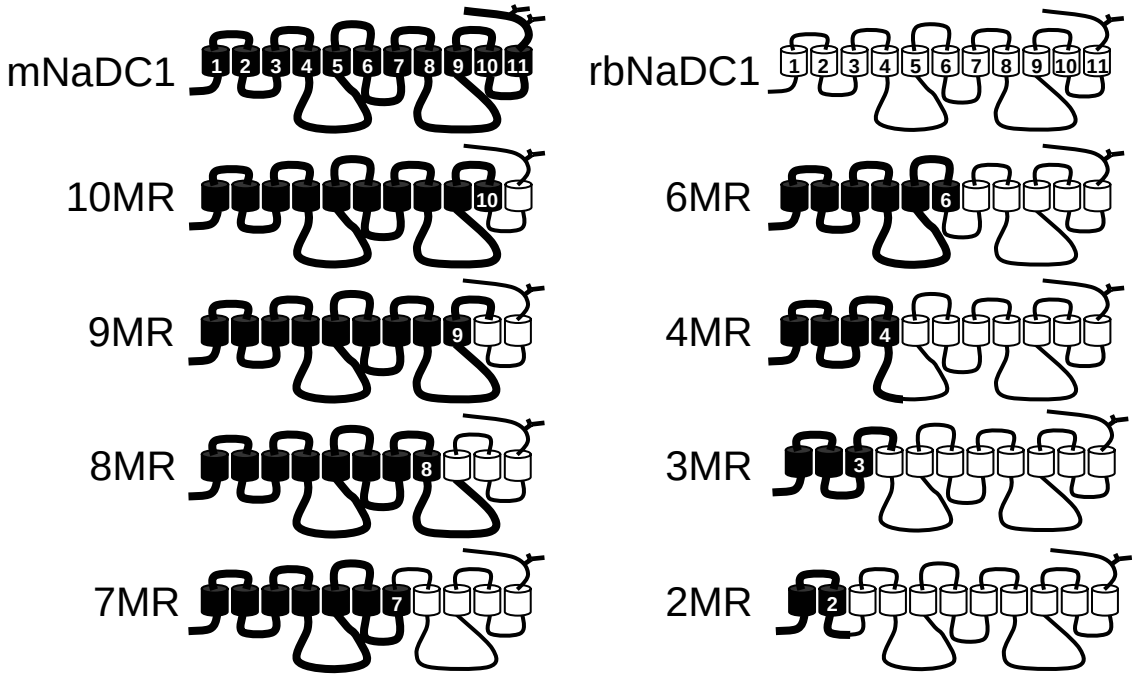

Figure 2.5 Secondary structure models of chimeric NaDC1 transporters used in this study. The cylinders and lines represent predicted transmembrane helices (TM) and associated loops of mouse NaDC1 (filled cylinders, bold lines) and rabbit NaDC1 (unfilled cylinders, narrow lines). The chimeric transporters are designated using the letters M (mouse), R (rabbit), and the number of TM contributed by mNaDC1 at the amino terminus. For example, 2MR contains TM 1-2 from mNaDC1 and 3-11 from rbNaDC1. The junctions to construct the chimeras are located at amino acid positions 74 (2MR), 120 (3MR), 177 (4MR), 284 (6MR), 341 (7MR), 427 (8MR), 489 (9MR), and 518 (10MR) relative to the amino acid sequence of mNaDC1. The Y indicates the *N*-glycosylation site. The extracellular side is at the top of the figure.

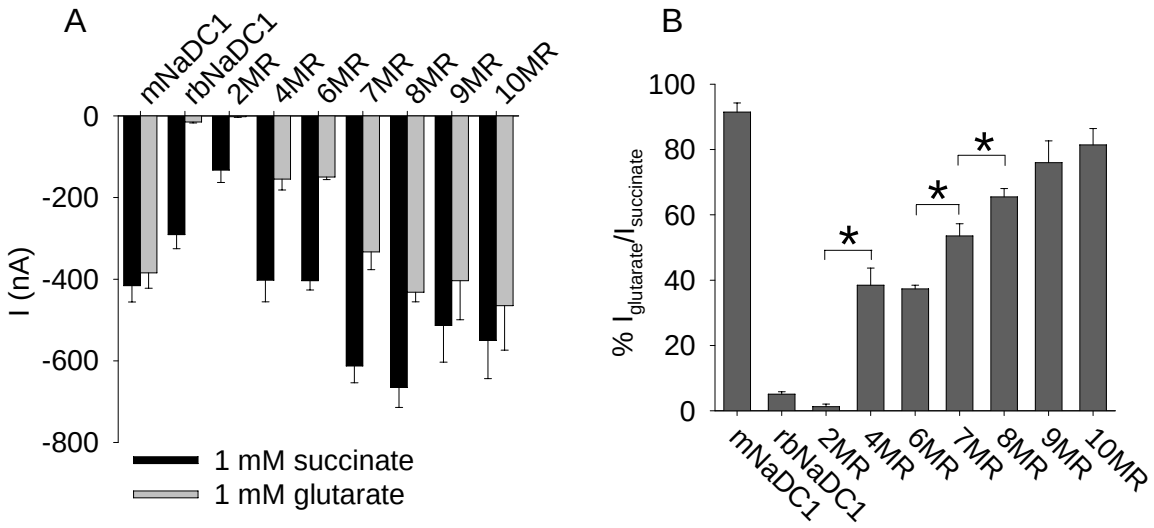

Figure 2.6 Currents in chimeric NaDC1 transporters. (A) Glutarate- and succinate-induced currents at -50 mV in wild type and chimeric NaDC1 transporters. The bars represent mean ± SEM, $n = 25$ (mNaDC1), $n = 18$ (rbNaDC1), $n = 3$-10 (chimeras). The concentration of each substrate was 1 mM. (B) Glutarate-induced currents expressed as a percentage of succinate-induced currents (from A). Asterisks represent $p < 0.05$. In addition, the 9MR chimera is significantly different from mNaDC1.

The currents induced by glutarate in mNaDC1 were almost as large as the succinate-induced currents, approximately 92% at -50 mV, whereas in rbNaDC1 the currents with glutarate were approximately 5% of those measured in succinate (Figure 2.6A, B). The chimeras that contained more TM from mNaDC1 also had increased glutarate-induced currents relative to the succinate-induced currents. There were significant differences between the 4MR and 2MR chimeras, the 7MR and 6MR chimeras, and the 8MR and 7MR chimeras (Figure 2.6B). Therefore, TM 3-4, 7, and 8 contribute to the glutarate-dependent currents, but the largest contribution is made by TM 3-4. The 9MR chimera results were significantly different from wild-type mNaDC1 but not different from the 10MR chimera. Therefore, it is possible that TM 10 is involved in glutarate transport, but the contribution is not large. TM 1, 2, 5, 6, and 11 do not appear to be involved in glutarate transport. However, this assumption can not be concluded from this study and remains to be studied. The results suggest that the difference between the mouse and rabbit NaDC1 in handling glutarate is determined primarily by

residues in TM 3-4 including the associated loop, but other residues in the C-terminal half of the protein also contribute.

Contribution of TM 3-4 to Glutarate-Induced Currents

The R(M3-4) chimera was constructed to investigate further the contribution of TM 3-4 in determining species differences in handling glutarate. The R(M3-4) chimera contains TM 3-4 from mNaDC1, and the rest of the protein is from rbNaDC1 (Figure 2.7A). The chimeric transporter was expressed in *Xenopus* oocytes, and substrate-dependent currents were measured (Figure 2.7B). Succinate-induced currents were decreased compared to the wild-type transporters, which may be due to lower expression of the chimeric protein. The glutarate-dependent currents relative to the succinate-evoked currents were 47.5 ± 5.7% (n = 6) in the R(M3-4) chimera compared with 5% for rbNaDC1 (Figure 2.6B), verifying that TM 3 and 4 contribute considerably to a difference in glutarate transport in NaDC1. The kinetics of the R(M3-4) chimera with glutarate and succinate were also measured. Substitution of TM 3-4 of mNaDC1 into rbNaDC1 resulted in a large decrease in $K_{0.5}^{glutarate}$ to 3.6 mM in the experiment shown in Figure 2.7C and a mean $K_{0.5}^{glutarate}$ of 4.1 ± 1.1 mM (mean ± SEM, n = 5). For comparison, the $K_{0.5}^{glutarate}$ in rbNaDC1 was 15 mM (Figure 2.3). The R(M3-4) chimera had no change in the $K_{0.5}$ for succinate, 219 ± 29 μM (mean ± range, n = 2, Figure 2.7D), compared with 203 μM for rbNaDC1 (76).

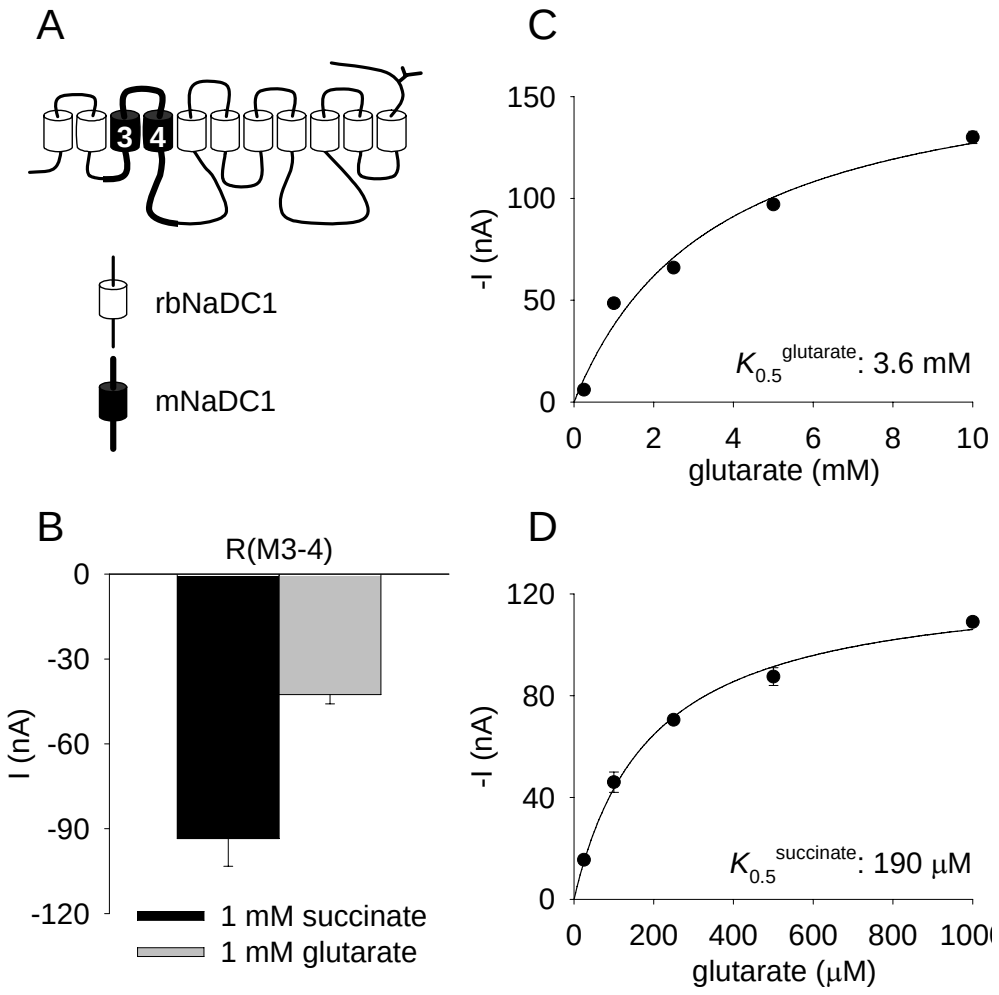

Figure 2.7 Currents in the R(M3-4) chimera. (A) Secondary structure model of the R(M3-4) chimera, containing TM 3-4 and associated loops of mNaDC1 (amino acids 75-177) in rbNaDC1 background. The filled cylinders represent mNaDC1. (B) Currents induced by 1 mM glutarate or succinate in the R(M3-4) chimera, measured at -50 mV. The bars represent mean ± SEM, $n = 6$. (C) Glutarate kinetics in theR(M3-4) chimera (same procedure as in Figure 2.3). The $K_{0.5}^{glutarate}$ is 3.6 mM and the I_{max} is -173 nA. (D) Succinate kinetics in the R(M3-4) chimera. The $K_{0.5}^{succinate}$ is 190 μM and the I_{max} is -126 nA.

Transport Specificity Ratio (TSR) Analysis of TM 3-4 Chimeras

The results of this study have shown that TM 3 and 4 in NaDC1 are important in determining the $K_{0.5}$ for glutarate. However, the catalytic efficiency of a transporter depends on both $K_{0.5}$ (or K_m) and k_{cat}. In transport experiments, including these, it is often difficult to determine the k_{cat} for lack of a measurement of the amount of transporter protein, or the fraction of that protein that is properly folded and active. The Transport Specificity Ratio (TSR) is a protein-independent constant that reflects a change in substrate specificity for two competing substrates and provides information on the relative catalytic efficiency (41) (see Methods). Since the TSR calculation is based on initial uptake rates, the time course of uptake of 150 μM ^{14}C-glutarate and 50 μM ^{3}H-succinate was measured between 10 s and 15 min to determine the initial rate of competitive uptake (Figure 2.8). The time courses were linear for at least 1 min with both substrates and both transporters. Therefore, 1-min uptakes were used for subsequent experiments. The TSR value calculated using 1 min uptakes for mNaDC1 is 0.54 in the experiment shown in Figure 2.8, compared with a TSR value of 0.043 for rbNaDC1, indicating large differences in catalytic efficiency for glutarate relative to succinate between these two transporters. The mean TSR values are 0.40 ± 0.04 in mNaDC1 and 0.046 ± 0.001 for rbNaDC1 (mean ± SEM, n = 5) (Table 2.1).

Because the TSR value is the ratio of k_{cat}/K_m for the two substrates, I can use the measured $K_{0.5}$ and TSR values to estimate the ratio of k_{cat} for glutarate relative to k_{cat} for succinate ($k_{cat}^{glutarate/succinate}$). Using the following equation:

$$k_{cat}^{glutarate/succinate} = TSR \left(\frac{K_{0.5}^{glutarate}}{K_{0.5}^{succinate}} \right) \qquad [Eqn.5]$$

the $k_{cat}^{glutarate/succinate}$ for mNaDC1 is 1.03 compared with 3.45 for rbNaDC1. The k_{cat} ratio value in rbNaDC1 implies that the $k_{cat}^{glutarate}$ is more than 3-fold greater than the $k_{cat}^{succinate}$. Although somewhat counterintuitive, this could be related to the very low

affinity for glutarate in rbNaDC1. Very often in transporters a low substrate affinity is correlated with a high transport capacity, probably a consequence of weaker binding and faster release of the substrate after translocation. Nevertheless, since physiological concentrations of succinate and glutarate in plasma are below 20 μM (8; 46), the rabbit NaDC1 functions primarily as a succinate transporter.

I next examined chimeras based on rbNaDC1 containing single or double substitutions of TM 3 or TM 4 from mNaDC1, called R(M3) and R(M4) (Figure 2.9A). Figure 2.9B shows competitive uptakes of ^{3}H-succinate and ^{14}C-glutarate in wild-type, single TM substituted chimeras and the double TM substituted chimera, R(M3-4). All three chimeras had measurable uptake activity with glutarate and succinate although the R(M3-4) and R(M3) chimeras exhibited lower activity compared with that of the R(M4) chimera (Figure 2.9B). The mean TSR values for the chimeras were significantly larger than the TSR value for the wild-type rbNaDC1 (Table 2.1). For comparison with the wild-type transporters, the $k_{cat}^{glutarate/succinate}$ ratio is 1.33 in the R(M3-4) chimera.

To determine whether there is functional interaction between TM 3 and 4, I calculated the free energy change ($\Delta(\Delta\Delta G_b)$) produced by each TM substitution (summarized in Table 2.1). This parameter is an indication of the change in discrimination between the two substrates as a result of the TM substitution. The free energy change of the double TM chimera R(M3-4) is -1.07 kJ/mol compared with the sum of free energies of the two single TM chimeras (R(M3) and R(M4)) of -2.81 kJ/mol (Table 2.1). The difference in free energy of the double TM chimera is not equal to the sum of the individual TM chimeras; thus, there is likely to be functional interaction between amino acid side chains in TM 3 and 4 (110).

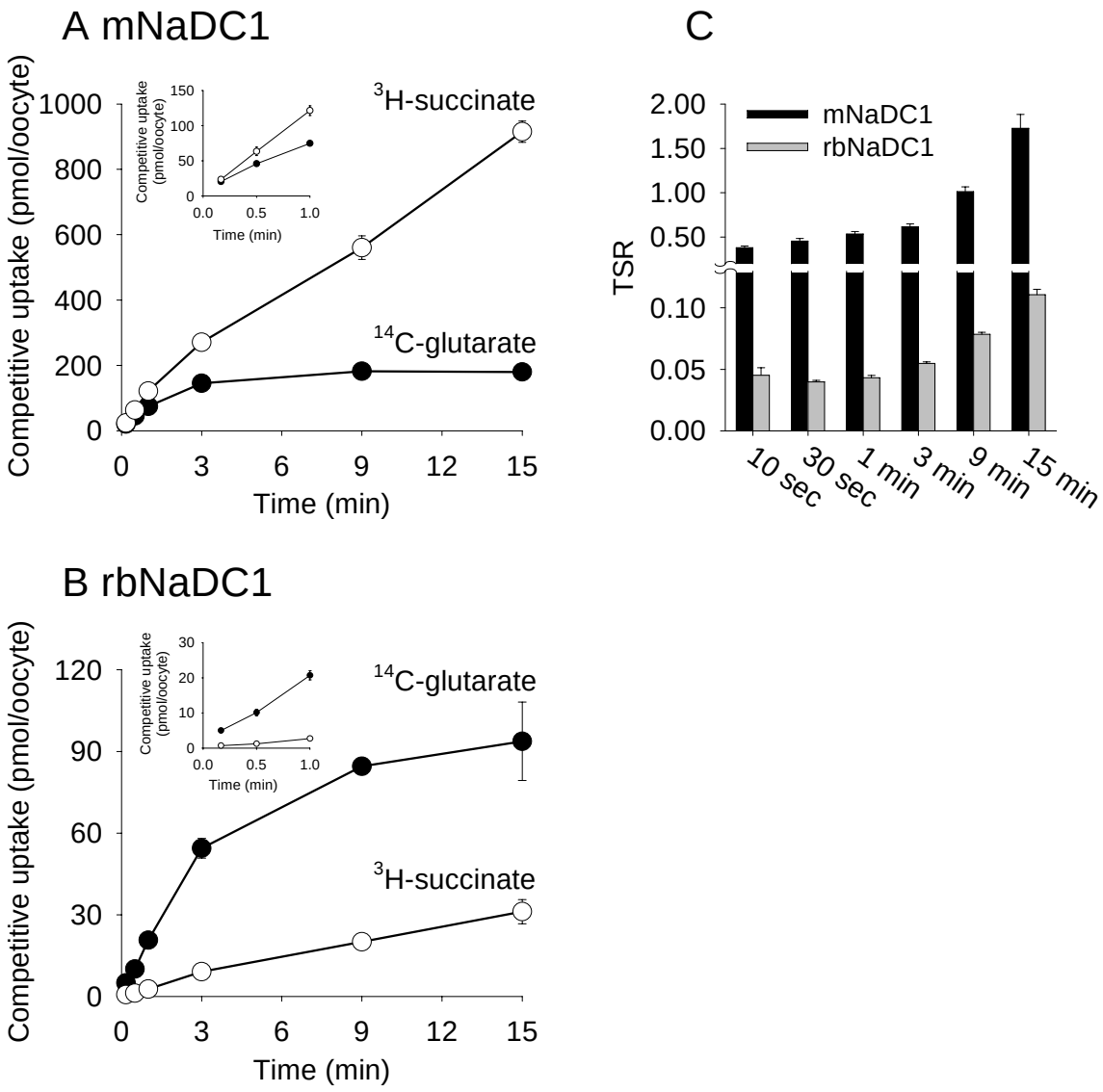

Figure 2.8 Time courses of competitive uptakes in wild-type NaDC1 transporters. Competitive uptakes using oocytes expressing mNaDC1 (A) and rbNaDC1 (B) were measured at different time points, from 10 s to 15 min. The concentrations of ^{14}C-glutarate and ^{3}H-succinate in the transport solution were 150 and 50 μM, respectively. The closed circles represent succinate, and the open circles represent glutarate, mean ± SEM, n = 5 oocytes. (C) TSR values calculated at different time points for the two wild-type NaDC1 transporters using the data shown in A and B.

Table 2.1 Comparison of TSR and free energy calculations in wild-type rbNaDC1, rbNaDC1 with single TM substitutions (TM 3 or 4) and with double TM substitution

Protein	TSR	$\Delta\Delta G_b$ (kJ/mol)[a]	$\Delta(\Delta\Delta G_b)$ (kJ/mol)[b]
rbNaDC1	0.046 ± 0.001 (5)	7.57	-
R(M3-4)	0.071 ± 0.01* (2)	6.51	-1.07
R(M3)	0.070 ± 0.003* (3)	6.54	-1.03
R(M4)	0.095 ± 0.01* (3)	5.79	-1.78

The numbers in parentheses under TSR values refer to sample size and the * denotes significant difference from wild-type, $p < 0.05$.

[a] $\Delta\Delta G_b = -RT \ln(\text{TSR})$.

[b] The change in free energy associated with binding glutarate relative to succinate as a result of chimera formation.

$\Delta(\Delta\Delta G_b) = \Delta\Delta G_{b(\text{chimera})} - \Delta\Delta G_{b(\text{wild-type})} = -RT \ln[(k_{cat}/K_m)_{\text{chimera}}/(k_{cat}/K_m)_{\text{wild-type}}] = -RT \ln[(\text{TSR}_{\text{chimera}})/(\text{TSR}_{\text{wild-type}})]$.

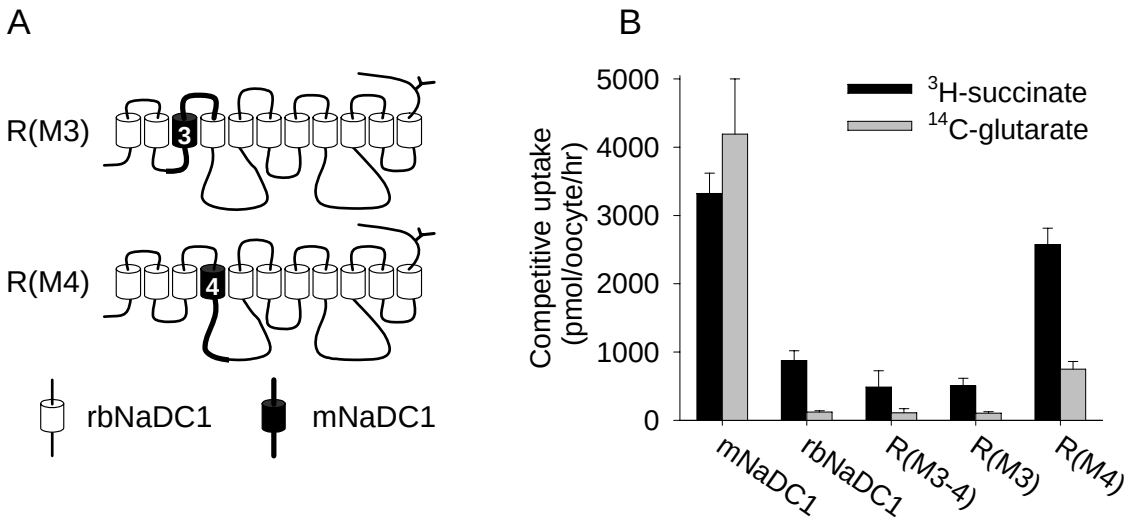

Figure 2.9 Competitive uptake assay in chimeric NaDC1 transporters. (A) Secondary structure models of the R(M3) and R(M4) chimeras containing substitutions of either TM 3 or TM 4 from mNaDC1 (shown by filled cylinders) in rbNaDC1 background. (B) Competitive uptake of glutarate and succinate by wild-type and chimeric NaDC1 transporters expressed in *Xenopus* oocytes. The transport reactions were carried out for 1 min with 150 μM ^{14}C-glutarate and 50 μM ^{3}H-succinate. The bars represent mean ± SEM, $n = 5$ (wild-type), $n = 3$ (R(M3) and R(M4) chimeras), and mean ± range, $n = 2$ (R(M3-4) chimera). TSR values are shown in Table 2.1.

Mutants in TM 3-4

To identify the individual amino acids in TM 3 and 4 that determine differences in glutarate $K_{0.5}$ and TSR, site-directed mutagenesis was done using the 4MR chimera as a parental transporter. There are 26 amino acid differences between mouse and rabbit NaDC1 between amino acids 75 and 177 (the TM 3-4 region). In my initial screen, I chose seven amino acids that are identical between mNaDC1 and mNaDC3, the high affinity transporter that also carries glutarate, but are different from rbNaDC1. Four out of the seven amino acids, Cys-79, Phe-83, Leu-149, and Gly-161, are also conserved in other NaDC3 orthologs. These seven amino acids were mutated from the mNaDC1 sequence to the amino acid found in rbNaDC1 at the same position. The mutants were:

K77E, C79G, F83L, L149V, G161N, K164S, and D165N. The mutants were first screened for inward currents in the presence of glutarate and succinate. Most did not show any changes, but the G161N mutant appeared to have a decrease in glutarate currents relative to those of succinate (Figure 2.10). In the single experiment shown in Figure 2.11, the $K_{0.5}^{glutarate}$ in the G161N mutant was 7.7 mM and I_{max} was -520 nA, and the $K_{0.5}^{glutarate}$ in the parental transporter, the 4MR chimera, was 2.3 mM and I_{max} was -453 nA. In three experiments, the mean $K_{0.5}^{glutarate}$ in the G161N mutant was 6.1 ± 1.3 mM (mean ± SEM, n = 3), significantly different from the $K_{0.5}^{glutarate}$ of 2.5 ± 0.2 mM (n = 3) in the 4MR chimera. However, when I tested TSR values of the mutants, there were no major differences among them or with the 4MR parental transporter (Figure 2.12). Therefore, Gly-161 appears to be a determinant of binding in the initial Michaelis complex ($K_{0.5}^{glutarate}$) but not in the transition state complex, which is addressed by the TSR results.

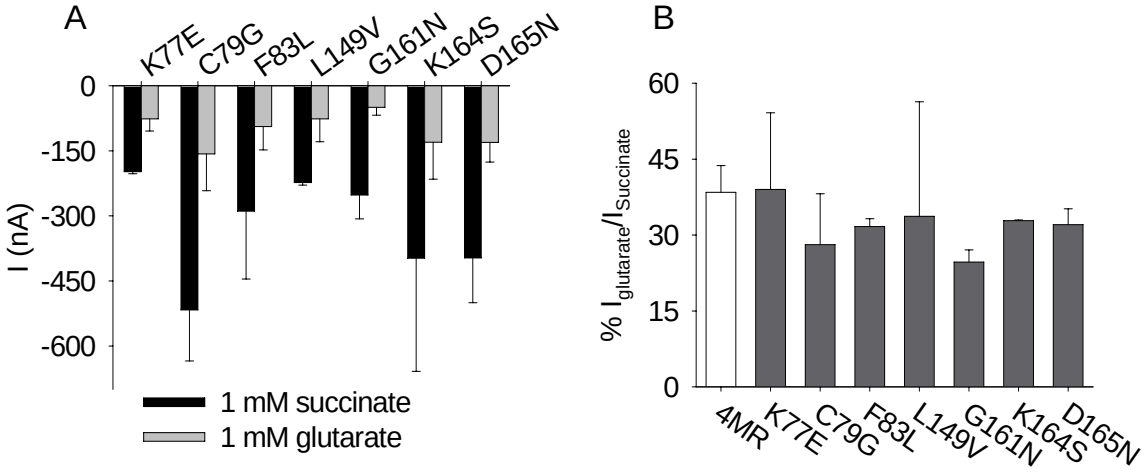

Figure 2.10 Currents in the TM 3-4 mutants. (A) Glutarate- and succinate- dependent currents at -50 mV in the TM 3-4 mutants and the parental 4MR chimera. The bars represent mean ± SEM, n = 11 (4MR), n = 5 (G161N), and mean ± range, n = 2 (K77E, C79G, F83L, L149V, K164S, and D165N). The concentration of each substrate was 1 mM. (B) Glutarate-evoked currents expressed as a percentage of succinate-induced currents (from A).

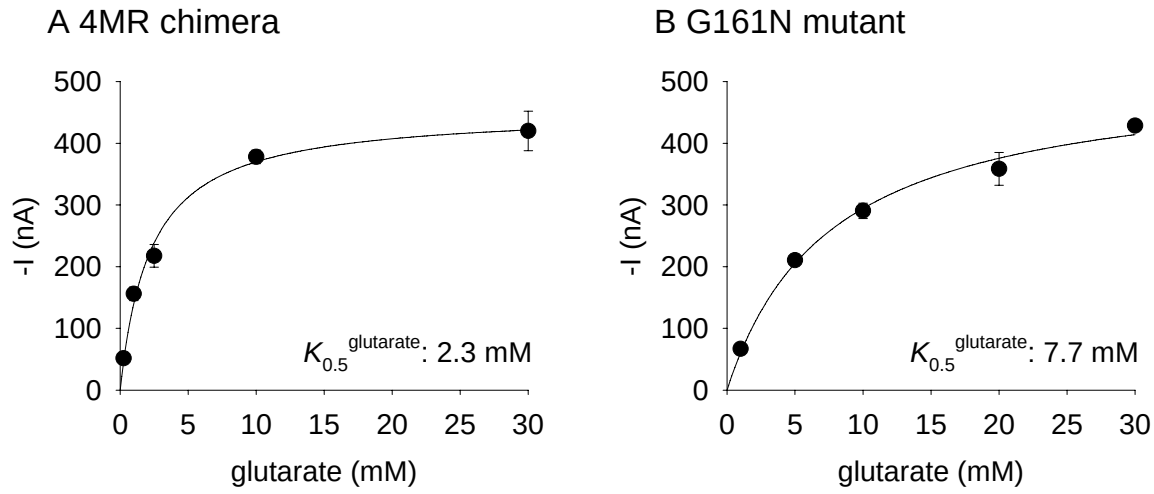

Figure 2.11 Glutarate kinetics in oocytes expressing the 4MR chimera (A) and the G161N mutant (B). Steady-state glutarate-induced currents at -50 mV are shown as a function of different concentrations of the substrate. Each data point shows the mean ± range of duplicate measurements in a single oocyte. The concentrations of glutarate were between 0.25 and 30 mM for 4MR and between 1 and 30 mM for the G161N mutant. In the parental 4MR transporter, the $K_{0.5}^{glutarate}$ is 2.3 mM, and the I_{max} is -453 nA. In the G161N mutant, the $K_{0.5}^{glutarate}$ is 7.7 mM, and the I_{max} is -520 nA.

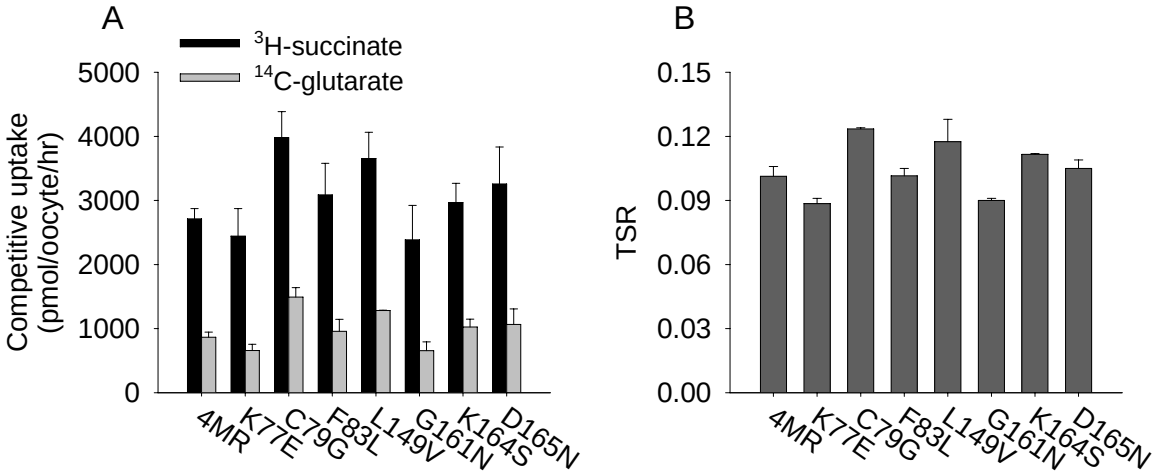

Figure 2.12 Competitive uptake assay in TM 3-4 mutants. (A) Competitive uptake of glutarate and succinate by the TM 3-4 mutants and the 4MR chimera (parental). The transport assay was performed for 1 min with 150 μM ^{14}C-glutarate and 50 μM ^{3}H-succinate. The bars represent mean ± SEM, n = 6 for the 4MR chimera, and mean ± range, n = 2 for the mutants.

DISCUSSION

This study is based on the observation that the mouse and rabbit NaDC1 orthologs exhibit differences in their handling of glutarate, which differs from succinate by only one carbon. A series of chimeras was made and tested by the two-electrode voltage clamp to identify the regions of the protein responsible for transport of glutarate. I found that differences in glutarate transport are determined by residues found throughout the protein, including transmembrane helices (TM) 7, 8 and possibly 10, but the largest contribution is made by TM 3 and 4 and their associated loops. TM 3-4 make significant contributions both to the $K_{0.5}$ for glutarate and to the relative catalytic specificity, measured using the Transport Specificity Ratio (TSR). The results provide evidence of functional coupling between amino acids located in the TM 3-4 region, possibly indicating either a direct interaction between amino acid side chains or cooperative interaction between the amino acids to form a substrate binding site.

Some domains of the NaDC1 protein that affect glutarate transport have been shown in our previous studies to be involved in transport of other substrates. For example, the difference in citrate affinity between the human and rabbit NaDC1 is determined by residues in TM 7, 10, and 11 (38). The arginine at position 349, at the extracellular face of TM 7, is required for succinate transport, and the aspartic acid at position 373 in TM 8 is a conformationally sensitive residue (118). TM 9-10 appear to form part of the permeation pathway in NaDC1, and this region contains functionally important residues that are alternately accessible and inaccessible to the extracellular medium during the transport cycle (71; 79). Previous studies have also shown that residues that affect the K_m for succinate are also found in TM 1-4, before amino acid 139 (83), which corresponds well with the finding in the present study that TM 3-4, including the glycine at position 161, are important in determining the $K_{0.5}$ for glutarate.

Transport specificity ratio (TSR) analysis provides information on changes in catalytic efficiency with glutarate and succinate as a consequence of chimera formation (42). The mouse and rabbit NaDC1 transporters differ in their TSR values by more than 10-fold, reflecting the large differences in substrate specificity of glutarate relative to succinate. Since the TSR is based on a change in free energy of transition-state binding for two competitive substrates, $\Delta\Delta G_b$, the TSR measurement can be used to estimate the effect of a mutation or chimera on the relative heights of the translocation energy barrier for the two substrates. Previous studies have shown that changes in free energy of single and double mutants relative to the wild-type proteins can provide information on whether the mutated amino acids interact in the transition state (110). If two residues are not close to one another and not functionally coupled, then the sum of changes in transition-state stabilization energy for two individual mutations is equal to that for the corresponding double mutation (110). However, a difference between the sum of changes in free energy of two single mutations compared with the double mutant indicates that the mutations alter the interactions between these residues. TSR analysis is somewhat more complex because two substrates are involved, succinate and glutarate. However, adaptation of these principles to the particular circumstances of TSR analysis leads to the conclusion that there is transition-state interaction energy between TM 3 and 4, and this interaction has a functional role in determining the relative specificities for glutarate versus succinate. My single and double chimeras exhibit nonadditivity since the sum of $\Delta(\Delta\Delta G_b)$ for the two single TM chimeras (-2.81 kJ/mol) is not the same as that for the chimera containing both TM 3 and 4 (-1.07 kJ/mol) (Table 2.1). This suggests that the function of TM 3 is coupled with that of TM 4 in the transition state. However, comparison of $\Delta(\Delta\Delta G_b)$ between the R(M3), R(M4), and R(M3-4) chimeras indicates a negative effect of TM 3 on TM4 in the transition state. Alternatively, in the R(M3) chimera, mouse TM 3 might have more thermodynamically unfavorable interaction with rabbit TMs, with compared to the interaction between mouse TM 4 and rabbit TMs in the R(M4) chimera. This effect may be seen in the R(M3-4) chimera in a value of $\Delta(\Delta\Delta G_b)$. In other studies, a similar difference between the free energy changes of single and

double mutants was found for polar residues in TM 4 and 5 of the dopamine transporter, suggesting the residues interact in the initial Michaelis complex (36).

The amino acids responsible for differences in glutarate handling in NaDC1 appear to be distributed throughout the protein, with contributions from TM 7, 8, and possibly 10 adding to the effects of TM 3-4. This indicates that amino acids found on multiple helical surfaces contribute to transport of glutarate in NaDC1, which is in agreement with other studies of transport proteins. For example, the affinity for glucose in the facilitative glucose transporters Hxt1 and Hxt2 from *Saccharomyces cerevisiae* is determined by at least four amino acids found in TM 1, 5, 7, and 8 (39). In the mammalian facilitative glucose transporters, glucose affinity is determined by residues in TM 9-12, whereas TM 1-2 and 6-11 contain determinants of fructose transport (12; 114). In addition, amino acids in TM 7 and 2 in GLUT7 appear to form a selectivity filter that restricts access of some substrates to the substrate binding site (59). Crystal structures of transport proteins, such as the recent structures of the bacterial Na^+/Cl^--dependent leucine transporter and the lactose permease, show that substrate binding sites are within hydrophilic cavities formed by multiple helices (1; 116).

The differences between rabbit and mouse NaDC1 in handling glutarate are more likely related to differences in transition state rather than the initial binding of substrate to the transporter. In transporters, the substrate specificity (k_{cat}/K_m) or the ability to discriminate between two substrates depends on the height of the activation energy barrier (41). As shown by the differences in TSR values, mNaDC1 has very similar transition-state stabilization (small $\Delta\Delta G_b$) for glutarate and succinate, which limits discrimination between them. In contrast, rbNaDC1 does a better job of discriminating between the two substrates, and this is reflected in the larger difference in binding energy used for transition-state stabilization. The best fit to the substrate is most likely during the transition-state complex (43), and the observed differences between the transporters could reflect differences in accommodating the two substrates in the transition state. For

example, the mNaDC1 protein could be more flexible to orient the critical residues in the protein with substrates of different structures.

In conclusion, the mouse and rabbit NaDC1 exhibit differences in handling the five-carbon dicarboxylate, glutarate. The mNaDC1 exhibits substrate-dependent currents with glutarate as large as those with succinate, and the TSR value of 0.4 reflects a relatively high efficiency of transporting glutarate relative to succinate. The rbNaDC1 has only small currents in the presence of glutarate and a succinate affinity similar to that of mNaDC1, reflected in a very low TSR value of 0.046. The results of this study show that the differences in glutarate transport are determined primarily by the interaction of multiple amino acids found in TM 3 and 4, with contributions from TM 7, 8, and 10 or the associated loops. TM 3-4 make important contributions to substrate affinity and specificity in NaDC1. Furthermore, there is evidence of functional coupling between amino acids in TM 3 and TM 4.

CHAPTER 3: Ala-504 IS A DETERMINANT OF SUBSTRATE BINDING AFFINITY IN THE MOUSE Na^+/DICARBOXYLATE COTRANSPORTER

(Studies in this chapter have been accepted for publication in Biochimica et Biophysica Acta-Biomembranes)

INTRODUCTION

Preliminary experiments showed that the mouse and rabbit NaDC1 orthologs also differ in their ability to handle adipate, a six-carbon terminal dicarboxylate (Figure 2.1). The rabbit does not transport adipate, whereas the mouse transports adipate quite well. Therefore, the purpose of the study in this Chapter was to identify domains and amino acids that determine adipate transport using the same chimeras used in the study in Chapter 2. In the previous chapter, I found that transmembrane helices (TM) 3, 4, 7, and 8 are involved in glutarate transport in mNaDC1. Particularly, the region of TM 3-4 made the greatest contribution to glutarate-induced currents (Figure 2.6). Furthermore, the result of TSR analysis using chimeras, consisting of rbNaDC1 with substitution of TM 3 and/or TM4 of mNaDC1, indicates that TM 3 and TM 4 are likely to have functionally coupling in the transition state carrier-substrate complex (Table 2.1).

Similar to the previous study in Chapter 2, I found that multiple TMs are involved in producing adipate-induced inward currents. However, the main determinants of adipate transport are found in the C-terminal half of the protein, particularly TM 10 with contributions from TM 8 and 9, very different from the domains involved in glutarate transport (Figure 2.6). Since TM 10 showed considerable contribution to adipate-induced currents, site-directed mutagenesis was performed. Within TM 10, Ala-504 appears to be a determinant of adipate transport. Mutation from the mouse to the rabbit sequence at this position, mNaDC1-A504S, results in increases in the $K_{0.5}$ for both adipate and succinate, suggesting that Ala-504 is important for substrate binding in NaDC1. Unlike

the study in the previous chapter, TSR analysis was not possible in this study due to high background of ^{14}C-adipate uptake in control oocytes (Figure 3.1).

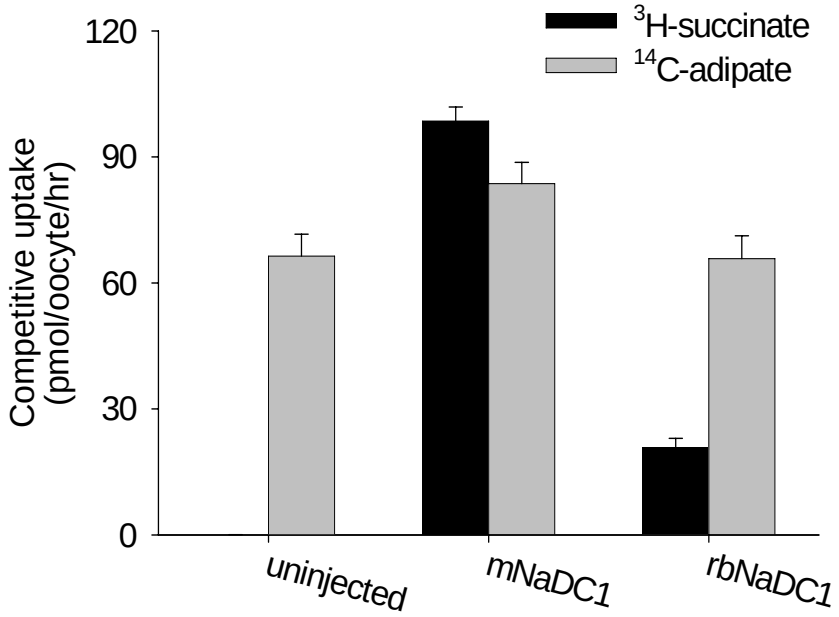

Figure 3.1 Dual-label competitive uptake of succinate and adipate in oocytes expressing wild-type NaDC1 transporters. The transport reactions were carried out for 1 min with 1 μM ^{3}H-succinate and 10 μM ^{14}C-adipate. The bars represent mean ± SEM, n = 5 oocytes from a single frog.

METHODS

All methods are described in Chapter 2.

RESULTS

Voltage-dependent currents in wild-type NaDC1 transporters

In the previous chapter, I found that mNaDC1 and rbNaDC1 have functional differences in glutarate transport, although glutarate is only one carbon longer than

succinate as shown Figure 1.2. Therefore, in this study I tested whether these transporters also differ in their handling of adipate, a six-carbon terminal dicarboxylic acid. As shown in Figure 3.2, mNaDC1 had large substrate-dependent inward currents induced by both adipate and succinate at all tested membrane potentials, whereas rbNaDC1 had inward currents with only succinate. Adipate- and succinate-dependent currents were not detected in control oocytes (Figure 3.3).

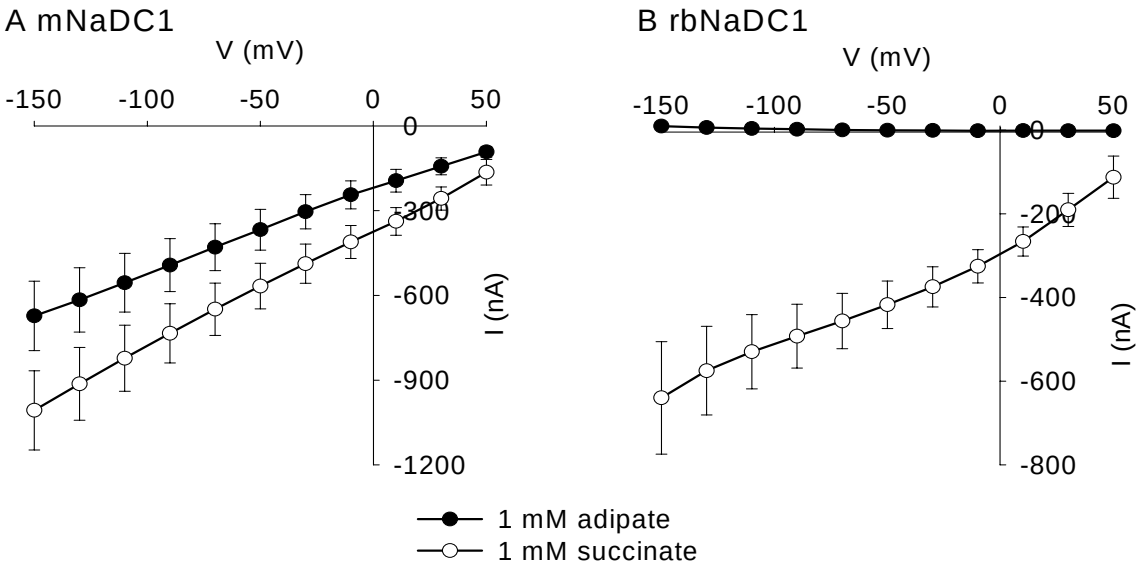

Figure 3.2 The voltage dependence of steady-state substrate-dependent currents in mNaDC1 and rbNaDC1 expressed in Xenopus oocytes. Adipate- and succinate-induced currents in mNaDC1 (A) and rbNaDC1 (B) are shown as a function of different voltages. The concentration of the substrates was 1 mM. The mNaDC1-mediated inward currents were seen in the presence of both adipate and succinate at all tested voltages. In contrast, rbNaDC1-mediated inward currents were only detected in the presence of succinate. The data shown are mean ± SEM, n = 14 frogs.

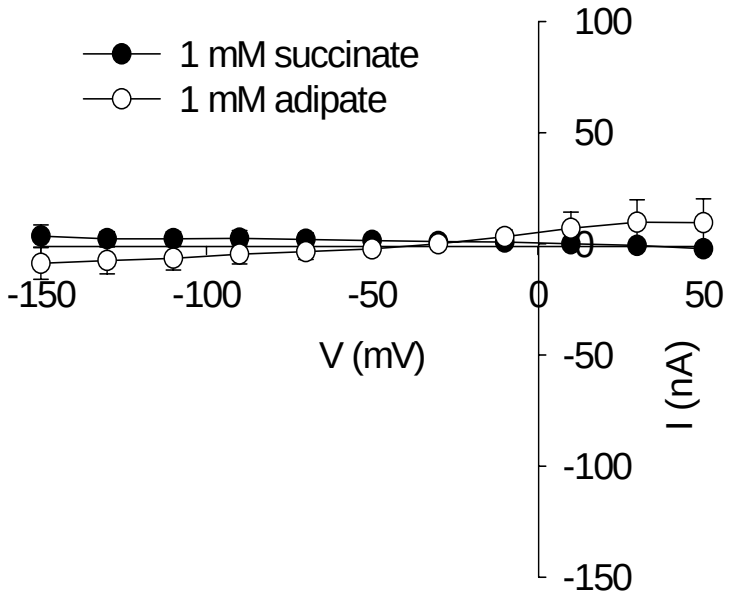

Figure 3.3 Substrate-induced currents in control, uninjected oocytes. Data was calculated from the difference between currents in the presence and absence of 1 mM succinate (closed circles) and adipate (open circles) in buffer containing sodium. Data are mean ± SEM, n=3.

Kinetics of adipate-induced currents in mNaDC1

The concentration dependence of steady-state adipate-induced currents was examined in oocytes expressing mNaDC1. The results of a single experiment at -50 mV are shown in Figure 3.4A and the means of three experiments at different voltages are in Figures 3.4B, C. The $K_{0.5}$ for adipate was 0.54 mM, and the I_{max} was -348 nA (Figure 3.4A). In three experiments, the mean $K_{0.5}^{adipate}$ was 0.70 ± 0.12 mM (mean ± SEM), and the $I_{max}^{adipate}$ was -239 ± 55 nA at -50 mV. The voltage dependence of $K_{0.5}^{adipate}$ and $I_{max}^{adipate}$ are shown in Figures 3.4B, C. The $K_{0.5}^{adipate}$ was voltage-insensitive at potentials more negative than -50 mV and gradually increased as the membrane potential became more positive. For example, at -150 mV, $K_{0.5}^{adipate}$ was 0.47 ± 0.06 mM, and at +50 mV, $K_{0.5}^{adipate}$ was 2.22 ± 0.37 mM (mean ± SEM, n = 3) (Figure 3.4B). The

maximum adipate-induced inward currents, $I_{max}^{adipate}$, were sensitive to the membrane potential, with a 3.6-fold increase between +50 and -150 mV (Figure 3.4C).

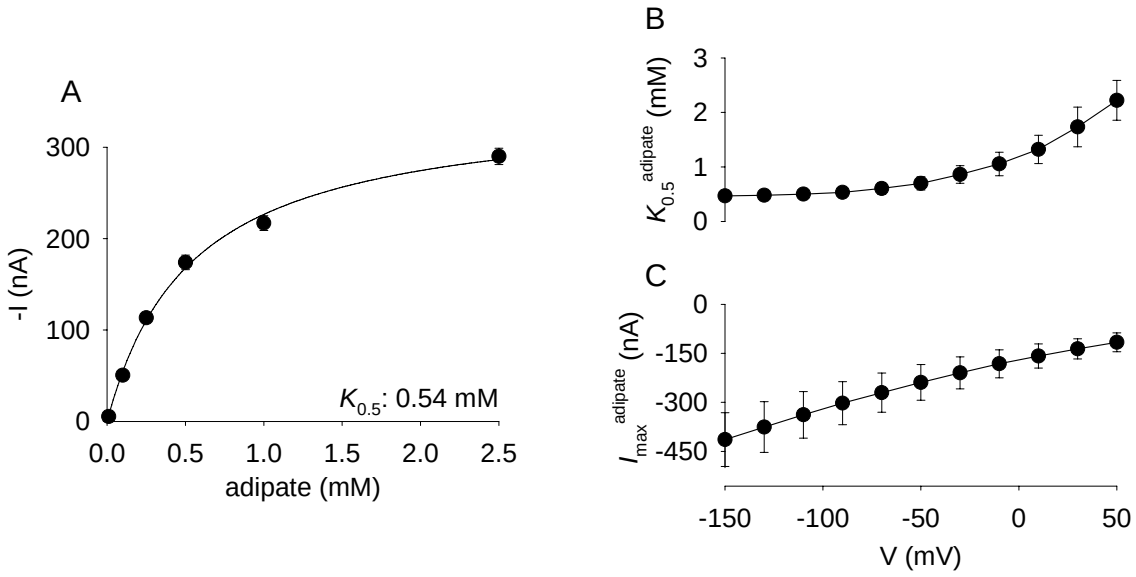

Figure 3.4 Kinetics of adipate-induced currents mediated by mNaDC1. (A) The concentration dependence of steady-state adipate-induced currents at -50 mV in oocytes expressing mNaDC1. The result from a single experiment is shown in this panel, and each data point represents the mean ± range of duplicate measurements in a single oocyte. The adipate concentrations were between 0.01 mM and 2.5 mM. The $K_{0.5}$ for adipate is 0.54 mM and I_{max} is -348 nA. (B) and (C), The voltage dependence of the mean $K_{0.5}$ and I_{max} for adipate, respectively. The data shown are mean ± SEM, n = 3 frogs.

Substrate-induced currents in chimeric NaDC1 transporters

A series of chimeras, consisting of increasing substitutions by mNaDC1 at the N-terminus (Figure 3.5) were used to examine adipate-dependent currents after expression in *Xenopus* oocytes. The substrate-induced currents were measured using the same pulse protocol as the one shown in Figure 3.2, but for simplicity only the data at -50 mV are shown (Figure 3.6). The results were similar at all voltages. All of the chimeras exhibited succinate-induced currents similar to those of the wild-type mouse or rabbit NaDC1, but differed in their adipate-induced currents (Figure 3.6A). I also tested some

chimeras containing rabbit NaDC1 at the N-terminus: 7RM (containing TM 1-7 of rbNaDC1 and TM 8-11 of mNaDC1) and 8RM (TM 1-8 of rbNaDC1 and TM 9-11 of mNaDC1). However, the succinate-induced currents were too small for further experiments, similar to previous observations (38).

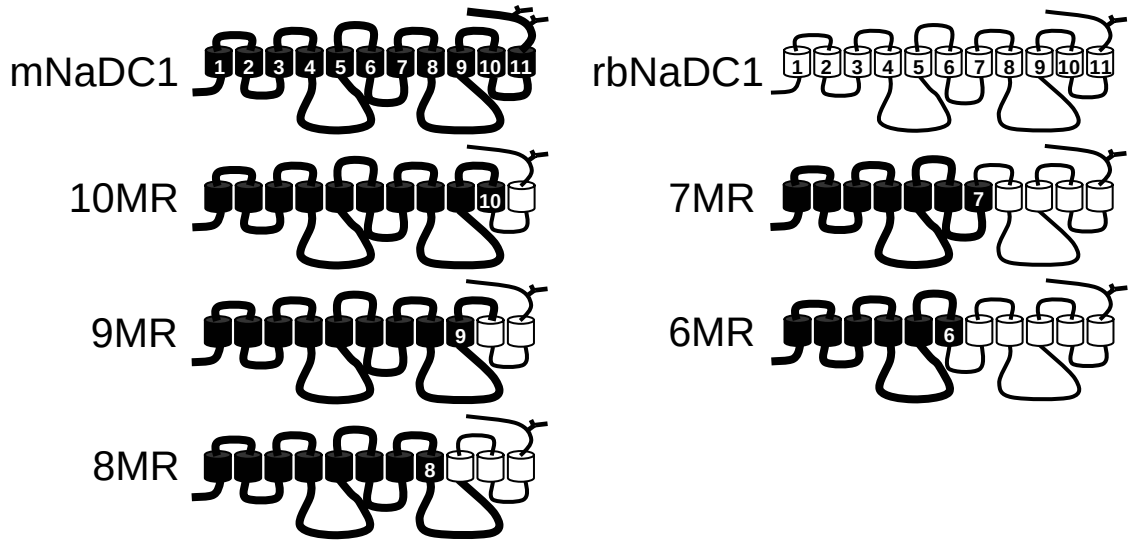

Figure 3.5 Secondary structure models of the mNaDC1-rbNaDC1 chimeras used in this chapter. These chimeras were used in the study of Chapter 2 to examine glutarate transport. (Figure 2.5)

At -50 mV, the adipate-dependent currents in mNaDC1 were 61% of the succinate-induced currents, whereas in rbNaDC1 there were no detectable currents in the presence of adipate (Figures 3.6A, B). The chimeras showed increases in adipate-dependent currents relative to the succinate-induced currents, depending on the number of TM from mNaDC1 at the amino terminus. There were statistically significant differences between rbNaDC1 and the 6MR chimera, the 7MR and 8MR chimeras, the 8MR and 9MR chimeras, and the 9MR and 10MR chimeras (Figure 3.6B). Overall, the most important contributions to adipate-dependent currents were made by TM 10 with some contributions from TM 8 and 9. Although TM 7 and 11 do not appear to be involved in adipate transport since there were no differences between the 6MR and 7MR chimeras or between the 10 MR chimera and wild-type mNaDC1, it cannot be concluded

from this study. The interaction of TM 7 and 11 with other TMs in the protein may situate TM 8, 9, and 10 at the ideal conformations during adipate transport. The study in Chapter 2 using glutarate examined both substrate-dependent currents and the transport specificity ratio (TSR), a protein expression-independent constant calculated with values from dual-label competitive uptakes of two competing substrates, to investigate changes in relative substrate specificity in the transition state. However, it was not possible to measure the TSR for adipate and succinate in this study due to high background uptake of ^{14}C-adipate in control oocytes, resulting in inaccurate TSR values (Figure 3.1).

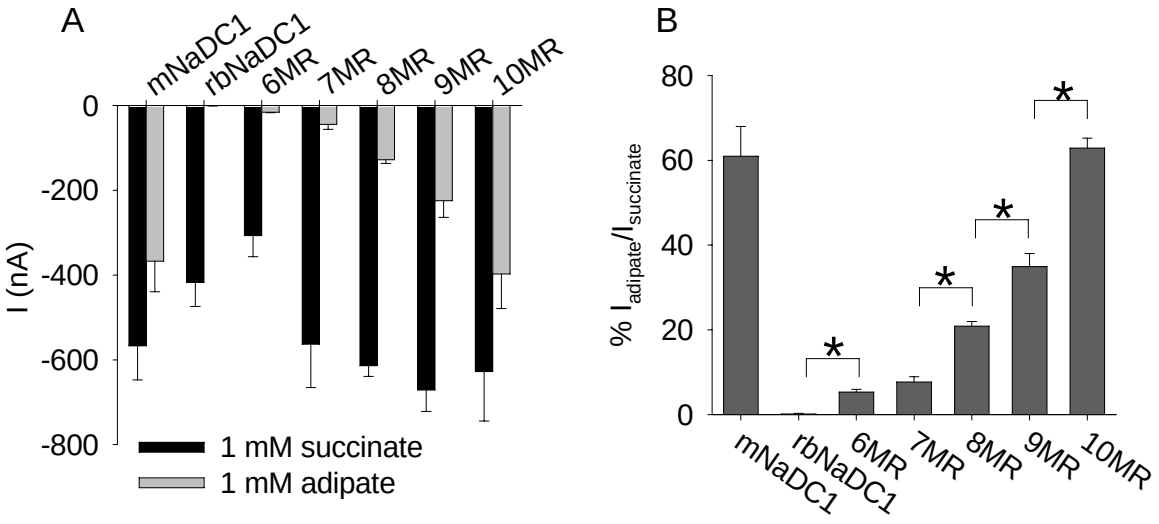

Figure 3.6 Substrate-induced currents mediated by chimeric NaDC1 transporters. (A) Substrate-dependent currents at -50 mV in the presence of 1 mM adipate or succinate in oocytes expressing wild-type and chimeric NaDC1. The bars represent mean ± SEM, n = 14 (mNaDC1), n = 9 (rbNaDC1), n = 3-6 (chimeras). (B) Adipate-dependent currents expressed as a percentage of the succinate-dependent currents (from A). Asterisks represent significant differences, $p < 0.05$.

Mutagenesis in TM 10

The largest contribution to adipate-induced currents appears to be from TM 10, containing amino acids 519-586 (mNaDC1 numbering). There is only one amino acid difference between mouse and rabbit NaDC1 in TM10. The mNaDC1 has an alanine at

position 504 whereas rbNaDC1 has a serine at the equivalent position 512. The A504S mutant of mNaDC1 was expressed in *Xenopus* oocytes in paired experiments with the wild-type mNaDC1, and substrate-dependent currents were measured in the presence of adipate and succinate (Figure 3.7A). As shown in Figure 3.7B, the adipate-dependent currents relative to the succinate-dependent currents were 40.4 ± 3.9% in the A504S mutant, significantly lower than the adipate currents relative to succinate in mNaDC1 of 59.3 ± 0.8% (n = 3 paired experiments). Since TM 11 does not seem to participate in adipate transport, the A504S mutant of mNaDC1 should correspond to the 9MR chimera, which contains rabbit sequence from TM 10 and 11 (Figure 3.5). In fact, there were no significant differences in adipate:succinate currents between the A504S mutant and the 9MR chimera (Figure 3.6B). The S512A mutant of rbNaDC1 was also tested but the mutation of only one residue is not enough to add function to rbNaDC1, compared with removing one of at least three residues in the A504S mutant of mNaDC1. The currents in the rbNaDC1-S512A mutant were the same as in wild-type rbNaDC1 (Figure 3.8).

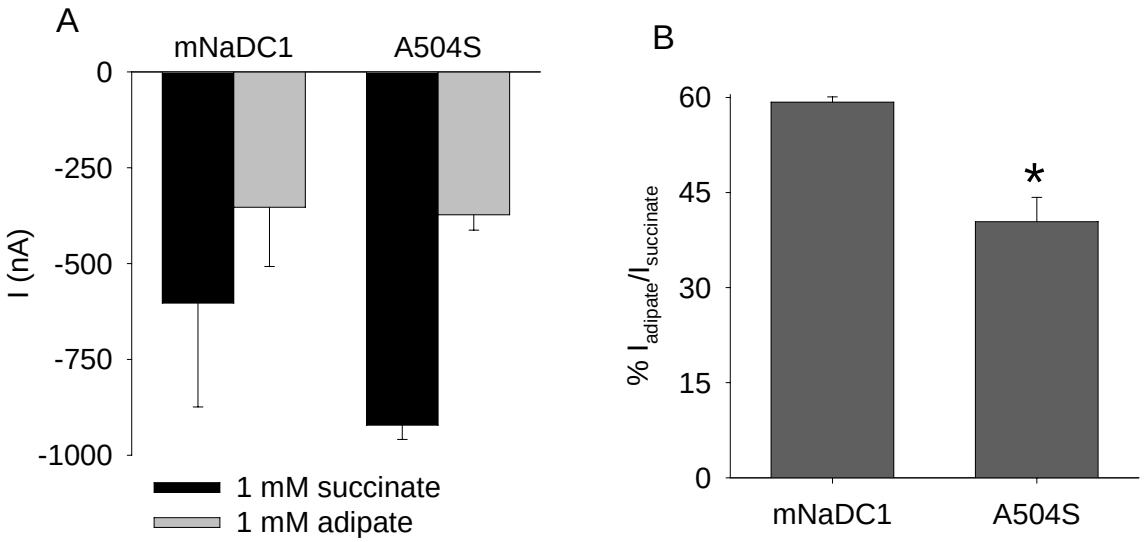

Figure 3.7 Substrate-dependent currents in the A504S mutant of mNaDC1. (A) Adipate- and succinate- induced currents measured at -50 mV with substrate concentrations of 1 mM. The bars represent mean ± SEM, n = 3 paired experiments. (B) Adipate-dependent currents expressed as a percentage of the succinate-dependent currents (from A). The A504S mutant is significantly different from the parental mNaDC1 transporter, $p < 0.05$.

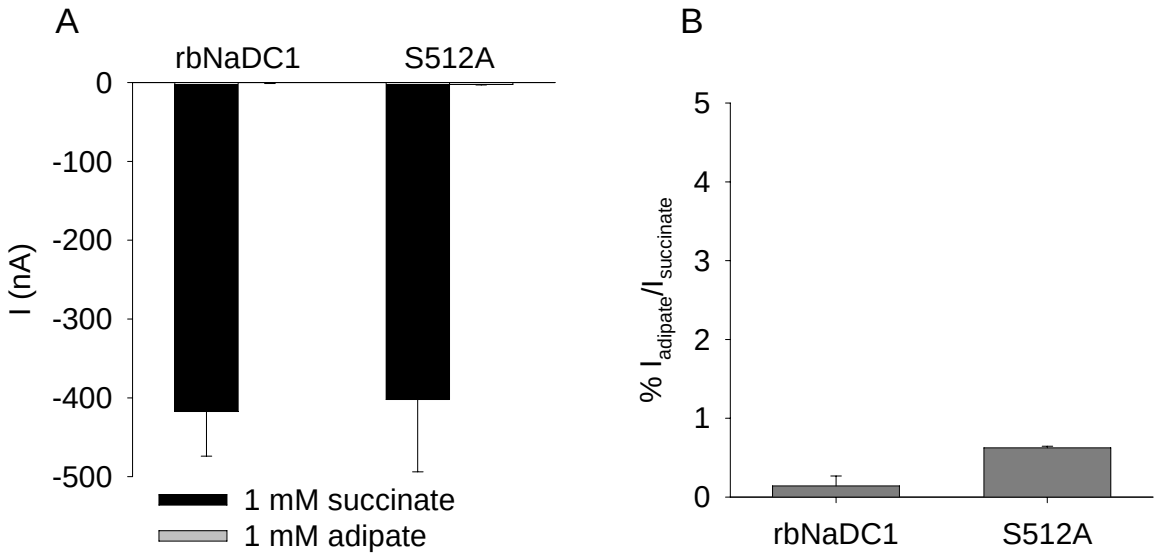

Figure 3.8 Substrate-dependent currents in the S512A mutant of rbNaDC1. (A) Adipate- and succinate- induced currents measured at -50 mV with substrate concentrations of 1 mM. The bars represent mean ± SEM, n = 9 for rbNaDC1 and mean ± range, n = 2 for the S512A mutant. (B) Adipate-dependent currents expressed as a percentage of the succinate-dependent currents (from A). The S512A mutant is no notable difference from the parental rbNaDC1 transporter.

The kinetics of the A504S mutant of mNaDC1 were examined with both adipate and succinate. This single mutation at position 504 resulted in increases in the $K_{0.5}$ for both adipate and succinate compared with the parental transporter, mNaDC1 (Figures 3.9 and 3.10). In the single experiment shown in Figure 3.9A, the $K_{0.5}^{adipate}$ for the A504S mutant was 1.25 mM and $I_{max}^{adipate}$ was -797 nA at -50 mV. In three experiments, the mean $K_{0.5}^{adipate}$ was 1.25 ± 0.04 mM (mean ± SEM, n = 3), significantly different from the mean $K_{0.5}^{adipate}$ of 0.7 mM in mNaDC1 (Figure 3.4). The voltage dependence of $K_{0.5}^{adipate}$ and $I_{max}^{adipate}$ are shown in Figure 3.9B, C (n=3 experiments). The $K_{0.5}^{adipate}$ gradually increased from 0.84 mM at -150 mV to 4.61 mM at +50 mV (Figure 3.9B). The $I_{max}^{adipate}$ was also voltage sensitive with almost a 5-fold increase in adipate-induced currents between +50 mV (-364 nA) and -150 mV (-1743 nA) (Figure 3.9C).

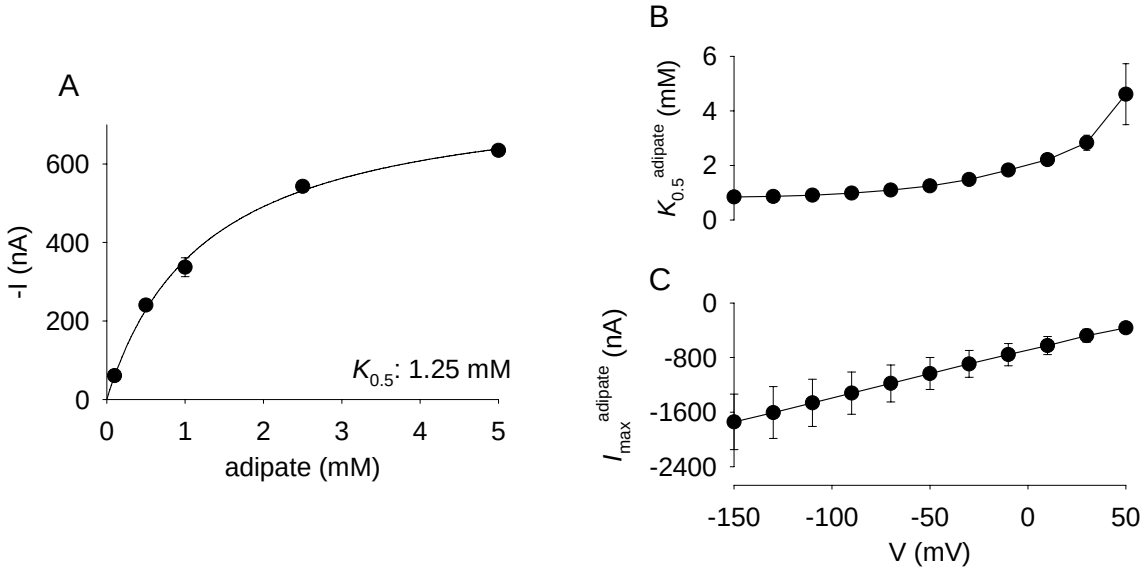

Figure 3.9 Adipate kinetics in oocytes expressing the mNaDC1-A504S mutant. (A) The concentration dependence of the steady-state adipate-induced currents at -50 mV in a single oocyte expressing the A504S mutant. Each data point represents mean ± range of duplicate measurements in a single oocyte. The adipate concentrations were between 0.01 mM and 2.5 mM. The $K_{0.5}$ for adipate is 1.25 mM and I_{max} is -797 nA. The voltage dependence of the (B) $K_{0.5}$ and (C) I_{max} for adipate. The data shown are mean ± SEM, n = 3 frogs.

Interestingly, the affinity for succinate in the mNaDC1-A504S mutant also changed. The A504S mutant had a $K_{0.5}^{succinate}$ of 291 μM and $I_{max}^{succinate}$ of -1319 nA at -50 mV in the single experiment shown in Figure 3.10A. The mean $K_{0.5}^{succinate}$ for this mutant was 270 ± 32 μM (mean ± SEM, n = 3), significantly different from 99 ± 15 μM for the parental mNaDC1 but similar to 203 ± 30 μM for rbNaDC1 as described previously in Chapter 2. The voltage dependence of $K_{0.5}^{succinate}$ was altered in the A504S mutant compared with the parental mNaDC1 (Figure 3.10B for A504S, Figure 3.11A for mNaDC1). The $K_{0.5}^{succinate}$ was relatively insensitive to voltage between -50 and +50 mV, but increased at more negative voltages (427 μM at -150 mV and 257 μM at +50 mV). The $I_{max}^{succinate}$ in the A504S mutant and mNaDC1 was sensitive to membrane potential

with an increase of about 6-fold between +50 (-331 nA) and -150 mV (-2118 nA) (Figure 3.10C for A504S, Figure 3.11B for mNaDC1).

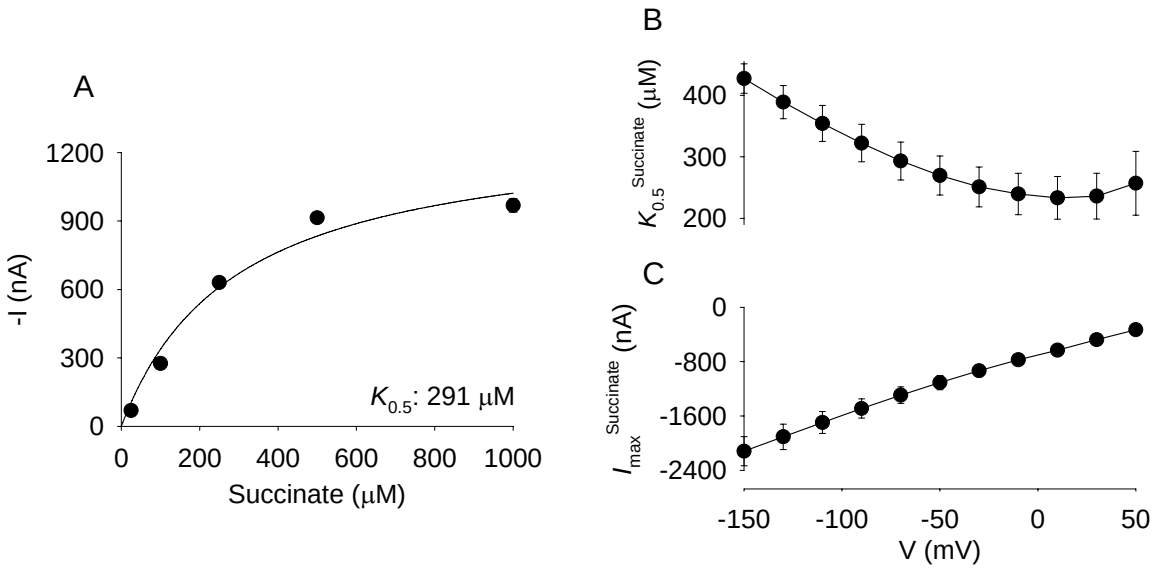

Figure 3.10 Succinate kinetics in the mNaDC1-A504S mutant. (A) Steady-state succinate-induced currents at -50 mV in the presence of different concentrations of succinate between 25 μM and 1 mM. Duplicate measurements in a single oocyte are expressed as mean ± range at each data point. The $K_{0.5}$ for succinate is 291 μM and I_{max} is -1319 nA. The (B) $K_{0.5}$ and (C) I_{max} for succinate at different voltages. The data shown are mean ± SEM, n = 3 frogs.

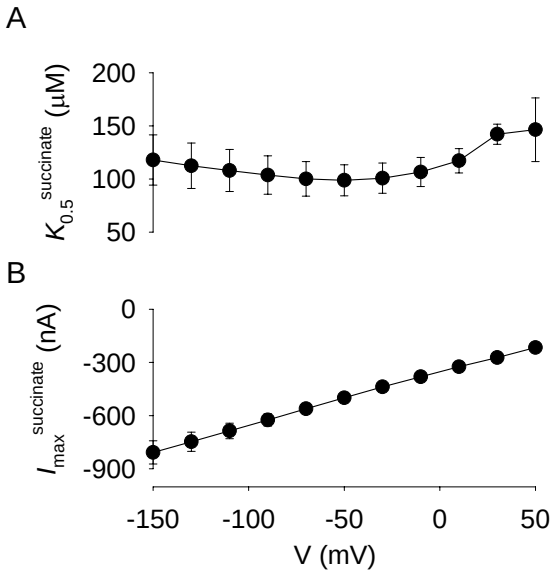

Figure 3.11 Voltage-dependence of $K_{0.5}^{succinate}$ and I_{max} in the mouse NaDC1 transporter. The voltage dependence of the (A) $K_{0.5}$ and (B) I_{max} for adipate. The data shown are mean ± SEM, n = 3 frogs.

DISCUSSION

The mouse and rabbit NaDC1 transporters differ in their ability to transport adipate, a six-carbon dicarboxylate. The mNaDC1 exhibits large adipate-induced inward currents whereas rbNaDC1 has no measurable currents in the presence of adipate. To identify protein domains involved in determining differences in adipate transport, a series of chimeras was constructed between mNaDC1 and rbNaDC1, and substrate-dependent currents were measured using two-electrode voltage clamp. I found that multiple transmembrane helices (TM) including TM 8, 9, and 10 are involved in adipate transport. Furthermore, the mNaDC1-A504S mutant exhibited changes in $K_{0.5}$ for both adipate and succinate, suggesting that Ala-504 in TM 10 is involved in recognition of both adipate and succinate in NaDC1.

The domains in NaDC1 involved in adipate transport are also involved in transport of other substrates. For example, the differences in the affinity for citrate between the human and rabbit NaDC1 are determined by residues in TM 7, 10, and 11 (38). Asp-373 in TM 8 is important in both substrate and cation binding, and exhibits differences in accessibility depending on conformational state (118). TM 9 and 10 appear to form part of the substrate translocation pathway in NaDC1 (71; 79). Interestingly, different TMs are involved in handling glutarate and adipate in NaDC1. TM 3-4 are the most important in determining differences between mNaDC1 and rbNaDC1 in the transport of glutarate, with some contributions also from TM 7 and 8 as described in Chapter 2.

One possible explanation for this difference could be that the preferred conformations of adipate and glutarate are different and bind to different protein domains. The preferred conformation in aqueous solution of the four-carbon succinate is planar with the dicarboxylate groups in *trans* conformation (66; 90). However, computational models of the structures of glutarate (5 carbons) and adipate (6 carbons) show that they are more complex than succinate (66). Although adipate can assume at

least five stable conformations in aqueous solution, the most stable conformation is planar with the dicarboxylates in *trans* conformation in (66). Glutarate adopts at least three stable conformations in aqueous solution, not all of which are planar, and the most stable has the dicarboxylates in *cis* conformation (66).

The mutation of alanine 504 in mNaDC1 to the serine found at the equivalent position in rbNaDC1 produced increases in the $K_{0.5}$ for both adipate and succinate. The wild-type rbNaDC1 exhibits very high discrimination between the two substrates since there were no currents induced by adipate. Although the decrease in adipate affinity in mNaDC1-A504S is approaching the rabbit phenotype, the discrimination between substrates has not increased, since the $K_{0.5}$ increased for both succinate and adipate. This result suggests that Ala-504 may be an important determinant of dicarboxylate binding but not of distinguishing between substrates. Possibly the interaction between Ala-504 and residues in TM 8 and 9 is required for discrimination between substrates. In contrast to the functional changes in the mNaDC1-A504S mutant, we observed no changes in the rbNaDC1-S512A mutant. In a previous study, the rbNaDC1-S512C mutant was not expressed on the plasma membrane, suggesting that a cysteine at this position produces a misfolded protein (79). In the present study, the rbNaDC1-S512A mutant had similar substrate-dependent inward currents as the wild-type rbNaDC1. Since multiple amino acids are likely to be required for the transport of adipate, changing a single residue in rbNaDC1 may not be enough to add function. In the mNaDC1, changing a single residue in the A504S mutant still leaves other residues in TM 8 and 9, with the result of reducing substrate affinity but not completely abolishing transport of adipate. However, I cannot completely rule out the possibility that the changes in $K_{0.5}$ for substrates in the mNaDC1-A504S mutant are due to indirect effects on the substrate binding site as a result of changes in overall protein structure or in the number of water molecules in the substrate binding pocket.

At present, the reason for the functional difference between alanine and serine in binding adipate in NaDC1 has not been determined. The size of alanine and serine

residues are not very different, 26.3 and 30.4 Å^3, respectively, and serine is thought of as a hydroxylated version of alanine (19). However, the hydroxyl group in serine renders it more hydrophilic than alanine. In addition, serine residues can introduce a bend angle into a transmembrane helix compared with alanine, which could potentially displace other residues (7). Serines have been shown to participate in substrate and cation binding in transport proteins. In the Na^+/sulfate transporter, also a member of the SLC13 family, serines are found at positions 260 and 288, whereas alanines are found at the equivalent positions in the dicarboxylate transporters. Mutation of these serines to alanine decreases affinity for sulfate and alters cation specificity (50). A similar involvement of serines in substrate and cation binding has been seen in the vesicular monoamine transporter, VMAT (63), the Na^+-Cl^--dependent serotonin transporter (103), and the Na^+/K^+-ATPase (10).

The voltage-dependence of adipate transport in the wild-type mNaDC1 is very similar to the voltage-dependence of succinate transport in other NaDC1 orthologs from rabbit, human (76; 117) and mouse (Figure 3.11) and in high-affinity NaDC3 orthologs from human, mouse and flounder (14; 75; 108). The maximal substrate-dependent inward current, I_{max}, increases with more negative voltages indicating that voltage-dependent steps are a general property of sodium-dependent transporters from the SLC13 family. This voltage dependence suggests that a rate-limiting step in the transport cycle involves translocation of negative charges through the electric field as the empty carrier reorients to face the outside of the cell (14; 26). The $K_{0.5}$ in these transporters is relatively insensitive to negative voltages, indicating that substrate binding is not affected by electric field, despite the fact that the substrates are divalent anions. Many of these transporters also exhibit an increase in $K_{0.5}$ at positive voltages. The voltage-dependence of adipate transport in the mNaDC1-A504S mutant is very similar to that of the wild-type mNaDC1. In contrast, the voltage-dependence of succinate transport in the mutant is different from the parental transporter, with an increase in $K_{0.5}^{succinate}$ as the voltage becomes more negative. A similar effect of voltage on $K_{0.5}$ has been observed for citrate binding in wild-type rat NaDC1 (18), the Na^+/Cl^-/GABA transporter (56), and the H^+-

coupled oligopeptide transporter (54). At least one of the cation binding sites and the substrate binding site appear to be located close together in the C-terminal half of NaDC1 (28), so it is possible that the A504S mutation may affect the voltage-dependent binding of Na^+ ions, leading to a change in voltage-dependence in $K_{0.5}^{succinate}$. Nevertheless, it is not clear why substitution of one neutral amino acid by another in the mNaDC1-A504S mutant should result in an alteration in voltage dependence of succinate binding but not adipate.

In conclusion, the mouse and rabbit NaDC1 exhibit differences in the transport of the six-carbon dicarboxylate, adipate. The mNaDC1 has adipate-dependent inward currents whereas rbNaDC1 exhibits no currents in the presence of adipate. The results of the chimera and mutagenesis studies show that the differences in adipate transport between mNaDC1 and rbNaDC1 are determined predominantly by Ala-504 found in TM 10, with contributions from residues in TM 8 and 9. Interestingly, the amino terminal half of mNaDC1 does not play a major role in adipate recognition, unlike our previous findings with glutarate transport described in Chapter 2 of this dissertation, although adipate and glutarate differ in length by only one carbon. I conclude that TM 8, 9 and 10 are involved in adipate transport in NaDC1. Ala-504 in TM 10 is an important determinant of dicarboxylate binding in the initial Michaelis complex, and other residues in TM 8 and 9 also participate in adipate recognition.

CHAPTER 4: FUNCTIONAL CHARACTERIZATION OF HIGH-AFFINITY Na^+/DICARBOXYLATE COTRANSPORTER FOUND IN *Xenopus laevis* KIDNEY AND HEART

(Studies in this chapter have been published and partially reproduced with permission from: Oshiro, N. and Pajor A. M. (2005) Functional characterization of high-affinity Na^+/dicarboxylate cotransporter found in *Xenopus laevis* kidney and heart, *American Journal of Physiology Cell Physiology 289*, C1159-C1168. Copyright 2005 American Physiological Society.)

INTRODUCTION

There is relatively little known about NaDCs in non-mammalian vertebrates. A type of NaDC3 that functionally resembles the NaDC3 from mammals has been cloned from winter flounder kidney (fNaDC3) (101). Also, the *Xenopus* NaDC1 (xNaDC1) transporter has been cloned from *Xenopus laevis* intestine (6). Recently, another member of the NaDC3 transporter has been identified from *Xenopus laevis*, designated xNaDC3. The amino acid sequence of xNaDC3 is approximately 70% identical to other mammalian NaDC3 transporters. The initial functional characterization using radiotracer assay reveals that the transport properties of xNaDC3 are similar to those of other NaDC3 orthologs. For, example, the K_m for succinate in xNaDC3 is about 5 μM, which falls into the range of 2–15 μM measured for rat NaDC3 in different expression systems (17; 40), and 2,3-dumethylsuccinate (2,3-DMS) and α-ketoglutarate are preferable substrates for xNaDC3 as well as mouse, human, rat, and flounder NaDC3 transporters (13; 17; 40; 75; 101; 108). For cation selectivity, the xNaDC3 transporter shows partial succinate transport when sodium is replaced with lithium, yet lithium does not inhibit succinate uptake in the presence of sodium by competing the same cation binding site with sodium, which is similar to mouse NaDC3 (75). Transport mediated by xNaDC3 is sodium-dependent as all other members of SLC13 family, and a likely transport stoichiometry is

3 Na^+:1 $succinate^{2-}$. However, the lithium activation of succinate uptake shows unique profile. The activation curve appears to be sigmoidal, but it cannot reach to plateau phase at the highest tested concentration of lithium. The expression of xNaDC3 mRNA is detected from not only kidney, intestine, and livers but also heart.

The NaDCs are electrogenic. Transport of one molecule of dicarboxylate with three sodium ions leaves one net positive charge inside the cell, which allows me to measure currents when dicarboxylates are being transported by NaDCs. By measuring steady state currents, there are two distinct currents that NaDCs mediate: substrate-induced currents and leak currents. The substrate-induced currents activated by translocation of fully loaded carrier proteins with three sodium ions and one dicarboxylate (Figure 1.4). The substrate-evoked currents in NaDCs are voltage dependent, showing larger inward currents at more negative membrane potentials (13; 14; 18; 75; 76; 85; 117). The leak currents are activated by substrate-uncoupled cation transport, involving translocation of cation-loaded carrier proteins. The leak currents in NaDCs are smaller than the substrate-induced currents (117). The cation-dependent substrate-independent leak currents are also specific to each transporter and not all membrane transporters exhibit. Previous reports for rat (r)and human (h) NaDC1 as well as other members of SLC families such as Na^+/glucose cotransporter (SGLT1), Na^+/phosphate cotransporter (NaPi-2), and thyroid Na^+/I^- symporters (NIS) show sodium-dependent substrate-uncoupled leak currents (18; 21; 25; 88; 117). Therefore, since xNaDC3 exhibits unique lithium activation curve of succinate uptake, it is interesting to investigate electrophysiological properties of xNaDC3 with comparison to other members of SLC13 family.

In this chapter, I performed initial functional characterization of the high affinity Na^+/dicarboxylate cotransporter from *Xenopus laevis* (xNaDC3) using the two-electrode voltage clamp (TEVC). The xNaDC3 exhibits large cation-activated leak currents with sodium and lithium, which affects the voltage-dependence of substrate-induced currents. Moreover, the leak currents are not carried by either sodium or lithium but may be carried

by anions. This finding suggests that xNaDC3 has unique electrophysiological properties compared with other members in SCL13 family and might have anion transport activity independent of substrate transport.

METHODS

Most methods are described in Chapter 2. For cation replacement experiments using the two-electrode voltage clamp, the test solutions of 1 mM succinate were prepared in a buffer containing either (in mM) 100 NaCl, 100 cholineCl, or 100 LiCl in this chapter. The sodium buffer was composed of (in mM) 100 NaCl, 2 KCl, 1 $MgCl_2$, 1 $CaCl_2$, and 10 HEPES, adjusted to pH 7.5 with 1 M Tris. Choline and lithium buffers contained 100 mM cholineCl or LiCl in place of NaCl. For the sodium buffers containing different concentrations of sodium to measure Na^+-activated leak currents, 100 mM NaCl was replaced by cholineCl. The lithium buffers for Li^+-activated leak currents were prepared as with the sodium buffers. The sodium concentrations were between 10 and 100 mM, and the lithium concentrations were between 5-100 mM. In chloride replacement experiments for Na^+-activated current in the absence of substrate, the NaCl was replaced with other sodium salts, NaBr, NaI, $NaNO_3$, NaSCN, and Na-gluconate. The solutions also contained (in mM) 6 Cl^- as 2 KCl, 1 $MgCl_2$, and 1 $CaCl_2$ to minimize liquid junction potentials with a use of agar bridge as a reference electrode. In chloride replacement for Li^+-activated currents without substrate, the test solution was Cl^- free by replacing the LiCl with lithium acetate, and 2 mM KCl, 1 mM $MgCl_2$, and 1 mM $CaCl_2$ with 4 mM K^+-, 2 mM Mg^{2+}-, and 2 mM Ca^{2+}-gluconate. In the voltage-clamp experiments, each oocyte was superfused with Na^+, Li^+, or choline containing buffer, and the voltage pulse protocol was applied. Substrate-induced currents were measured in the same cation buffer containing 1 mM succinate.

RESULTS

Electrophysiological measurements

The function of xNaDC3 was assessed by TEVC of *Xenopus* oocytes injected with xNaDC3 cRNA. In the absence of substrate, sodium and lithium-dependent leak currents were measured in oocytes expressing xNaDC3. Figure 4.1A-C shows currents in an individual oocyte expressing xNaDC3 in the presence of different cation-containing solutions, with or without 1 mM succinate. The summary results from five different experiments are shown in Figure 4.1D and E. The cation-evoked currents are largest in lithium, followed by sodium (Figure 4.1D). The difference between currents measured in sodium or Li vs. choline, abbreviated Ch, ($I_{Na} - I_{Ch}$ or $I_{Li} - I_{Ch}$) represents the cation-induced leak current. The leak currents are not seen in control, uninjected oocytes (Figure 4.2A), similar to what we reported previously (117). The total succinate-dependent currents in different cations are shown in Figure 4.1E (xNaDC3-injected oocytes) and Figure 4.2B (control oocytes). These currents are calculated from the difference in the presence and absence of substrate for a given cation (for example, $I_{succinate+Na} - I_{Na}$). The small outward current seen in choline with substrate is also present in control oocytes, and thus probably represents succinate inhibition of an endogenous current. There were outward-directed substrate-dependent currents in lithium in xNaDC3. The corresponding currents in control oocytes are much smaller. A previous study has reported similar outward currents in substrate and lithium in oocytes expressing mouse NaDC3 (75). These lithium and substrate-dependent outward currents probably represent inhibition of the lithium-induced leak current by substrate, although this remains to be tested in more detail. There may also be a small Li^+/succinate cotransport current but it is obscured by the larger leak current. The substrate-dependent measurements in sodium probably represent a combination of the activation of Na^+/succinate cotransport currents and inhibition of the Na^+-leak current. This produces an inward current that appears independent of voltage (Figure 4.1E). However, a more accurate estimate of Na^+/substrate cotransport current is shown in Figure 4.3A.

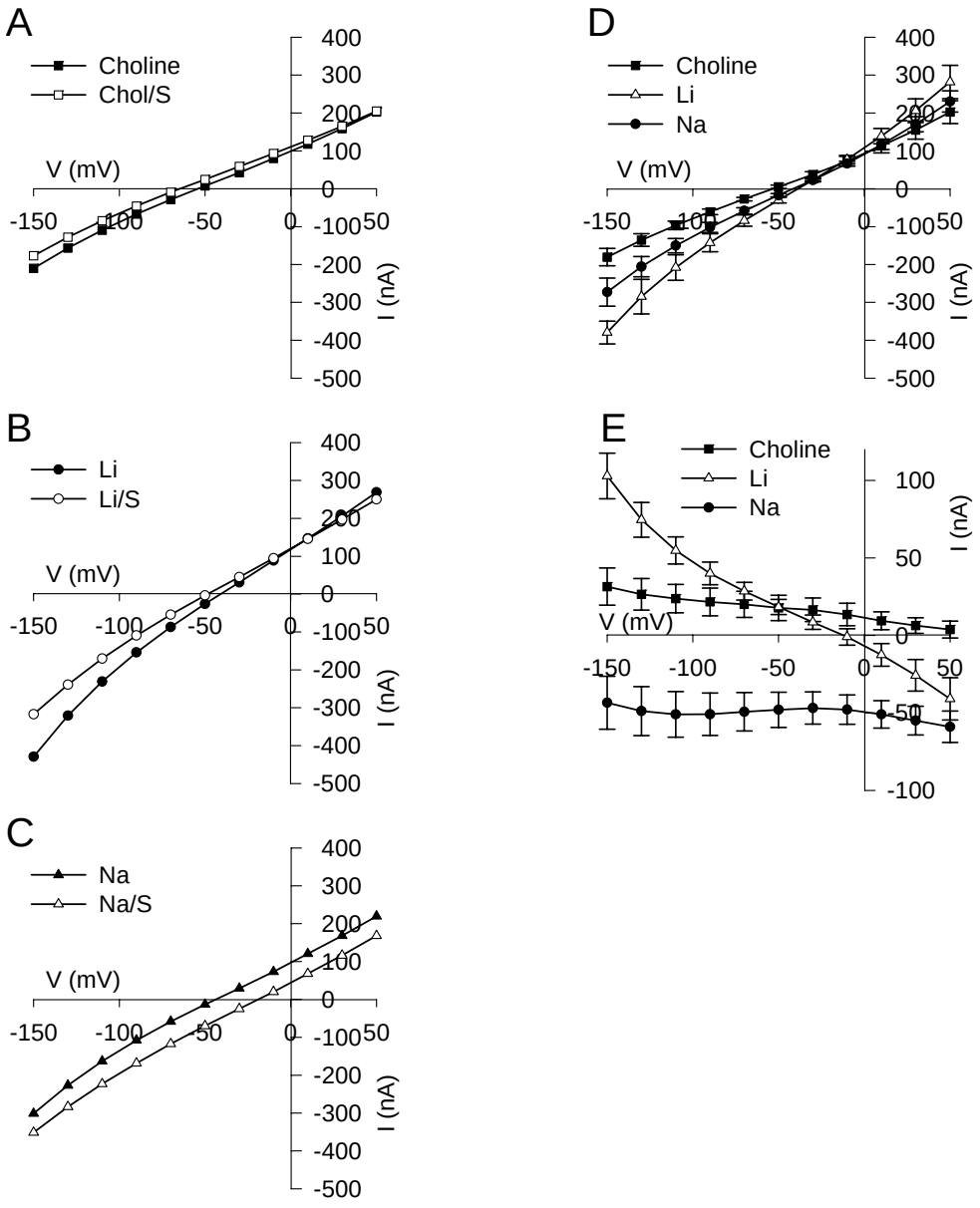

Figure 4.1 Voltage dependence of substrate and cation-dependent currents in Xenopus oocytes expressing xNaDC3. A–C: currents in the presence and absence of 1 mM succinate (S) in a single oocyte expressing xNaDC3 superfused with choline (A), lithium (B), or sodium (C) buffers. (D) Summary of currents in oocytes expressing xNaDC3 superfused with choline-, lithium-, or sodium-containing buffers. (E) Total succinate-dependent currents in oocytes expressing xNaDC3, calculated from the difference between currents in the presence and absence of 1 mM succinate in buffers containing choline, lithium, or sodium. Data are means ± SE from 5 separate batches of oocytes.

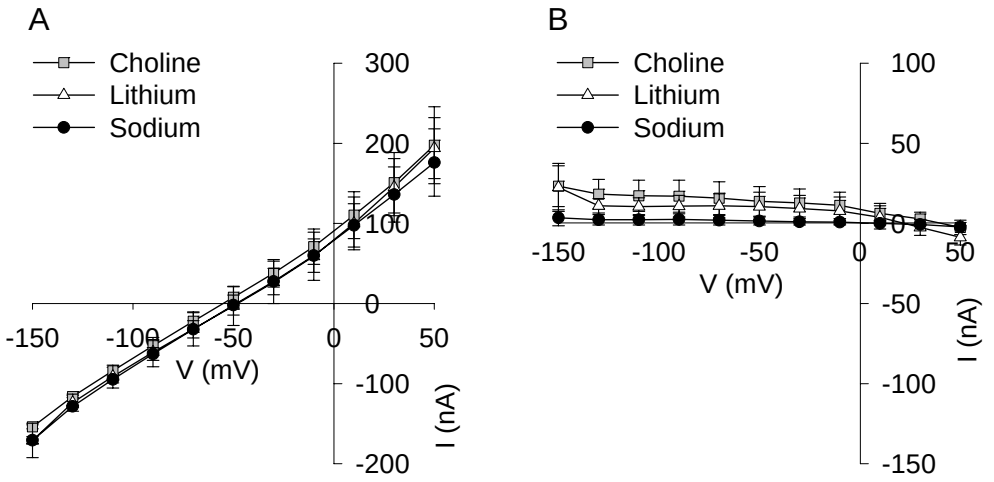

Figure 4.2 Cation and substrate-dependent currents in control, uninjected oocytes. (A) Steady-state currents in oocytes superfused with choline, lithium, or sodium (compare with Figure 4.1D). (B) Succinate-dependent currents in control oocytes, calculated from the difference between currents in the presence and absence of 1 mM succinate in buffers containing choline, lithium, or sodium. Data are means ± SE, n = 3.

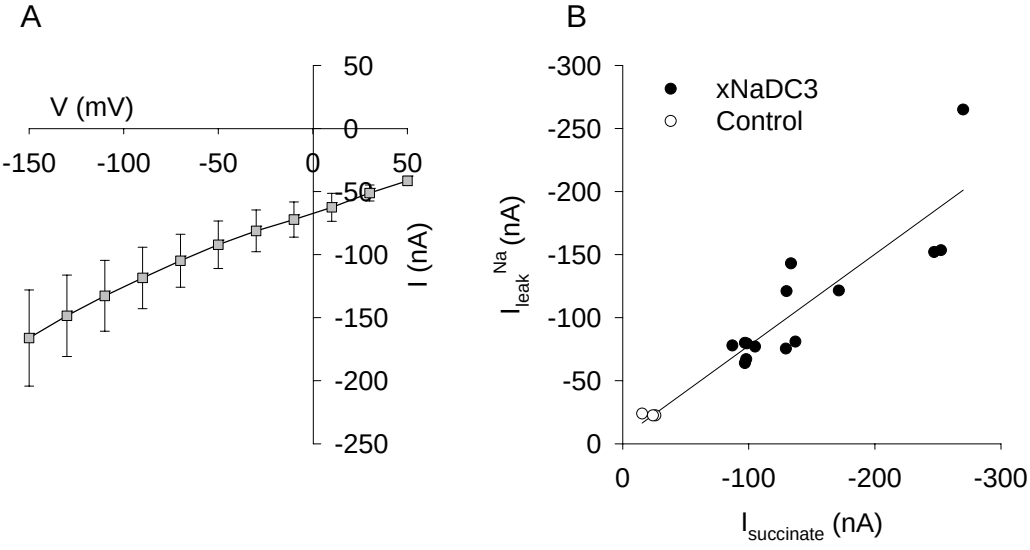

Figure 4.3 Voltage dependence of succinate-dependent currents in oocytes expressing xNaDC3. (A) The succinate-dependent currents are calculated from the difference between currents in sodium + 1 mM succinate and currents in choline because of the large leak current activated by sodium, which should have the smallest leak current. Data are means ± SE of oocytes from 5 batches of oocytes. (B) Relationship between substrate-dependent currents and Na^+-induced leak current at –150 mV in control oocytes or oocytes expressing xNaDC3.

The substrate-dependent current in xNaDC3 was determined from the difference between current in sodium + succinate and the current in choline. Because control oocytes have similar currents in sodium and choline, the current measured in choline in xNaDC3 injected oocytes probably represents the baseline current. This current-voltage relationship resembles those of the other members of the SLC13 family (14; 76). The magnitude of the leak currents induced by sodium or lithium are a linear function of the amount of expression of xNaDC3 (Figure 4.3B), which supports the hypothesis that the leak currents are a property of xNaDC3.

I then tested the concentration dependence of the Na^+-activated (Figure 4.4) and Li^+-activated (Figure 4.5) leak currents. The leak currents were determined from the difference between currents in Na^+ or Li^+ and choline (see total currents in Figure 4.1D). The reversal potentials in both sodium and lithium were independent of cation concentration, although the magnitude of the currents changed with cation concentration (Figures 4.4A and 4.5A). The reversal potentials were approximately –5 to –10 mV. This result suggests that the cations activate a current but do not carry it. The kinetics of Na^+-activated and Li^+-activated leak currents were hyperbolic (Figures 4.4B and 4.5B), rather than sigmoidal, suggesting that there is a single binding site for leak current activation. In contrast to the low affinity for sodium or lithium activation of transport, the $K_{0.5}$ for activation of the leak current was ~20 mM for Na^+ and 15 mM for Li^+. The $K_{0.5}$ for the activation was relatively insensitive to voltage, but the maximum current induced by cations was sensitive to voltage (Figures 4.4C and 4.5C).

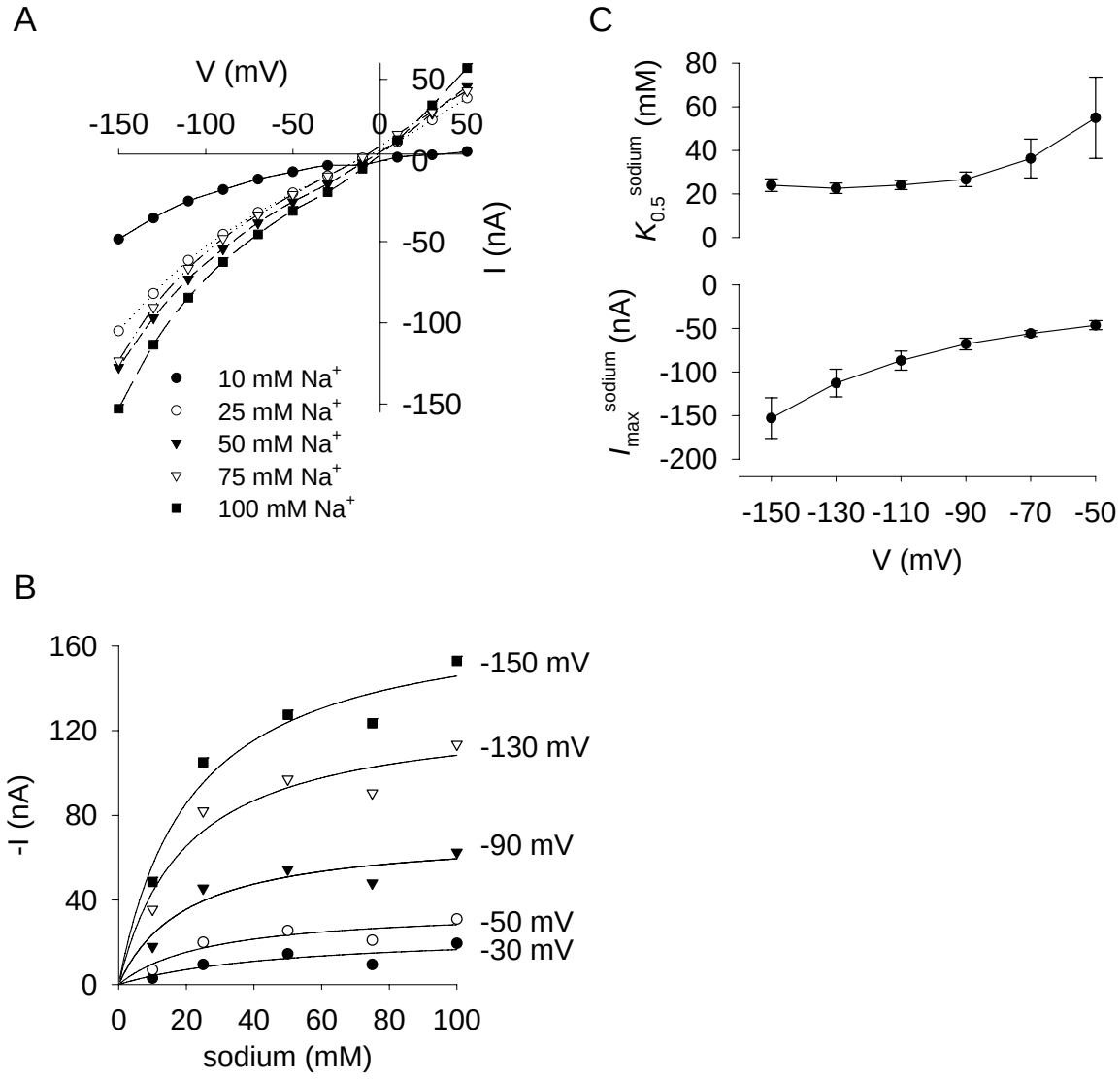

Figure 4.4 Sodium-activated leak currents associated with xNaDC3 expression in oocytes. (A) Voltage and concentration dependence of sodium-activated currents in a single oocyte expressing xNaDC3. (B) The data from A replotted as a function of sodium concentration. (C) Voltage dependence of $K_{0.5}$ (top) and maximum current (I_{max}; bottom) for leak currents activated by sodium in oocytes expressing xNaDC3. Data are means ± SE, n = 5.

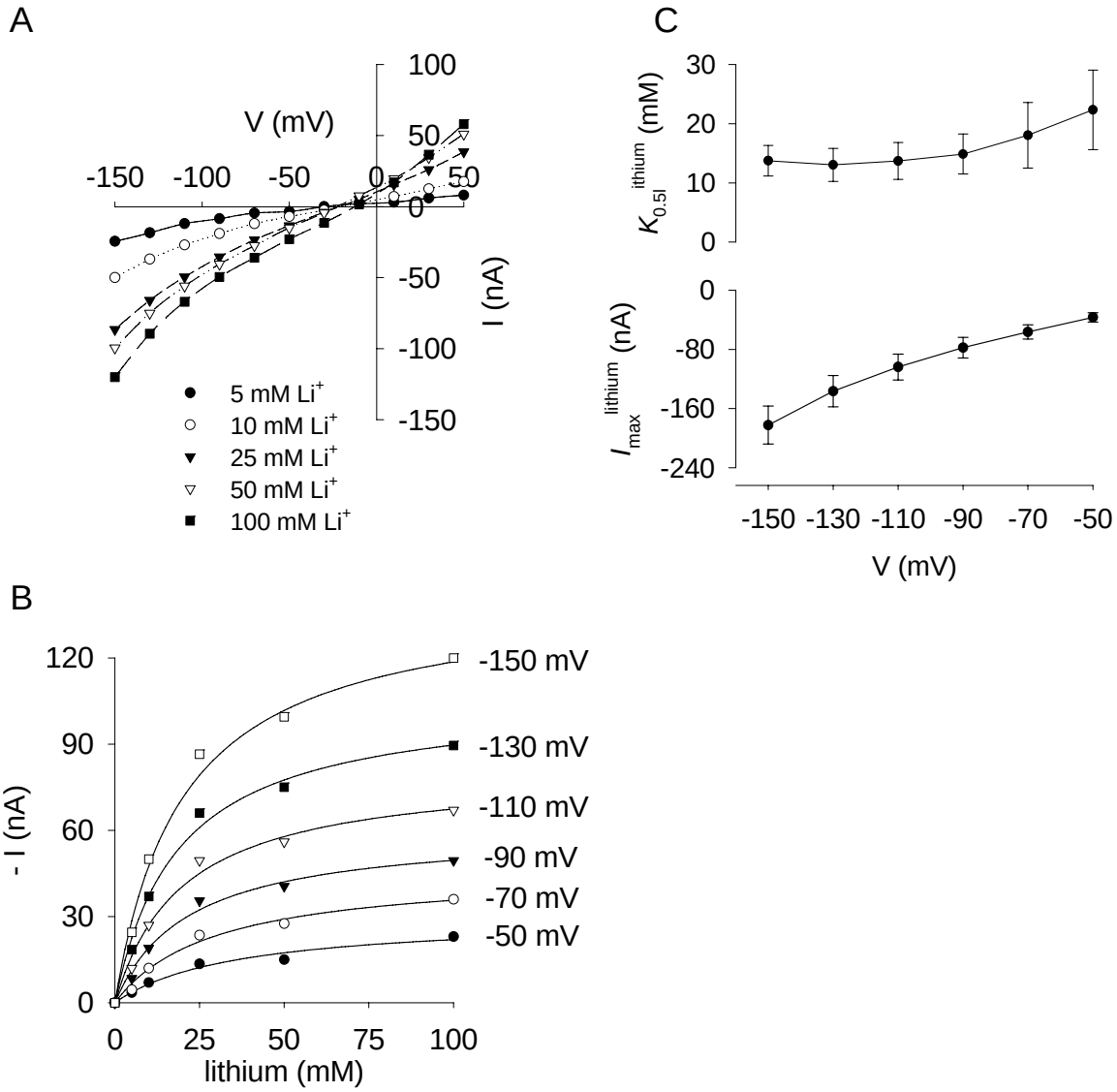

Figure 4.5 Lithium-activated leak currents associated with xNaDC3 expression in oocytes. (A) Voltage and concentration dependence of lithium-activated currents in a single oocyte expressing xNaDC3. (B) The data from A replotted as a function of sodium concentration. (C) Voltage-dependence of $K_{0.5}$ (upper panel) and I_{max} (lower panel) for leak currents activated by lithium in oocytes expressing xNaDC3. The data represent mean ± SEM, n=5.

I further investigated whether the leak currents in xNaDC3 are sensitive to Cl^- replacement. The reversal potential for Cl^- in *Xenopus* oocytes in 96 mM extracellular Cl

is approximately –22 to –25 mV (22). Note that the total currents in different anions were determined, rather than the difference between sodium and choline as in Figure 4.4 because different choline salts are not available. As shown in Figure 4.6, replacement of NaCl by Na^+-gluconate had no effect on the inward currents but reduced the outward currents by approximately 50%, suggesting that at least part of the leak current may be carried by anions. A similar result was seen with replacement of LiCl by Li-acetate (Figure 4.7). Substitution of NaCl with NaBr, NaI, $NaNO_3$, and NaSCN resulted in a negative shift of the reversal potential, leading to a general anion selectivity sequence of $SCN^- > NO_3^- = I^- > Br^- > Cl^- > Gluconate^-$ (Figure 4.6).

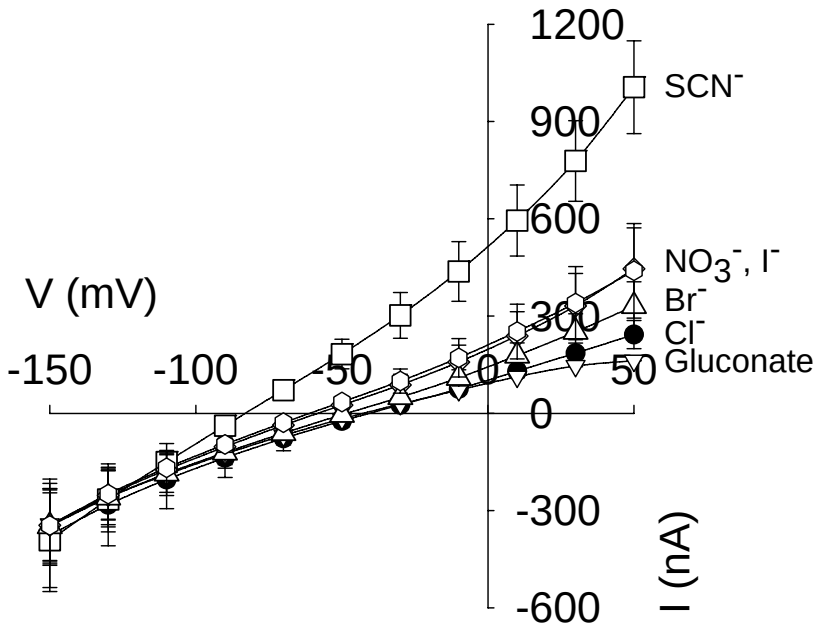

Figure 4.6 Anion-induced currents in oocytes expressing xNaDC3. Oocytes were superfused with bath solutions containing 100 mM sodium salts of different test anions (shown to the right of each curve). Each solution also contained a total of 6 mM Cl^- as KCl, $MgCl_2$, and $CaCl_2$. The data points show the mean ± range or SEM (n=2 (gluconate) or 3 different donor frogs).

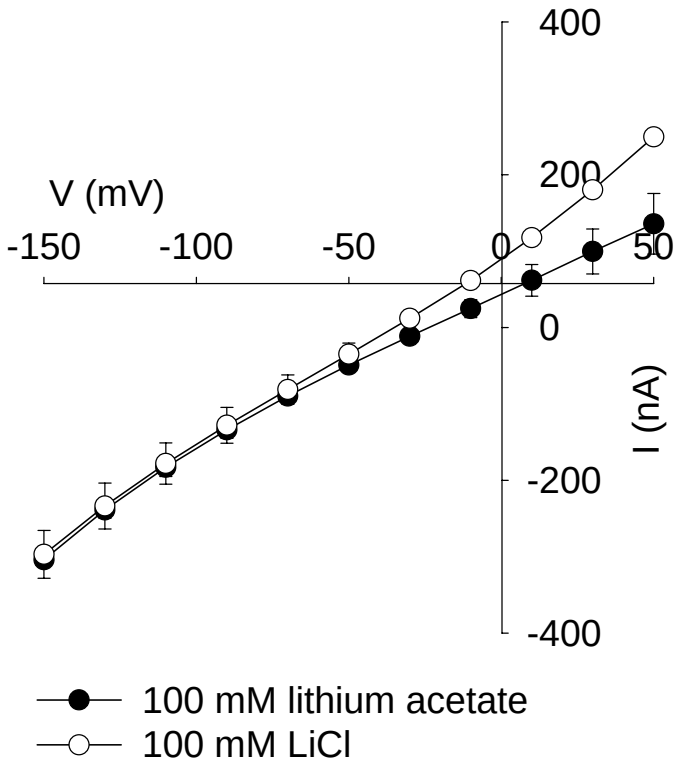

Figure 4.7 Chloride replacement for Li^+-activated currents in oocytes expressing xNaDC3. Li^+-activated currents in the absence of substrate were measured and compared with the currents with LiCl. In the Cl^- free solution, LiCl was replaced with lithium acetate, and other chloride ions were substituted with gluconate. Oocytes were superfused with bath solutions containing 100 mM LiCl and lithium acetate. The data points show the mean ± range, n = 2.

DISCUSSION

Despite the fact that the transport properties of xNaDC3 are very similar to those of other NaDC3 orthologs, the electrophysiological properties of xNaDC3 have some differences. The presence of sodium or lithium activates large leak currents in xNaDC3 that appear to be inhibited by substrate. The leak currents are not carried by sodium or lithium, as shown by their reversal potential that is independent of the cation concentration. The results of the anion replacement experiments are consistent with at

least part of the current being carried by anions, such as Cl^-. The general anion permeability sequence was $SCN^- > NO_3^- = I^- > Br^- > Cl^- > Gluconate^-$. Unlike the activation of substrate-dependent transport, which involves multiple cations, the activation of the leak currents likely involves binding of sodium or lithium to a single site, which has a higher affinity than the coupled-transporter cation binding sites. The half-saturation constant for Na^+ or Li^+ for activation of the leak was about 15–20 mM, compared with about 50 mM for uptake of succinate.

As shown in Figure 1.4, the substrate-induced currents are activated by translocation of NaDC proteins in which all of sodium binding sites and a substrate binding site are occupied prior to the translocation (states 5). As the fully loaded protein orients inwardly to the face intracellular space, one positive net change movement takes place (Stage 6). This positive charge flow from the outside to the inside of the cell generates currents, call substrate-induced currents. The substrate-induced currents in NaDCs are voltage dependent. Therefore, when a membrane potential is hyperpolarized, NaDC mediated inward currents increase (13; 14; 18; 75; 76; 85; 117).

The NaDCs also show cation-dependent leak currents activated by cation transport independent of substrate translocation, and inhibited by substrate. The substrate-uncoupled leak currents are generated by translocation of cation-loaded carrier proteins (Figure 1.4, states 2 and 9). The leak currents observed in NaDCs are smaller than the substrate-induced currents (117). The cation leak current is not a general characteristics of membrane transport protein. Depending on a change in net charge movement, magnitude of leak alters. Therefore, the specific leak currents are detected on different proteins. The rat (r) and human (h) NaDC1 transporters have been reported to exhibit cation-dependent leak currents (18; 117). Also, other membrane transport proteins from different gene families show leak current with the similar mechanism to NaDCs. The Na^+/glucose cotransporter (SGLT1), Na^+/phosphate cotransporter (NaPi-2), and thyroid Na^+/I^- symporters (Na^+/I^+ symporters)(21; 25; 88). Some of the GABA transporters, such as GAT1 and GAT3, exhibit leak currents in lithium, which also represent partial

reactions of the transporter, uncoupled to substrate (29; 53; 55). A different type of current is seen in the Na^+/glutamate transporters, such as EAAT1, which exhibit chloride channel activity in the presence of substrate (107).

The leak currents in xNaDC3 are very different from those seen in other Na^+-coupled transporters. The xNaDC3 mediated leak currents do not appear to be carried by sodium or lithium, and they are not activated by substrate, which makes them very different from previously reported leak currents in other transporters. The currents measured in xNaDC3 in the presence of substrate and cation are consistent with a mixture of activation of cation/substrate cotransport current and inhibition of the cation-dependent leak current. In lithium, the leak current is predominant. In sodium, the Na^+/substrate cotransport current is larger than in lithium and the leak current is smaller. Therefore, currents in the presence of substrate appear to be inward but independent of voltage. When choline is used to estimate the substrate-dependent current, however, the voltage dependence resembles that of other NaDC transporters. Since the leak currents of xNaDC3 might be carried by anions independent of substrate transport, xNaDC3 may have channel-like activity as in EAAT1 although this needs to be tested.

In short, because of its unusual cation dependence on substrate transport, which is addressed in the primary functional characterization by radiotracer assay, the study in this chapter has identified electrophysiological properties of the high affinity Na^+/dicarboxylate cotransporter from *Xenopus laevis*, xNaDC3. The electrophysiological properties of xNaDC3 are unique and exhibit large leak currents that are activated by sodium and lithium to the same extent. However, sodium and lithium do not carry the leak current. The result of chloride replacement suggests that xNaDC3 may carry anions independently of substrate.

CHAPTER 5: CONCLUSIONS

THE Na^+/DICARBOXYLATE COTRANSPORTERS IN THE SLC13 GENE FAMILY

The Na^+/dicarboxylate cotransporters (NaDCs) are members of the SLC13 gene family in human gene nomenclature. Two isoforms of NaDCs have been identified, and they are coded for two genes, SLC13A2 and SLC13A3 (74). SLC13A2 codes for the low affinity Na^+/dicarboxylate cotransporter designated NaDC1, and SLC13A3 codes for the high affinity Na^+/dicarboxylate cotransporter named NaDC3. The major differences between NaDC1 and NaDC3 can be found in their affinity for substrates, tissue distribution, and cellular localization in addition to the amino acid sequences (Table 1.1). The NaDC1 transporter has a K_m for succinate about 0.8 mM in human NaDC1 (hNaDC1) (69), and is expressed on the apical membrane of the epithelium in renal proximal tubules and small intestine (18; 94). The NaDC3 transporter has higher affinity for dicarboxylates than NaDC1, evidenced by approximately 20 μM of the K_m for succinate in human NaDC3 (hNaDC3) (108), and is detected on the basolateral membrane of renal proximal tubule epithelial cells, brain, liver, and placenta (17; 31; 40; 75). The studies in this dissertation were conducted on the basis of two different research interests of each isoform: the identification of transmembrane helices (TM) and amino acid residues responsible for different substrate specificity between the mouse and rabbit NaDC1 transporters, and functional characterization of *Xenopus laevis* NaDC3 using the two-electrode voltage clamp.

TRANSMEMBRANE HELICES AND AMINO ACID RESIDUES RESPONSIBLE FOR DIFFERENT SUBSTRATE SPECIFICITY BETWEEN THE NaDC1 TRANSPORTERS

The mammalian NaDC1 orthologs show more than 70% identity in amino acid sequences. However, there are also differences in functional properties with respect to substrate specificity. The previous studies done by Pajor and her colleagues found that mouse NaDC1 (mNaDC1) and rabbit NaDC1 (rbNaDC1) transport some dicarboxylates differently such as α-ketoglutarate and 2,3-dimethylsuccinate (2,3-DMS) (72; 76; 85). These dicarboxylates are longer and bulkier than succinate (Figure 1.2). Despite the evidence that there are differences in substrate specificity between the NaDC1 orthologs, the structures responsible for functional differences are very limited. Under the two-electrode voltage clamp (TEVC) condition, the preliminary screening for substrate specificity in mNaDC1 and rbNaDC1was performed using dicarboxylates tested previously in the different experimental conditions. At -50 mV, mNaDC1-expressing oocytes exhibit large substrate-induced currents relative to succinate-dependent currents with all tested substrates. On the other hand, oocytes expressing rbNaDC1 have little currents with glutarate, α-ketoglutarate, and 2,3-DMS, and there are no detectable currents with adipate. Therefore, Chapters 2 and 3 in this dissertation focused on the identification of transmembrane helices (TM) and amino acids responsible for differences in glutarate and adipate transport between the mouse and rabbit NaDC1 transporters.

Glutarate and adipate recognition in wild-type NaDC1 transporters

The studies were performed using an electrophysiological approach as well as dual label competitive uptake assay to detect changes in relative substrate specificity. Using a series of NaDC1 chimeras constructed between mNaDC1 and rbNaDC1, I found that the chimeric transporters containing more potion of mNaDC1 at the N-terminus show more glutarate- and adipate-induced currents relative to succinate-dependent

currents. These results point to TMs that are involved in glutarate-and adipate-induced currents such as a region of TM 3-4, 7, and 8 of mNaDC1 for glutarate and that of TM 8, 9, and 10 for adipate due to changes observed in the ratio of substrate-dependent currents in the tested chimeras. However, the gradual increases in glutarate- and adipate-dependent currents in the chimeras imply that other TMs in the protein which did not show increases in the ratio of substrate-induced currents are also involved in glutarate and adipate transport by interacting with those TMs showing changes in the ratio of substrate-evoked currents.

To extend the kinetic data reflecting substrate binding at the initial Michaelis complex to the transition state carrier-substrate complex in the transport process, a new experimental approach proposed by King, called the Transport Specificity Ratio (TSR), was employed in this dissertation (41). The strength of TSR analysis is that TSR is a protein expression-independent constant reflecting a difference in substrate affinity for two competing substrates in their transition states. Unless kinetic parameters for two substrates are measured in the same oocyte, comparison of a catalytic efficiency, k_{cat}/K_m, for the two substrates is not relevant due to the lack of information for protein expression. For this respect, measuring uptake activity for two competing substrates in the same oocyte rules out the concern for protein expression level. Also, TSR is substrate concentration independent. Lastly, TSR can provide information on the changes in binding energy ($\Delta\Delta G_b$) between two competing substrates in their transition states, which further contributes to detection of intramolecular interaction without crystallography. Nevertheless, there are also a few limitations for TSR analysis. The uptake activity of two competing substrates by transporters needs to be at least three times higher than that by the control expression system. For this respect, when background uptake is high in a control as observed in ^{14}C-adipate uptake in uninjected oocytes, TSR values cannot be accurate. Also, when mutants of chimeras show low uptake activities, accurate TSR cannot be calculated. Also, independence of substrate concentrations in TSR values is valid when concentrations of two substrates are less than K_m and result in at least three

times higher uptake compared to the control. Finally, availability of proper radiotracer can be a problem.

In my study, the chimeras incorporating each TM 3, 4, and 3-4 of mNaDC1 into rbNaDC1 were tested by TSR analysis using both ^{3}H-succinate and ^{14}C-glutarate. Addition of mNaDC1 segments to rbNaDC1 significantly increases TSR values, suggesting that both regions of TM 3 and TM 4 of mNaDC1 appear to be involved in determination of relative glutarate specificity in mNaDC1. There is another important finding addressed by the results of the TSR analysis: TM 3 and TM 4 of mNaDC1 are functionally interacting in the transition state complex. Based on the equation described by Wells, when there is a functional coupling between positions x and y, the sum of the free energy change caused by a single mutation x and y is not equal to that by double mutations xy, expressed as $\Delta\Delta G(xy) \neq \Delta\Delta G(x) + \Delta\Delta G(y)$ (110). Wells's thermodynamic equation is explained using only one substrate. However, the principle of this idea has been adapted into a two-substrate circumstance as in TSR analysis by calculating differences between $\Delta\Delta G_b$ for rbNaDC1 and the R(M3-4), R(M3), and R(M4) chimeras, expressed as $\Delta(\Delta\Delta G_b)$. It is obvious that the sum of $\Delta(\Delta\Delta G_b)$ for the single-TM substituted chimeras, R(M3) and R(M4), is not equal to that for the double-TM substituted chimera, R(M3-4) (Table 2.1). Therefore, the amino acid residues in the regions of TM 3 and TM 4 of mNaDC1 are likely to couple functionally. Also, the intramolecular interaction between TM 3 and 4 of mNaDC1 and other TMs of rbNaDC1 shown as $\Delta(\Delta\Delta G_b)$ in this study is about ten times smaller than the energy of a single hydrogen bond.

Although TSR analysis cannot be used for adipate recognition studies in Chapter 3 due to the high background of ^{14}C-adipate in control oocytes, I found that multiple TMs, TM 8, 9, and 10, participate in adipate-induced currents. However, TMs involved in adipate-evoked currents are not the same as those of glutarate-induced currents. In particular, the N-terminal half of the protein is not required for adipate-dependent inward

currents unlike glutarate. Based on the results in the chimera studies, mutagenesis in TM 10 was performed. The alanine residue at position 504 in mNaDC1 was mutated to serine found at equivalent position in rbNaDC1. The A504S mutant leads to significant decrease in adipate-dependent currents and increase in $K_{0.5}^{adipate}$. The change in $K_{0.5}$ in the A504S mutant is also seen with succinate. Therefore, Ala-504 may be an important residue for dicarboxylate binding but not for discriminating between adipate and succinate binding. Structurally, serine residues can introduce alterations by bending TMs, which could displace other TMs and residues (7). The rearrangement of TMs due to a single mutation was also seen in the hexose transporter from *Plasmodium falciparum*, a homolog of the mammalian facilitative glucose transporter (GLUT1). A single mutation in TM 5 appears to displace TM 4 away from the recognition site and the substrate permeation pathway. This new TM arrangement is assumed to change a hydrogen bond that inhibits the binding of fructose (58). Therefore, a hydroxyl group in the serine residue in the A504S mutant might lead to change in electrostatic environment in the protein by creating hydrogen bonds with other residues, resulting in decrease in affinity for dicarboxylate binding.

A considerable change in the voltage dependence of $K_{0.5}^{succinate}$ was observed in the A504S mutant showing steep increase in the range of negative potentials. By contrast, the $K_{0.5}$ for succinate in the parental mNaDC1 transporter is relatively voltage-insensitive during hyperpolarization. The reason for the change in voltage-dependence of $K_{0.5}$ for succinate in the A504S mutant needs to be studied further. Based on a previous study in NaDC1, at least one of cation binding sites appears to be located close to the substrate binding site in the C-terminal half of the protein (28). Additionally, a recent crystal structure of the Na^+/Cl^--dependent leucine transporter from *Aquifex aeolicus* revealed that one of two sodium ions in the binding pocket interacts with the leucine carboxy oxygen through an ionic bond (116). This result suggests that changes in sodium binding may affect stable binding of leucine. It can be hypothesized, therefore, that the mutation of A504S may change the voltage-dependent binding of sodium ions, leading to a change in voltage-dependence of succinate binding. However, I do not know why the

change in voltage-dependence of $K_{0.5}$ in the A504S mutant is seen with only succinate but not adipate although the apparent affinity for both adipate and succinate decreased due to the A504S mutation.

The studies in both Chapters 2 and 3 show an involvement of multiple TMs in substrate transport or substrate-induced currents. Multiple TMs have also been reported to participate in substrate recognition in other membrane transport proteins. For example, atomic resolution crystal structures of three bacterial transporters show multiple TMs throughout the proteins form substrate translocation pathway (1; 32; 116). In the translocation pathway, multiple amino acid resides project into the aqueous pore to interact with the substrates and ions through electrostatic interaction such as hydrogen bonds. The yeast hexose transporters (Hxt) and mammalian facilitative glucose transporters (GLUTs) also show multiple TMs and amino acids involved in determination of substrate affinity and specificity (12; 39; 59; 114). Therefore, my findings of multiple TM contribution to glutarate- and adipate-evoked currents are in agreement with these previous findings in the membrane transport proteins. Moreover, the involvement of different TMs to recognize different substrates, which is the case of glutarate and adipate, has been reported using glucose and fructose in GLUTs (12; 114). In conclusion, amino acid residues from multiple TMs are necessary to create a perfect fit with a substrate, leading to an efficient transport activity.

Electrophysiological properties of the high affinity Na^+/dicarboxylate cotransporter

Isolation and functional characterization of NaDC3 have been performed using radiotracer assay and the two-electrode voltage clamp (TEVC) in the last decade. However, there is only one report for the NaDC3 transporter isolated from non-mammalian vertebrates (101). Recently, a new member of NaDC3 was found from *Xenopus laevis*, designated as xNaDC3. The sequence alignment and the initial functional characterization of xNaDC3 by radiotracer uptake show similar properties to other members of NaDC3. The xNaDC3 transporter is an electrogenic transporter as with

other members in the SLC13 family, with a transport stoichiometry of 3 Na^+: 1 dicarboxylate (70; 73; 74). However, different characteristics were found in the unique tissue distribution and lithium activation of succinate uptake. The succinate transport is stimulated by lithium, but the uptake does not reach a plateau phase at the highest tested concentration of lithium. Since xNaDC3 has an unusual transport activity of succinate in the presence of lithium, in Chapter 4 of this dissertation, electrophysiological properties of xNaDC3 was investigated using TEVC with *Xenopus* oocyte expression system.

The major findings in Chapter 4 are the xNaDC3 transporter has large cation-activated leak currents in the presence of sodium and lithium, which appears to be inhibited by substrate. In addition, the cation-activated leak currents in xNaDC3 are neither carried by sodium nor lithium but may partially anions such as chloride. In general, the leak currents in transporters are triggered by substrate-uncoupled cation transport due to a higher affinity for the cation to the binding sites in the protein in the absence of substrate. However, the substrate-independent leak currents are specific to each transporter and not detected in every membrane transporter. Previous reports for rat (r)and human (h) NaDC1, Na^+/glucose cotransporter (SGLT1), Na^+/phosphate cotransporter (NaPi-2), and thyroid Na^+/I^- symporters (NIS) exhibit sodium-dependent and substrate-uncoupled leak currents (18) (21; 25; 88; 117). The GABA transporter, GAT1, has different electrophysiological properties in terms of leak currents. GAT1 shows no leak currents in the presence of sodium but lithium (52). The lithium-dependent leak currents in GAT1 is insensitive to the addition of GABA (53), which is different from the effect of succinate on the sodium leak currents in hNaDC1 (117). Some transporters involve more than one cation in their substrate transport cycles and anion channel conductance, resulting in two distinct currents can be detected. For example, the glutamate transporter, EAAT1, has currents due to the flux of $Na^+/K^+/H^+$, coupled to glutamate transport and the flux of chloride, uncoupled to glutamate flux. The uncoupled chloride conductance is activated by glutamate but also partially activated without glutamate (107). Since cation-activated leak currents in xNaDC3 might partially carried by anions, like EAAT1, xNaDC3 might form the anion channel pore in the

protein. Therefore, an experimental approach to test the hypothesis with regard to the unique cation-activated currents seen in the absence of substrate in xNaDC3 would be addition of various ion channel inhibitors to the sodium and lithium buffers such as tetraethylammonium, DIDS, amiloride, tetrodotoxin, Gd^{3+}, and niflumic acid to see changes in the xNaDC3 involved leak currents.

Besides the leak currents, majority of members in SLC13 family exhibit substrate-dependent inward currents with di- and tricarboxylates in the presence of sodium. The substrate-induced currents in the members of SLC13 family show larger inward currents at more negative membrane potentials (13; 14; 18; 75; 76; 85; 117). Nevertheless, this profile is not the case for xNaDC3. Because of large cation-activated leak currents, xNaDC3 shows unique substrate-induced currents in the presence of sodium and lithium. The succinate-induced currents in the presence of sodium are voltage insensitive, showing about -50 nA at all tested membrane potentials. This electrophysiological profile in xNaDC3 may be both effects of the inhibition of sodium-activated leak currents by succinate and the activation of succinate-evoked currents although this hypothesis needs to be tested. During negative potentials, succinate-induced currents in the presence of lithium exhibit outward currents, which may be due to the same mechanism as those in sodium.

FUTURE DIRECTION

In a typical organism, membrane proteins are estimated to be coded in 20-30% of all genes (44). However, these proteins have proven to be difficult to study due to their hydrophobic and amphiphilic properties. As a result, the structures of only a limited number of transport proteins have been solved to a resolution that allows molecular analysis. In the absence of detailed structural information of the vast majority of transport proteins, the structure-function relationships in transporters have relied on molecular biological and biochemical methods for analysis. Such an approach was employed to the study of the NaDC transporters in the SLC13 gene family.

To date, a great deal is known about the SLC13 gene family with respect to physiological function, tissue distribution, and substrate preference (see Introduction). However, the information of the structure-function relationships that helps to understand substrate specificity and transport function in members of this family is limited. To obtain a better understanding of these relationships, I employed an experimental method that was a combination of molecular biology, electrophysiology, and TSR analysis. This approach provided evidence that differences in substrate specificity between the NaDC orthologs are determined by multiple domains throughout these proteins, and that these domains interact functionally.

The information gained as well as methods utilized in this study allow a more detailed analysis of the structure and function of the SLC 13 gene family. For example, it can be applied to study different parts of the NaDC1 proteins that have not been investigated in this dissertation in order to dictate more details of differences in substrate specificity between NaDC1 orthologs. Also, differences in substrate specificity and affinity between NaDC1 and NaDC3 can be studied using the same type of the experimental approach to find out domains and amino acid residues determining differences in functional properties between these two transporters. The combination of electrophysiology and TSR analysis can detect changes in not only substrate affinity but also relative substrate specificity. With the information, the thermodynamic approach based on TSR analysis can provide more insight with regard to which TMs are interacting while a substrate is transported by the NaDC transporters although how they interact needs to be investigated further.

The methods used in this work can also be applied to the analysis of transport proteins in general. With the availability of radiotracers showing low background in control expression system, the TSR analysis can be a useful tool to detect changes in relative substrate specificity and functional interaction in the transport membrane proteins, which may not be obvious by electrophysiological approaches. However, to

measure currents evoked by electrogenic membrane transport proteins can provide different aspects of transport kinetics with respect to changes in an apparent substrate affinity as well as transport mechanisms. The studies in cotransport mechanisms of the NaDC transporters have been limited to steady-state current measurements. Although transport model for the human (h) NaDC1 transporter has been proposed earlier, the rate-limiting steps and rate constants (k) of the transport reactions are not fully understood (117) (Figure 1.3). For further understanding of mechanism of the Na^+-couple cotransporters, analysis of presteady-state currents is important. The information for the population of the transporters at the each transport reaction state and rate constant for every transport step will be determined at different membrane potentials. Moreover, the rate-limiting step of the transport reaction should be identified at different tested membrane potentials using presteady-state currents. Theses analytical data and information will be great insights for transport mechanism of the Na^+-coupled cotransporters.

REFERENCES

1. Abramson J, Smirnova I, Kasho V, Verner G, Kaback HR and Iwata S. Structure and mechanism of the lactose permease of *Escherichia coli*. *Science* 301: 610-615, 2003.

2. Abuladze N, Azimov R, Newman D, Sassani P, Liu W, Tatishchev S, Pushkin A and Kurtz I. Critical amino acid residues involved in the electrogenic sodium-bicarbonate cotransporter kNBC1-mediated transport. *J Physiol* 565: 717-730, 2005.

3. Aruga S, Pajor AM, Nakamura K, Liu L, Moe OW, Preisig PA and Alpern RJ. OKP cells express the Na-dicarboxylate cotransporter NaDC-1. *Am J Physiol Cell Physiol* 287: C64-C72, 2004.

4. Aruga S, Wehrli S, Kaissling B, Moe OW, Preisig PA, Pajor AM and Alpern RJ. Chronic metabolic acidosis increases NaDC-1 mRNA and protein abundance in rat kidney. *Kidney Int* 58: 206-215, 2000.

5. Bacconi A, Virkki LV, Biber J, Murer H and Forster IC. Renouncing electroneutrality is not free of charge: switching on electrogenicity in a Na^+-coupled phosphate cotransporter. *Proc Natl Acad Sci U S A* 102: 12606-12611, 2005.

6. Bai L and Pajor AM. Expression cloning of NaDC-2, an intestinal Na^+- or Li^+-dependent dicarboxylate transporter. *Am J Physiol* 273: G267-G274, 1997.

7. Ballesteros JA, Deupi X, Olivella M, Haaksma EE and Pardo L. Serine and threonine residues bend alpha-helices in the chi(1) = g(-) conformation. *Biophys J* 79: 2754-2760, 2000.

8. Baric I, Wagner L, Feyh P, Liesert M, Buckel W and Hoffmann GF. Sensitivity and specificity of free and total glutaric acid and 3-hydroxyglutaric acid measurements by stable-isotope dilution assays for the diagnosis of glutaric aciduria type I. *J Inher Metab Dis* 22: 867-881, 1999.

9. Beck L and Markovich D. The mouse Na^+-sulfate cotransporter gene Nas1. Cloning, tissue distribution, gene structure, chromosomal assignment, and transcriptional regulation by vitamin D. *J Biol Chem* 275: 11880-11890, 2000.

10. Blostein R, Wilczynska A, Karlish SJ, Arguello JM and Lingrel JB. Evidence that Ser^{775} in the alpha subunit of the Na,K-ATPase is a residue in the cation binding pocket. *J Biol Chem* 272: 24987-24993, 1997.

11. Boehmer C, Embark HM, Bauer A, Palmada M, Yun CH, Weinman EJ, Endou H, Cohen P, Lahme S, Bichler KH and Lang F. Stimulation of renal Na^+ dicarboxylate cotransporter 1 by Na^+/H^+ exchanger regulating factor 2, serum and glucocorticoid inducible kinase isoforms, and protein kinase B. *Biochem Biophys Res Commun* 313: 998-1003, 2004.

12. Buchs AE, Sasson S, Joost HG and Cerasi E. Characterization of GLUT5 domains responsible for fructose transport. *Endocrinology* 139: 827-831, 1998.

13. Burckhardt BC, Lorenz J, Kobbe C and Burckhardt G. Substrate specificity of the human renal sodium dicarboxylate cotransporter, hNaDC-3, under voltage-clamp conditions. *Am J Physiol Renal Physiol* 288: F792-F799, 2005.

14. Burckhardt BC, Steffgen J, Langheit D, Muller GA and Burckhardt G. Potential-dependent steady-state kinetics of a dicarboxylate transporter cloned from winter flounder kidney. *Pflugers Arch* 441: 323-330, 2000.

15. Busch W and Saier MH, Jr. The transporter classification (TC) system, 2002. *Crit Rev Biochem Mol Biol* 37: 287-337, 2002.

16. Chan TO, Rittenhouse SE and Tsichlis PN. AKT/PKB and other D3 phosphoinositide-regulated kinases: kinase activation by phosphoinositide-dependent phosphorylation. *Annu Rev Biochem* 68: 965-1014, 1999.

17. Chen X, Tsukaguchi H, Chen XZ, Berger UV and Hediger MA. Molecular and functional analysis of SDCT2, a novel rat sodium-dependent dicarboxylate transporter. *J Clin Invest* 103: 1159-1168, 1999.

18. Chen XZ, Shayakul C, Berger UV, Tian W and Hediger MA. Characterization of rat Na^+-dicarboxylate cotransporter. *J Biol Chem* 273: 20972-20981, 1998.

19. Cohen A, Ellis P, Kresge N and Soltis SM. MAD phasing with krypton. *Acta Crystallogr D Biol Crystallogr* 57: 233-238, 2001.

20. Dantzler WH and Evans KK. Effect of αKG in lumen on PAH transport by isolated perfused proximal tubules. *Am J Physiol* 271: F521-F526, 1996.

21. Eskandari S, Loo DDF, Dai G, Levy O, Wright EM and Carrasco N. Thyroid Na^+/I^- symporter. *J Biol Chem* 272: 27230-27238, 1997.

22. Fairman WA, Vandenberg RJ, Arriza JL, Kavanaugh MP and Amara SG. An excitatory amino-acid transporter with properties of a ligand-gated chloride channel. *Nature* 375: 599-603, 1995.

23. Fei YJ, Inoue K and Ganapathy V. Structural and functional characteristics of two sodium-coupled dicarboxylate transporters (ceNaDC1 and ceNaDC2) from

Caenorhabditis elegans and their relevance to life span. *J Biol Chem* 278: 6136-6144, 2003.

24. Fei YJ, Liu JC, Inoue K, Zhuang L, Miyake K, Miyauchi S and Ganapathy V. Relevance of NAC-2, an Na^+-coupled citrate transporter, to life span, body size and fat content in *Caenorhabditis elegans*. *Biochem J* 379: 191-198, 2004.

25. Forster I, Hernando N, Biber J and Murer H. The voltage dependence of a cloned mammalian renal type II Na^+/P_i cotransporter (NaP_i-2). *J Gen Physiol* 112: 1-18, 1998.

26. Geck P and Heinz E. Coupling in secondary transport. Effect of electrical potentials on the kinetics of ion linked co-transport. *Biochim Biophys Acta* 443: 49-63, 1976.

27. Girard JP, Baekkevold ES, Feliu J, Brandtzaeg P and Amalric F. Molecular cloning and functional analysis of SUT-1, a sulfate transporter from human high endothelial venules. *Proc Natl Acad Sci U S A* 96: 12772-12777, 1999.

28. Griffith DA and Pajor AM. Acidic residues involved in cation and substrate interactions in the Na^+/dicarboxylate cotransporter, NaDC-1. *Biochemistry* 38: 7524-7531, 1999.

29. Grossman TR and Nelson N. Effect of sodium lithium and proton concentrations on the electrophysiological properties of the four mouse GABA transporters expressed in *Xenopus* oocytes. *Neurochem Int* 43: 431-443, 2003.

30. Hamm LL. Renal handling of citrate. *Kidney International* 38: 728-735, 1990.

31. Hentschel H, Burckhardt BC, Scholermann B, Kuhne L, Burckhardt G and Steffgen J. Basolateral localization of flounder Na^+-dicarboxylate cotransporter (fNaDC-3) in the kidney of *Pleuronectes americanus*. *Pflugers Arch* 446: 578-584, 2003.

32. Huang Y, Lemieux MJ, Song J, Auer M and Wang DN. Structure and mechanism of the glycerol-3-phosphate transporter from *Escherichia coli*. *Science* 301: 616-620, 2003.

33. Inoue K, Fei YJ, Zhuang L, Gopal E, Miyauchi S and Ganapathy V. Functional features and genomic organization of mouse NaCT, a sodium-coupled transporter for tricarboxylic acid cycle intermediates. *Biochem J* 378: 949-957, 2004.

34. Inoue K, Zhuang L and Ganapathy V. Human Na^+-coupled citrate transporter: primary structure, genomic organization, and transport function. *Biochem Biophys Res Commun* 299: 465-471, 2002.

35. Inoue K, Zhuang L, Maddox DM, Smith SB and Ganapathy V. Structure, function, and expression pattern of a novel sodium-coupled citrate transporter (NaCT) cloned from mammalian brain. *J Biol Chem* 277: 39469-39476, 2002.

36. Itokawa M, Lin Z, Cai NS, Wu C, Kitayama S, Wang JB and Uhl GR. Dopamine transporter transmembrane domain polar mutants: ΔG and ΔΔG values implicate regions important for transporter functions. *Mol Pharmacol* 57: 1093-1103, 2000.

37. Jenkins AD, Dousa TP and Smith LH. Transport of citrate across renal brush border membrane: effects of dietary acid and alkali loading. *Am J Physiol* 249: F590-F595, 1985.

38. Kahn ES and Pajor AM. Determinants of substrate and cation affinities in the Na^+/dicarboxylate cotransporter. *Biochemistry* 38: 6151-6156, 1999.

39. Kasahara T and Kasahara M. Transmembrane segments 1, 5, 7 and 8 are required for high-affinity glucose transport by *Saccharomyces cerevisiae* Hxt2 transporter. *Biochem J* 372: 247-252, 2003.

40. Kekuda R, Wang H, Huang W, Pajor AM, Leibach FH, Devoe LD, Prasad PD and Ganapathy V. Primary structure and functional characteristics of a mammalian sodium-coupled high affinity dicarboxylate transporter. *J Biol Chem* 274: 3422-3429, 1999.

41. King SC. The "Transport Specificity Ratio": a structure-function tool to search the protein fold for loci that control transition state stability in membrane transport catalysis. *BMC Biochem* 5: 2004.

42. King SC, Hu LA and Pugh A. Induction of substrate specificity shifts by placement of alanine insertions within the consensus amphipathic region of the *Escherichia coli* GABA (γ-aminobutyric acid) transporter encoded by GabP. *Biochem J* 376: 645-653, 2003.

43. Klingenberg M. Ligand-protein interaction in biomembrane carriers. The induced transition fit of transport catalysis. *Biochemistry* 44: 8563-8570, 2005.

44. Krogh A, Larsson B, Von HG and Sonnhammer EL. Predicting transmembrane protein topology with a hidden Markov model: application to complete genomes. *J Mol Biol* 305: 567-580, 2001.

45. Kunkel TA. Rapid and efficient site-specific mutagenesis without phenotypic selection. *Proc Natl Acad Sci USA* 82: 488-492, 1985.

46. Kushnir MM, Komaromy-Hiller G, Shushan B, Urry FM and Roberts WL. Analysis of dicarboxylic acids by tandem mass spectrometry. High-throughput

quantitative measurement of methylmalonic acid in serum, plasma, and urine. *Clin Chem* 47: 1993-2002, 2001.

47. Kyte J and Doolittle RF. A simple method for displaying the hydropathic character of a protein. *J Mol Biol* 157: 105-132, 1982.

48. Lang F and Cohen P. Regulation and physiological roles of serum- and glucocorticoid-induced protein kinase isoforms. *Sci STKE* 2001: RE17, 2001.

49. Lee A, Beck L and Markovich D. The human renal sodium sulfate cotransporter (SLC13A1; hNaSi-1) cDNA and gene: organization, chromosomal localization, and functional characterization. *Genomics* 70: 354-363, 2000.

50. Li H and Pajor AM. Serines 260 and 288 are involved in sulfate transport by hNaSi-1. *J Biol Chem* 278: 37204-37212, 2003.

51. Li H and Pajor AM. Mutagenesis of the N-glycosylation site of hNaSi-1 reduces transport activity. *Am J Physiol Cell Physiol* 285: C1188-C1196, 2003.

52. MacAulay N, Bendahan A, Loland CJ, Zeuthen T, Kanner BI and Gether U. Engineered Zn^{2+} switches in the γ-aminobutyric acid (GABA) transporter-1. Differential effects on GABA uptake and currents. *J Biol Chem* 276: 40476-40485, 2001.

53. MacAulay N, Zeuthen T and Gether U. Conformational basis for the Li^{+}-induced leak current in the rat γ-aminobutyric acid (GABA) transporter-1. *J Physiol* 544: 447-458, 2002.

54. Mackenzie B, Loo DD, Fei Y, Liu WJ, Ganapathy V, Leibach FH and Wright EM. Mechanisms of the human intestinal H^{+}-coupled oligopeptide transporter hPEPT1. *J Biol Chem* 271: 5430-5437, 1996.

55. Mager S, Kleinberger-Doron N, Keshet GI, Davidson N, Kanner BI and Lester HA. Ion binding and permeation at the GABA transporter GAT1. *J Neurosci* 16: 5405-5414, 1996.

56. Mager S, Naeve J, Quick M, Labarca C, Davidson N and Lester HA. Steady states, charge movements, and rates for a cloned GABA transporter expressed in *Xenopus* oocytes. *Neuron* 10: 177-188, 1993.

57. Mann SS, Hart TC, Pettenati MJ, von Kap-herr C and Holmes RP. Assignment of the sodium-dependent dicarboxylate transporter gene (SLC13A2 alias NaDC-1) to human chromosome region 17p11.1-q11.1 by radiation hybrid mapping and fluorescence in situ hybridization. *Cytogenet Cell Genet* 34: 89-90, 1999.

58. Manning SK, Woodrow C, Zuniga FA, Iserovich P, Fischbarg J, Louw AI and Krishna S. Mutational analysis of the hexose transporter of *Plasmodium falciparum* and development of a three-dimensional model. *J Biol Chem* 277: 30942-30949, 2002.

59. Manolescu A, Salas-Burgos AM, Fischbarg J and Cheeseman CI. Identification of a hydrophobic residue as a key determinant of fructose transport by the facilitative hexose transporter SLC2A7 (GLUT7). *J Biol Chem* 280: 42978-42983, 2005.

60. Markovich D, Forgo J, Stange G, Biber J and Murer H. Expression cloning of rat renal $Na^+/SO4^{2-}$ cotransport. *Proc Natl Acad Sci U S A* 90: 8073-8077, 1993.

61. Markovich D, Regeer RR, Kunzelmann K and Dawson PA. Functional characterization and genomic organization of the human Na^+-sulfate cotransporter hNaS2 gene (SLC13A4). *Biochem Biophys Res Commun* 326: 729-734, 2005.

62. Meinild AK, Loo DD, Pajor AM, Zeuthen T and Wright EM. Water transport by the renal Na^+-dicarboxylate cotransporter. *Am J Physiol Renal Physiol* 278: F777-F783, 2000.

63. Merickel A, Rosandich P, Peter D and Edwards RH. Identification of residues involved in substrate recognition by a vesicular monoamine transporter. *J Biol Chem* 270: 25798-25804, 1995.

64. Mohana Rao JK and Argos P. A conformational preference parameter to predict helices in integral membrane proteins. *Biochim Biophys Acta* 869: 197-214, 1986.

65. Nakada T, Zandi-Nejad K, Kurita Y, Kudo H, Broumand V, Kwon CY, Mercado A, Mount DB and Hirose S. Roles of Slc13a1 and Slc26a1 sulfate transporters of eel kidney in sulfate homeostasis and osmoregulation in freshwater. *Am J Physiol Regul Integr Comp Physiol* 289: R575-R585, 2005.

66. Nguyen TH, Hibbs DE and Howard ST. Conformations, energies, and intramolecular hydrogen bonds in dicarboxylic acids: implications for the design of synthetic dicarboxylic acid receptors. *J Comput Chem* 26: 1233-1241, 2005.

67. Oshiro N and Pajor AM. Functional characterization of high-affinity Na^+/dicarboxylate cotransporter found in *Xenopus laevis* kidney and heart. *Am J Physiol Cell Physiol* 289: C1159-C1168, 2005.

68. Ostermeier C and Michel H. Crystallization of membrane proteins. *Curr Opin Struct Biol* 7: 697-701, 1997.

69. Pajor AM. Molecular cloning and functional expression of a sodium-dicarboxylate cotransporter from human kidney. *Am J Physiol* 270: F642-F648, 1996.

70. Pajor AM. Molecular properties of sodium/dicarboxylate cotransporters. *J Membr Biol* 175: 1-8, 2000.

71. Pajor AM. Conformationally sensitive residues in transmembrane domain 9 of the Na^+/dicarboxylate co-transporter. *J Biol Chem* 276: 29961-29968, 2001.

72. Pajor, A. M. Sequence and functional characterization of a renal sodium/dicarboxylate cotransporter. *J Biol Chem* 270, 5779-5785. 1995.

73. Pajor AM. Sodium-coupled transporters for Krebs cycle intermediates. *Ann Rev Physiol* 61: 663-682, 1999.

74. Pajor AM. Molecular properties of the SLC13 family of dicarboxylate and sulfate transporters. *Pflugers Arch* 451: 597-605, 2006.

75. Pajor AM, Gangula R and Yao X. Cloning and functional characterization of a high-affinity Na^+/dicarboxylate cotransporter from mouse brain. *Am J Physiol Cell Physiol* 280: C1215-C1223, 2001.

76. Pajor AM, Hirayama BA and Loo DDF. Sodium and lithium interactions with the Na^+/dicarboxylate cotransporter. *J Biol Chem* 273: 18923-18929, 1998.

77. Pajor AM, Kahn ES and Gangula R. Role of cationic amino acids in the Na^+/dicarboxylate co-transporter NaDC-1. *Biochem J* 350: 677-683, 2000.

78. Pajor AM, Krajewski SJ, Sun N and Gangula R. Cysteine residues in the Na^+/dicarboxylate cotransporter, NaDC-1. *Biochem J* 344: 205-209, 1999.

79. Pajor AM and Randolph KM. Conformationally sensitive residues in extracellular loop 5 of the Na^+/dicarboxylate co-transporter. *J Biol Chem* 280: 18728-18735, 2005.

80. Pajor AM and Sun N. Characterization of the rabbit renal Na^+-dicarboxylate cotransporter using antifusion protein antibodies. *Am J Physiol* 271: C1808-C1816, 1996.

81. Pajor AM and Sun N. Functional differences between rabbit and human Na^+-dicarboxylate cotransporters, NaDC-1 and hNaDC-1. *Am J Physiol* 271: F1093-F1099, 1996.

82. Pajor AM and Sun N. Protein kinase C-mediated regulation of the renal Na^+/dicarboxylate cotransporter, NaDC-1. *Biochim Biophys Acta* 77654: 1-8, 1999.

83. Pajor AM, Sun N, Bai L, Markovich D and Sule P. The substrate recognition domain in the Na^+/dicarboxylate and Na^+/sulfate cotransporters is located in the

carboxy-terminal portion of the protein. *Biochim Biophys Acta* 1370: 98-106, 1998.

84. Pajor AM, Sun N and Valmonte HG. Mutational analysis of histidines in the Na^+/dicarboxylate cotransporter, NaDC-1. *Biochem J* 331: 257-264, 1998.

85. Pajor AM and Sun NN. Molecular cloning, chromosomal organization, and functional characterization of a sodium-dicarboxylate cotransporter from mouse kidney. *Am J Physiol Renal Physiol* 279: F482-F490, 2000.

86. Pak CYC. Etiology and treatment of urolithiasis. *Am J Kidney Diseases* 18: 624-637, 1991.

87. Pak CYC and Fuller C. Idiopathic hypocitraturic calcium-oxalate nephrolithiasis successfully treated with potassium citrate. *Ann Int Med* 104: 33-37, 1986.

88. Parent L, Supplisson S, Loo DDF and Wright EM. Electrogenic properties of the cloned Na^+/glucose cotransporter: I. Voltage-clamp studies. *J Membrane Biol* 125: 49-62, 1992.

89. Paulsen IT, Sliwinski MK, Nelissen B, Goffeau A and Saier MH, Jr. Unified inventory of established and putative transporters encoded within the complete genome of *Saccharomyces cerevisiae*. *FEBS Lett* 430: 116-125, 1998.

90. Price DJ, Roberts JD and Jorgensen WL. Conformational complexity of succinic acid and its monoanion in the gas phase and in solution: *Ab initio* calculations and Monte Carlo simulations. *J Am Chem Soc* 120: 9672-9679, 1998.

91. Pritchard JB and Miller DS. Mechanisms mediating renal secretion of organic anions and cations. *Physiological Reviews* 73: 765-796, 1993.

92. Rogina B, Reenan RA, Nilsen SP and Helfand SL. Extended life-span conferred by cotransporter gene mutations in *Drosophila*. *Science* 290: 2137-2140, 2000.

93. Saier MH, Jr. A functional-phylogenetic classification system for transmembrane solute transporters. *Microbiology and Molecular Biology Reviews* 64: 354-411, 2000.

94. Sekine T, Cha SH, Hosoyamada M, Kanai Y, Watanabe N, Furuta Y, Fukuda K, Igarishi T and Endou H. Cloning, functional characterization and localization of a rat renal Na^+-dicarboxylate cotransporter. *Am J Physiol* 275: F298-F305, 1998.

95. Shank RP and Bennett DJ. 2-Oxoglutarate transport: a potential mechanism for regulating glutamate and tricarboxylic acid cycle intermediates in neurons. *Neurochem Res* 18: 401-410, 1993.

96. Shank RP and Campbell GL. Avid Na^+-dependent, high affinity uptake of α-ketoglutarate by nerve terminal enriched material from mouse cerebellum. *Life Sciences* 28: 843-850, 1981.

97. Shenolikar S and Weinman EJ. NHERF: targeting and trafficking membrane proteins. *Am J Physiol Renal Physiol* 280: F389-F395, 2001.

98. Sheridan E, Rumrich G and Ullrich KJ. Reabsorption of dicarboxylic acids from the proximal convolution of rat kidney. *Pflugers Arch* 399: 18-28, 1983.

99. Smirnova IN and Kaback HR. A mutation in the lactose permease of *Escherichia coli* that decreases conformational flexibility and increases protein stability. *Biochemistry* 42: 3025-3031, 2003.

100. Smith U, Carvalho E, Mosialou E, Beguinot F, Formisano P and Rondinone C. PKB inhibition prevents the stimulatory effect of insulin on glucose transport and protein translocation but not the antilipolytic effect in rat adipocytes. *Biochem Biophys Res Commun* 268: 315-320, 2000.

101. Steffgen J, Burckhardt BC, Langenberg C, Kuhne L, Muller GA, Burckhardt G and Wolff NA. Expression cloning and characterization of a novel sodium-dicarboxylate cotransporter from winter flounder kidney. *J Biol Chem* 274: 20190-20196, 1999.

102. Stoll B, McNelly S, Buscher HP and Haussinger D. Functional hepatocyte heterogeneity in glutamate, aspartate and α-ketoglutarate uptake: a histoautoradiographical study. *Hepatology* 13: 247-253, 1991.

103. Sur C, Betz H and Schloss P. A single serine residue controls the cation dependence of substrate transport by the rat serotonin transporter. *Proc Natl Acad Sci U S A* 94: 7639-7644, 1997.

104. Sweet DH. Organic anion transporter (Slc22a) family members as mediators of toxicity. *Toxicol Appl Pharmacol* 204: 198-215, 2005.

105. Tate CG. Overexpression of mammalian integral membrane proteins for structural studies. *FEBS Lett* 504: 94-98, 2001.

106. Vallon V and Lang F. New insights into the role of serum- and glucocorticoid-inducible kinase SGK1 in the regulation of renal function and blood pressure. *Curr Opin Nephrol Hypertens* 14: 59-66, 2005.

107. Wadiche JI and Kavanaugh MP. Macroscopic and microscopic properties of a cloned glutamate transporter/chloride channel. *J Neuroscience* 18: 7650-7661, 1998.

108. Wang H, Fei YJ, Kekuda R, Yang-Feng TL, Devoe LD, Leibach FH, Prasad PD and Ganapathy V. Structure, function, and genomic organization of human Na^+-dependent high-affinity dicarboxylate transporter. *Am J Physiol Cell Physiol* 278: C1019-C1030, 2000.

109. Weinman EJ, Evangelista CM, Steplock D, Liu MZ, Shenolikar S and Bernardo A. Essential role for NHERF in cAMP-mediated inhibition of the Na^+-HCO_3^- co-transporter in BSC-1 cells. *J Biol Chem* 276: 42339-42346, 2001.

110. Wells JA. Additivity of mutational effects in proteins. *Biochemistry* 29: 8509-8517, 1990.

111. Windus DW, Cohn DE and Heifets M. Effects of fasting on citrate transport by the brush-border membrane of the rat kidney. *Am J Physiol* 251: F678-F682, 1986.

112. Wright SH, Kippen I, Klinenberg JR and Wright EM. Specificity of the transport system for tricarboxylic acid cycle intermediates in renal brush borders. *J Membrane Biol* 57: 73-82, 1980.

113. Wright SH, Kippen I and Wright EM. Effect of pH on the transport of Krebs cycle intermediates in renal brush border membranes. *Biochim Biophys Acta* 684: 287-290, 1982.

114. Wu L, Fritz JD and Powers AC. Different functional domains of GLUT2 glucose transporter are required for glucose affinity and substrate specificity. *Endocrinology* 139: 4205-4212, 1998.

115. Xie Z, Turk E and Wright EM. Characterization of the Vibrio parahaemolyticus Na^+/Glucose cotransporter. A bacterial member of the sodium/glucose transporter (SGLT) family. *J Biol Chem* 275: 25959-25964, 2000.

116. Yamashita A, Singh SK, Kawate T, Jin Y and Gouaux E. Crystal structure of a bacterial homologue of Na^+/Cl^--dependent neurotransmitter transporters. *Nature* 437: 215-223, 2005.

117. Yao X and Pajor AM. The transport properties of the human renal Na/dicarboxylate cotransporter under voltage clamp conditions. *Am J Physiol* 279: F54-F64, 2000.

118. Yao X and Pajor AM. Arginine-349 and aspartate-373 of the Na^+/dicarboxylate cotransporter are conformationally sensitive residues. *Biochemistry* 41: 1083-1090, 2002.

119. Yun CC, Chen Y and Lang F. Glucocorticoid activation of Na^+/H^+ exchanger isoform 3 revisited. The roles of SGK1 and NHERF2. *J Biol Chem* 277: 7676-7683, 2002.

120. Zhang FF and Pajor AM. Topology of the Na^+/dicarboxylate cotransporter: the N-terminus and hydrophilic loop 4 are located intracellularly. *Biochim Biophys Acta* 1511: 80-89, 2001.

121. Zhang YW and Rudnick G. Cysteine-scanning mutagenesis of serotonin transporter intracellular loop 2 suggests an alpha-helical conformation. *J Biol Chem* 280: 30807-30813, 2005.

122. Zimmerli B, O'Neill B and Meier PJ. Identification of sodium-dependent and sodium-independent dicarboxylate transport systems in rat liver basolateral membrane vesicles. *Pflugers Arch* 421: 329-335, 1992.

VITA

Naomi Oshiro, daughter of Hisashi and Yoko Oshiro, was born in Tokyo, Japan on December 24, 1974. After graduating from the Show University at Tokyo, Japan in 1998 with a Bachelor's degree in Pharmaceutical Sciences, Naomi further attended the university for her Master's degree. In 2001, Naomi matriculated in the Cellular Physiology and Molecular Biophysics graduate program at the University of Texas Medical Branch. Naomi was awarded the Student Travel Award for the Gordon Research Conference in 2004.

Naomi can be contacted through her parent at 1276 Takinoue-cho, Ome-shi, Tokyo, 198-0085, Japan.

Education

B.S., March 1998, The Showa University, Tokyo, Japan
M.S., March 2000, The Showa University, Tokyo, Japan

Publications

Oshiro N, King SC, and Pajor AM. Involvement of transmembrane helices 3 and 4 in substrate recognition by the Na^+/dicarboxylate cotransporter, NaDC1. *Biochemistry* 45: 2302-2310, 2006.

Oshiro N and Pajor AM. Functional characterization of high-affinity Na^+/dicarboxylate cotransporter found in *Xenopus laevis* kidney and heart. *Am J Physiol Cell Physiol* 289: C1159-C1168, 2005.

Kobayashi Y, Shibusawa A, Saito H, Ohshiro N, Ohbayashi M, Kohyama N, and Yamamoto T. Isolation and functional characterization of a novel organic solute carrier protein, hOSCP1. *J Biol Chem* 280: 32332-32339, 2005.

Kobayashi Y, Ohshiro N, Sakai R, Ohbayashi M, Kohyama N, and Yamamoto T. Transport mechanism and substrate specificity of human organic anion transporter 2 (hOat2 [SLC22A7]). *J Pharm Pharmacol* 57: 573-578, 2005.

Kobayashi Y, Sakai R, Ohshiro N, Ohbayashi M, Kohyama N, and Yamamoto T. Possible involvement of organic anion transporter 2 on the interaction of theophylline with erythromycin in the human liver. *Drug Metab Dispos* 33: 619-622, 2005.

Kobayashi Y, Ohshiro N, Tsuchiya A, Kohyama N, Ohbayashi M, and Yamamoto T. Renal transport of organic compounds mediated by mouse organic anion transporter 3

(mOat3): further substrate specificity of mOat3. *Drug Metab Dispos* 32: 479-483, 2004.

Kobayashi Y, Ohshiro N, Shibusawa A, Sasaki T, Tokuyama S, Sekine T, Endou H, and Yamamoto T. Isolation, characterization and differential gene expression of multispecific organic anion transporter 2 in mice. *Mol Pharmacol* 62: 7-14, 2002.

Kobayashi Y, Suzuki M, Ohshiro N, Sunagawa T, Sasaki T, Oguro T, Tokuyama S, Yamamoto T, and Yoshida T. Induction and inhibition of cytochrome P450 and drug-metabolizing enzyme by climbazole. *Biol Pharm Bull* 25: 53-57, 2002.

Kobayashi Y, Hirokawa N, Ohshiro N, Sekine T, Sasaki T, Tokuyama S, Endou H, and Yamamoto T. Differential gene expression of organic anion transporters in male and female rats. *Biochem Biophys Res Commun* 290: 482-487, 2002.

Kobayashi Y, Suzuki M, Ohshiro N, Sunagawa T, Sasaki T, Tokuyama S, Yamamoto T, and Yoshida T. Climbazole is a new potent inducer of rat hepatic cytochrome P450. *J Toxicol Sci* 26: 141-150, 2001.

Kobayashi Y, Ohshiro N, Sasaki T, Tokuyama S, Tobe T, Yoshida T, and Yamamoto T. Effect of 4-(4-chlorobenzyl)pyridine on rat hepatic microsomal cytochrome P450 and drug-metabolizing enzymes in vivo and in vitro. *Biol Pharm Bull* 24: 505-509, 2001.

Kobayashi Y, Ohshiro N, Suzuki M, Sasaki T, Tokuyama S, Yoshida T, and Yamamoto T. Sex-related effect on hemin on cytochrome P450 and drug-metabolizing enzymes in rat liver. *J Toxicol Sci* 25: 213-222, 2000.

Kobayashi Y, Ohshiro N, Okui E, Sasaki T, Tokuyama S, Yoshida T, and Yamamoto T. Concurrent induction of rat hepatic microsomal cytochrome P450 and haem oxygenase by 2,2'-dipyridyl ketone: comparison with the effect of 2,2'-dipyridyl amine. *Xenobiotica* 30: 683-692, 2000.

Abstracts

Oshiro N and Pajor AM. Involvement of glycine-161 in substrate selectivity in the mouse Na^+/dicarboxylate cotransporter. *Faseb J* 19: Abstract #671.78, 2005.

Oshiro N and Pajor AM. Transmembrane domains 3, 4, 7, and 9 of Na^+/dicarboxylate cotransporter 1 are involved in glutarate transport. Gordon Research Conference on Membrane Transport Proteins, Les Diablerets, Switzerland, 2004.

Oshiro N, Yao X, and Pajor AM. Transmembrane domain 9 of the sodium/dicarboxylate cotransporter 1 is involved in adipate transport. *Faseb J* 17: Abstract #330.5, 2003.